UNIVERSITÉ DE MONTRÉAL

ELECTRODEPOSITED POLY(3,4-ETHYLENEDIOXYTHIOPHENE) (PEDOT) FOR INVASIVE RECORDING AND STIMULATING NEURAL ELECTRODES

CÔME BODART

INSTITUT DE GÉNIE BIOMÉDICAL

ÉCOLE POLYTECHNIQUE DE MONTRÉAL

MÉMOIRE PRÉSENTÉ EN VUE DE L'OBTENTION

DU DIPLÔME DE MAÎTRISE ÈS SCIENCES APPLIQUÉES

(GÉNIE BIOMÉDICAL)

DÉCEMBRE 2018

UNIVERSITÉ DE MONTRÉAL

ÉCOLE POLYTECHNIQUE DE MONTRÉAL

Ce mémoire intitulé :

ELECTRODEPOSITED POLY(3,4-ETHYLENEDIOXYTHIOPHENE) (PEDOT) FOR INVASIVE RECORDING AND STIMULATING NEURAL ELECTRODES

présenté par : BODART Côme

en vue de l'obtention du diplôme de : Maîtrise ès sciences appliquées

a été dûment accepté par le jury d'examen constitué de :

M. HENRY Olivier, Ph. D, président

M. CICOIRA Fabio, Ph. D., membre et directeur de recherche

Mme MAUZEROLL Janine, Ph. D, membre

DEDICATION

To my girlfriend, my family and my colleagues for their continuous support

To the science that will help us build a better world

ACKNOWLEDGEMENTS

I would like first to thank my supervisor Professor Fabio Cicoira for integrating me into his research team and allowing me to discover the field of organic electronics. His support throughout the advancement of the project, his help and critical thinking made this project a success. I would also like to thank Professor Florin Amzica for his important contribution to the *in vivo* section of our work, which could not have been realized without him.

I would like to thank the research groups of professors Pierre-Paul Rompré and Louis-Eric Trudeau from Université de Montréal for their continuous help for the tissue analysis and the surgery procedure, as well as the veterinary Frédérique Chatigny.

I would like to thank Professor Francesca Soavi, for her helpful comments on our results that enlightened us during our research.

I would like to thank the technicians, without which most of our projects would not come to reality: Daniel Pilon and Yves Drolet.

I would like to thank Fabio Cicoira again and Patrice Chartrand for involving me in the tutorials of electrochemical classes for undergraduates students. I am most certain that this experience will serve me in the future.

I am grateful to the funding agencies and governmental groups without which this project would not have been possible: le Fond Québecois de la Recherche sur la Nature et les Technologies (FQRNT), the National Sciences and Engineering Research Council of Canada (NSERC), and le Ministère de l'Economie, des Sciences et des Technologies. I am also thankful to Polytechnique Montréal for the opportunity given to me to study science abroad. It was a very instructive stay in Québec.

I am deeply grateful to all of my colleagues, former and new, and friends that made my stay here so special. I would like to thanks Gaia, Guido, Shiming, Prajwal, Fanny, Irina and Eduardo for helping me settle at the beginning of my work. I would like to thank all my everyday colleagues for the fun times we had together, both inside and out of the lab: Yang, Tian, Julien, Xu, Nicolò, Ben, Tom, Shalin, Sam (both of them), Ada, Prabjot, Arun, Tim, Michael, Alexandra, Alexandre, Martin, Dominique, Mona, Natalie, Jo'elen, Manuel and Nils. I would like to thank Pauline for her great contribution during her internship among us. A special thanks to Xinda and Sanyasi for

thoroughly reviewing this Mémoire. I would like to thank my friends: Filipo, Ilaria, Arthur, Marie, Alexandre, Elisa, François, Pierre, Yann, Loïc, Moéa, Robin, Sophie, Anaëlle, Rodin, Paul and Pauline, for the great times we spent together.

I would like to dedicate these last lines to my family, especially my parents that helped me put everything together to go across the Atlantic for my studies. A special thanks to my girlfriend Emmanuelle, who managed to put up with me during our stay in Montréal.

RÉSUMÉ

Les électrodes neuronales sont un des outils médicaux utilisé pour soulager les symptômes des maladies neurodégénératives et pour étudier notre cerveau. Les électrodes neuronales conventionnelles souffrent de quelques inconvénients : leurs faibles dimensions leurs confèrent une haute impédance, et leur nature rigide et métallique couplée au traumatisme créé par la procédure d'implantation entraîne une réaction inflammatoire qui augmente encore plus l'impédance. Les polymères conducteurs sont des matériaux souples et organiques possédant une conductivité ionique-électronique mixte, et sont de candidats idéaux pour les interfaces biotique-abiotique. Ils sont régulièrement utilisés en tant que revêtement d'électrodes neuronales en raison de leur amélioration des propriétés électrochimiques et de leur supposée biocompatibilité. Une technique nommée électropolymérisation est généralement utilisée pour déposer les polymères conducteurs sur les microélectrodes neuronales. Un travail important a déjà été réalisé sur l'optimisation des paramètres de cette méthode de dépositionb. Cependant, les polymères conducteurs électropolymérisés souffrent d'une faible adhésion sur la plupart de leurs substrats. En plus de ce problème, il y a un manque d'études *in vivo* à long-terme confrontant les revêtements de polymères conducteurs aux conditions de stimulations électriques employés dans le domaine médical.

Dans notre étude, nous avons observé l'influence du solvant utilisé lors de la dépositions sur l'électropolymérisation, la stabilité électrochimique, et l'adhésion des revêtements en polymères conducteurs. Après avoir défini une procédure précise de déposition nous permettant de produire des revêtements stables, nous avons exploré l'utilité de ces revêtements pour des stimulations cérébrales profondes *in vivo.*

Du poly(3,4-éthylènedioxithipohène) (PEDOT) fut électropolymérisé dans trois solvants différents : acétonitrile, propylène carbonate et eau, sur des microélectrodes de platinium-iridium. Les microélectrodes enrobées furent soumises à différents tests de stabilité : sonication, vieillissement passif, stérilisation à la vapeur et stimulations électriques *in vitro*. Nous avons découvert que l'acétonitrile et le propylène carbonate nous fournissaient les revêtements les plus résistants. Tous les revêtements de PEDOT produits dans les différents solvants étaient suffisamment stable pour être utilisés dans un contexte médical. Ainsi, nous avons implanté des microélectrodes enrobées de PEDOT dans des rats et avons appliqué des stimulations électriques

quotidiennes tout en mesurant l'impédance des microélectrodes. Nous avons observé que les stimulations électriques entraînaient une diminution de l'impédance pour les microélectrodes enrobées de PEDOT et les microélectrodes de contrôle. La chute d'impédance était plus importante pour les microélectrodes de contrôle que pour les microélectrodes enrobées de PEDOT, ce qui remet en cause la pertinence de revêtements en PEDOT pour les stimulations cérébrales profondes et indique qu'un travail conséquent sera nécessaire pour optimiser les revêtements en polymère conducteur pour les électrodes neuronales de stimulation.

ABSTRACT

Neural electrodes are one of the medical tools to improve the symptoms of neurodegenerative diseases and/or to study the brain. Conventional neural electrodes suffer from some disadvantages such as: their smaller dimensions lead to high impedance, and their rigid and metallic nature coupled with the destructive insertion procedure leads to inflammatory response in the body that can further increase the impedance. Conducting polymers are soft and organic materials that possess a mixed electronic-ionic conductivity, and are ideal candidates for biotic-abiotic interfaces. They are regularly used for coating neural electrodes due to their enhanced electrochemical properties and biocompatibility. A technique called electropolymerization is generally used to deposit conducting polymers on neural microelectrodes. Extensive work has been done on the optimization of the parameters in this deposition method. However electrodeposited conducting polymers coatings suffer from poor adhesion on most of their substrates. Besides this issue, there is a lack of long-term *in vivo* studies subjecting conducting polymer coatings to electrical stimulation conditions used in medical studies.

In this work, we investigated the influence of the processing solvent on the electropolymerization, the electrochemical stability, and the adhesion of conducting polymer coatings. After having defined a precise deposition procedure to produce stable coatings, we investigated the role of these coatings for *in vivo* deep brain stimulations.

Poly(3,4-ethylenedioxithiophene) (PEDOT) was electropolymerized in three different solvent: acetonitrile, propylene carbonate and water, on platinum-iridium microelectrodes. The coated microelectrodes were subjected to different stability tests: sonication, passive aging, steam sterilization, and electrical stimulations *in vitro*. We found out that acetonitrile and propylene carbonate provided the most resistant PEDOT coatings. All the PEDOT coatings processed in different solvents were stable enough to be used in a medical context. We therefore implanted PEDOT-coated stimulating microelectrodes in rats and applied daily stimulation all the while monitoring the impedance of the microelectrodes. We observed that electrical stimulations decreased the impedance of both the PEDOT-coated microelectrodes and the uncoated control microelectrodes. The decrease in impedance was more prominent for control microelectrodes than for PEDOT-coated ones, which questions the relevance of PEDOT coatings for deep brain

stimulation purposes and indicates that more work is required to optimize conducting polymer coatings on neural electrodes for electrical stimulation studies.

TABLE OF CONTENTS

DEDICATION III

ACKNOWLEDGEMENTS IV

RÉSUMÉ VI

ABSTRACT VIII

TABLE OF CONTENTS X

LIST OF TABLES XIV

LIST OF FIGURES XV

LIST OF SYMBOLS AND ABBREVIATIONS XVIII

CHAPTER 1 INTRODUCTION 1

1.1 General context 1

1.1.1 Neural stimulation 1

1.1.2 Conducting polymers 2

1.2 Problematics 3

1.3 Objectives 3

1.4 Organization 4

CHAPTER 2 STATE OF THE ART 5

2.1 Deep Brain Stimulation (DBS) 5

2.1.1 Principles of bioelectricity 5

2.1.2 Principles of DBS 6

2.1.3 Parameters 8

2.2 Neural electrodes 10

2.2.1 Conventional electrodes 11

2.2.2 Materials 12

2.3 Foreign Body Reaction....15
2.3.1 Process of encapsulation....15
2.3.2 Causes of the FBR....18
2.4 Conducting polymers....20
2.4.1 Electron transport in conducting polymers....20
2.4.2 PEDOT coatings for neural electrodes....23
2.5 Processing of PEDOT....29
2.5.1 Choice of deposition method for PEDOT....29
2.5.2 Electropolymerization of PEDOT....29
CHAPTER 3 MATERIALS AND METHODS....35
3.1 Electropolymerization....35
3.1.1 Substrate cleaning....35
3.1.2 Solution preparation....36
3.1.3 Diazonium salt electrodeposition....36
3.1.4 PEDOT electrodeposition....37
3.1.5 Electrochemical characterization....38
3.1.6 Imaging....38
3.2 Stability tests *in vitro*....38
3.2.1 Sonication test....39
3.2.2 Passive aging....39
3.2.3 Steam sterilization....39
3.2.4 Electrical stimulation in PBS pH 7.4....40
3.3 *In vivo* stimulation....40
CHAPTER 4 RESULTS....42

4.1 Electropolymerization 42
4.1.1 Electrochemical properties 42
4.1.2 PEDOT morphologies 50
4.2 Stability of the organic coatings *in vitro* 52
4.2.1 Sonication test 52
4.2.2 Passive aging 55
4.2.3 Steam sterilization 57
4.2.4 Electrical stimulation in PBS pH 7.4 58
4.3 *In vivo* experiments 59
4.3.1 Voltage excursion 59
4.3.2 Electrochemical impedance measurements 61
CHAPTER 5 GENERAL DISCUSSION 65
5.1 Improved electrochemical properties *in vitro* 65
5.2 Stability *in vitro* 65
5.2.1 Use of thien-DS to improve adhesion 66
5.3 Differences in deposition kinetics 68
5.4 Electrochemical properties of PEDOT:BF_4 coatings *in vivo* 68
5.4.1 Impact of PEDOT coatings for DBS applications 69
CHAPTER 6 CONCLUSION AND RECOMMENDATIONS 71
6.1 Electropolymerization and adhesion 71
6.1.1 Thien-DS 71
6.1.2 Solvent 71
6.2 *In vivo* observations 72
6.3 Perspectives 73

BIBLIOGRAPHY 74

LIST OF TABLES

Table 1: Electropolymerization parameters of PEDOT:BF_4 on different substrates with different methods. 37

LIST OF FIGURES

Figure 1: Generation of an action potential across a cell membrane in 5 phases: (1) resting, (2) depolarization, (4) repolarization, (6) hyperpolarization and (7) resting. Taken from https://step1.medbullets.com/neurology/113052/action-potential-basics 6

Figure 2: Positions of the recurrently stimulated areas during DBS: GPi, STN and PPN. Taken from Hickey & Stacy [15]. 8

Figure 3: A) microwire-based electrode B) Michigan-style electrode C) Utah-style arrays. Taken from Jorfi et al [32]. 12

Figure 4: The Randles impedance model for electrode-solution interaction. Taken from Fernández-Sánchez et al [39]. 13

Figure 5: Astrocytes, brain-native immune cells, in their normal and reactive forms. Taken from Polikov et al [4]. 16

Figure 6: Microglias, brain-native immune cells, in their resting and activate forms. Taken from Polikov et al [4]. 16

Figure 7: Sheath resulting from chronic implantation of electrodes in brain after extraction of the electrodes at different time periods. Taken from Turner et al [49]. 18

Figure 8: The complex feedback loop mechanisms occurring during the FBR. Taken from Prodanov & Delbeke [42]. 20

Figure 9: The simple π-conjugated system of polyacetylene. Taken from Balint et al [58]. 21

Figure 10: A) Doping mechanism: oxidation or reduction of the polymer backbone, B) Charge carrier coupled with a lattice distortion, C) Polaron acting as an effective charge carrier and D) Travelling polaron. Taken from Balint et al [58]. 22

Figure 11: PEDOT polymerization consists of three main steps: (1) oxidation of EDOT, activation of the monomer, (2) EDOT radicals coupling, generation of a PEDOT dimer and (3) deprotonation of the dimer that reforms the π-conjugated structure and allows further polymerization. Taken from Ismail et al [90]. 31

Figure 12: PD deposition of 5 cycles at 100 mV/s of thien-DS on a recording PtIr microelectrode. A clear reduction peak is visible at 0.15 V, indicating the reduction of the amine moieties of the thien-DS.....43

Figure 13: a) CVs (3 cycles, 100 mV/s) in a ferrocene-containing solution before and after electrodeposition of a thien-DS layer on a Pt disk electrode and b) a zoom on the CVs obtained after deposition.....44

Figure 14: Deposition curves for PEDOT:BF_4 on Pt disk: a) PD depositions in ACN, PC and DW (last cycles out of 15, 100 mV/s), b) PD deposition in ACN (15 cycles, 100 mV/s) c) PS depositions in ACN, PC and DW and d) GS depositions in ACN, PC and DW. 45

Figure 15: Characterization of electropolymerized PEDOT:BF_4 coatings deposited in ACN, PC and DW using GS depositions: a) CV b) EIS ; PS depositions: c) CV d) EIS ; PD depositions: e) CV f) EIS. The scan rate for the CVs is 100 mV/s. The measurements were realized in PBS pH 7.4.....47

Figure 16: GS deposition curves of PEDOT:BF_4 in ACN, PC and DW on PtIr recording microelectrodes. 48

Figure 17: Characterization of electropolymerized PEDOT:BF4 galvanostatically deposited on PtIr recording microelectrodes using a) CV and b) EIS techniques. 49

Figure 18: Optical images of electropolymerized PEDOT:BF_4 on recording PtIr microelectrodes using 5 cycles of PD deposition in a) ACN and b) PC. 50

Figure 19: SEM imaging of PEDOT:BF4 on PtIr recording microelectrodes, galvanostatically deposited in PC: a) and b) ; ACN: c) and d) ; DW: e) and f). The acceleration voltage used was of 2.00 kV. 51

Figure 20: Time before appearance of large cracks and/or sudden changes in electrochemical properties (increase of impedance and decrease of CSC) for the PEDOT:BF_4 coating on the Pt disk during sonication, with different deposition method and different solvent used. The x axis represents the number of samples sonicated.....53

Figure 21: Delamination process of PEDOT:BF_4 galvanostatically deposited on the Pt disk in PC: a), b) and c) ; ACN: d), e) and f) ; DW: g), h) and i), under sonication for different time intervals. 54

Figure 22: Characterization of PEDOT:BF_4 coatings on PtIr microelectrodes immersed during 2 weeks in PBS pH 7.4: a) CV b) EIS. 56

Figure 23: Impedance measurements of PEDOT:BF4 coatings on recording PtIr microelectrodes before and after 30 minutes of steam sterilization at 121 °C. 57

Figure 24: Characterization of stimulating PEDOT:BF_4-coated PtIr microelectrodes before and after 2 hours of stimulations in PBS pH 7.4: a) CV, b) EIS. 58

Figure 25: Absolute values of the maximum of the negative peak measured before and after 90 minutes of stimulation at the PEDOT:BF_4-coated microelectrode and the bare PtIr microelectrode implanted in the first animal during the 15 days of stimulation. 59

Figure 26: Absolute values of the maximum of the negative peak measured before and after 90 minutes of stimulation at the PEDOT:BF_4-coated microelectrode and the bare PtIr microelectrode implanted in the second animal during the 7 days of stimulation. 60

Figure 27: Impedance at 1 kHz before and after stimulation of the PEDOT:BF4-coated microelectrode and the bare PtIr microelectrode implanted in the first animal during the 16 days of stimulation. 62

Figure 28: Bode impedance of the microelectrodes implanted in the first animal before and after 90 minutes of stimulation, after 9 days of stimulation. 63

Figure 29: Impedance at 1 kHz measured before and after 90 minutes of stimulation at the PEDOT:BF4-coated microelectrode and the bare PtIr microelectrode implanted in the second animal during the 7 days of stimulation. 63

Figure 30:(A) Electrodeposition of the thien-DS layer by reduction of the amine moieties (B) Electropolymerization of PEDOT on the thien-DS anchoring layer. 67

LIST OF SYMBOLS AND ABBREVIATIONS

The list of symbols and abbreviations presents the symbols and abbreviations used in the thesis or dissertation in alphabetical order, along with their meanings.

ACN	acetonitrile
Ag/AgCl	silver/silver-chloride
BBB	blood-brain barrier
BF_4^-	tetrafluoroborate
ClO_4^-	perchlorate
CP	conducting polymer
CSC	charge storage capacity
CV	cyclic voltammetry
DW	distilled water
DBS	deep brain stimulation
DS	diazonium salt
EDOT	ethylenedioxithiophene
EIS	electrochemical impedance spectroscopy
FBR	foreign body reaction
FDA	food and drug agency
GPi	global pallidus internal
GS	galvanostatic
Ir	Iridium
IrOx	iridium oxide
PBS	phosphate buffer solution
PC	propylene carbonate

PD	potentiodynamic
PEDOT	poly(3,4-ethylenedioxithiophene)
PPN	pedunculopontine nucleus
PPy	polypyrrole
Pt	platinum
PtIr	platinum-iridium
SEM	scanning electron microscopy
STN	subthalamic nucleus
Thien-DS	(4-thien-2-yl) diazonium salt
$TEABF_4$	tetraethylammonium tetrafluoroborate

CHAPTER 1 INTRODUCTION

1.1 General context

Healthcare has become a main concern in many countries, with the rise of life expectancy and the increasing prevalence of neurodegenerative diseases, such as Parkinson's disease. One of the common method used to treat movement disorders such as essential tremor and Parkinson's disease is Deep Brain Stimulation (DBS). DBS consists of applying electrical stimuli to a specific area of the brain and hence it heavily involves interactions between biology and electronics. The initial success of neural stimulation led to the creation of the field of bioelectronic medicine [1]. Since their discovery in the 70s, conducting polymers, i.e. organic materials capable of conducting charges, have allowed tremendous advances in electronics and gave birth to the field of organic electronics. Organic electronics comprises a wide range of applications, such as organic electrolyte-gated transistors, organic stretchable electronics and organic light-emitting diodes. Besides conductivity, the organic and soft nature of conducting polymers makes them ideal candidates for neural interfaces between conventional electronics and biological tissues. The use of conducting polymers in bioelectronic medicine could increase the efficiency of techniques such as neural recording and neural stimulation, and lead to exceptional discoveries about the human brain.

1.1.1 Neural stimulation

Neural stimulation is a wide family of techniques used to generate biosignals. This includes the DBS technique, used specifically to treat movement disorders.

1.1.1.1 Deep Brain Stimulation

Parkinson's disease is a neurodegenerative disease that affects dopaminergic neurons located in the substantia nigra region of the brain. In patients affected by Parkinson's disease, dopaminergic neurons, which are responsible for the production of dopamine, a crucial brain neurotransmitter, get attacked by immune cells. With aging, the symptoms tend to worsen leading heavy trembling and rigidity. DBS is a method to improve Parkinson's disease symptoms, approved since 2002 by the FDA [2]. Electrical pulses (1-9 V for human subjects) are delivered at high frequencies (130-180 Hz) in a specific area of the brain, usually the subthalamic nucleus (STN). Although the precise

mechanisms through which DBS achieves its effects are unknown, the most likely mode of action of DBS is through stimulation-based modulation of brain activity [3].

Bioelectricity and DBS will be discussed more in detail in chapter 2.

1.1.1.2 Foreign Body Reaction

The foreign body reaction (FBR) is the limiting factor for chronic implantation of medical device. The FBR consists of the spontaneous reaction of our immune system against intruders, including invasive devices such as stimulating and recording microelectrodes [4]. Despite its usefulness for protecting our body and destroying intruders, the FBR becomes problematic for treatments using DBS. Indeed, immune cells present in our brain, such as astrocytes and microglias, will attack the implanted electrodes. This will lead to an accumulation of cells, forming a sheath that obstructs the passage of electrical charges. With increasing implantation time, the usefulness of DBS decreases, as the electrical power necessary to alleviate the symptoms continuously increases, until the current and the voltage reach threatening levels for the neighboring cells. The FBR, which originates from various causes, is the main source of concern for long-term implantation of any devices, making the problem of biocompatibility paramount.

FBR will be discussed in more detail in chapter 2.

1.1.2 Conducting polymers

Conducting polymers are a large family of organic materials able to conduct electrical charges. The most commonly used for its robust stability is poly(3,4-ethylenedioxithiophene), also known as PEDOT. Its soft and organic nature combined with its electrochemical properties assert its relevance to bioelectronic medicine.

1.1.2.1 Electropolymerization

Several methods exists for the synthesis of conducting polymers, including chemical and electrochemical polymerization. In this work, we used electropolymerization to process PEDOT. Electropolymerization consists of applying a certain potential between a working electrode and a counter-electrode immersed into an electrolytic solution containing dissolved monomers. The application of the potential activates the monomers, transforming them into radicals that

subsequently polymerize together to form an insoluble polymer on the working electrode surface. Electropolymerization is the main method used to coat neural metallic electrodes [5].

This deposition technique will be discussed more in detail in chapter 2.

1.1.2.2 Adhesion

Despite their usefulness, PEDOT coatings tend to suffer from poor adhesion on most inorganic substrates. When confronted to harsh conditions, such as *in vivo* experiments, steam sterilization or repeated electrical stimulations, PEDOT coatings show signs of delamination or reduced electrochemical properties [6]. This is the most important limitation for the widespread use of conducting polymers in a biomedical context. Several elegant solutions were brought by the scientific community to solve this problem. In this work, specific tests were dedicated to ensuring the adhesion of PEDOT to the substrate. A solution, based on an anchoring layer for PEDOT, has also been explored [7].

This issue will be discussed in more detail in chapter 2.

1.2 Problematics

This Mémoire focuses on the following problematics:

- Is it possible to improve the electrochemical properties of neural microelectrodes using conducting polymers *in vitro* and *in vivo*?
- Is it possible to ensure the adhesion of conducting polymers on the microelectrodes to resist confrontation against harsh treatments?

1.3 Objectives

The objectives of this Mémoire are the following:

- Improve the electrochemical properties *in vitro* of invasive neural microelectrodes using a PEDOT coating.
- Ensure the adhesion and the electrochemical stability of the deposited PEDOT coating *in vitro*.
- Control the usefulness of the PEDOT-coated microelectrodes in DBS conditions *in vivo*.

1.4 Organization

This introductory chapter is followed by five other chapters. Chapter 2 provides the reader with a literature review about the main concepts introduced in chapter 1, i.e. Deep Brain Stimulation, foreign body reaction, conducting polymers, and electropolymerization. Chapter 3 details the methods and materials used in this work. Chapter 4 exposes the main results, followed by a discussion in chapter 5. Finally, chapter 6 concludes this Mémoire.

CHAPTER 2 STATE OF THE ART

2.1 Deep Brain Stimulation (DBS)

DBS is a FDA-approved method to treat movement disorders since 2002 [2]. This section consists in a description of the principles of bioelectricity followed by explanations about the mechanisms of DBS, and concludes by a review about the parameters used for DBS in humans and animals.

2.1.1 Principles of bioelectricity

Neuronal activity is characterized by trains of extracellular potentials, known as action potentials (APs). During the resting phase, the cell membrane exhibits a resting potential of -60 to -75 mV, due to an imbalance of ions, with an excess of K^+ inside the cell and an excess of Na^+ outside (figure 1, (1)). When a sufficiently positive voltage is applied, voltage-controlled Na^+ gates open, creating an influx of Na^+ ions that increases the membrane potential up to 40 mV (figure 1, (2)). This first phase is called depolarization. When the potential reaches a certain threshold, Na^+ gates close themselves and voltage-controlled K^+ gates start to open, putting a stop to the influx of Na^+ ions and generating an outflux of K^+ ions (figure 1, (3) and (4)). This phase, called repolarization, drives the membrane potential back down. A hyperpolarization phase, during which K^+ ions leach out of the cell before the K^+ gates close, generating an excessively negative membrane potential (figure 1, (6)), concludes the process [8]. This phase is also known as the refractory period. Indeed, no more APs can be generated during this period as the membrane potential is too low to activate the voltage-controlled ionic gates. Finally, after reaching a new ionic equilibrium, the membrane comes back to its initial resting phase (figure 1, (7)).

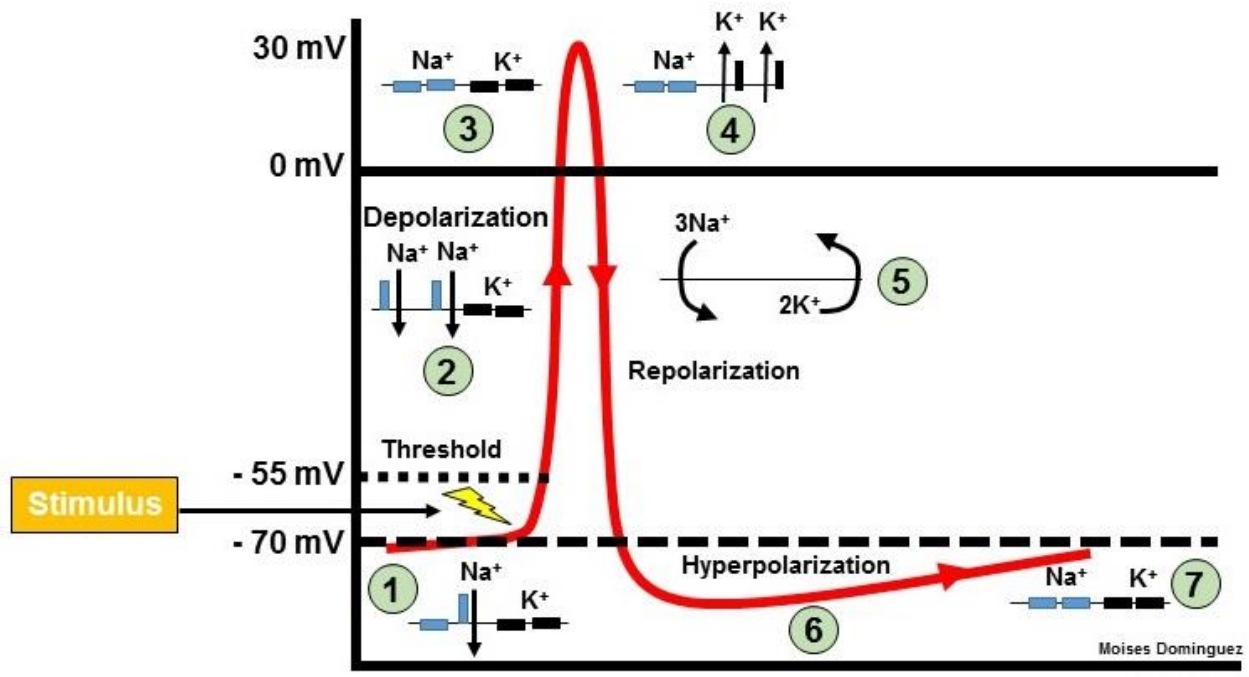

Figure 1: Generation of an action potential across a cell membrane in 5 phases: (1) resting, (2) depolarization, (4) repolarization, (6) hyperpolarization and (7) resting.
Taken from https://step1.medbullets.com/neurology/113052/action-potential-basics

2.1.2 Principles of DBS

Investigation of the brain activity using electrical stimulation has existed for almost 150 years. DBS, a technique derived from these early brain stimulations studies, is used nowadays to alleviate the symptoms of disorders such as Parkinson's disease, chronic pain, tremors and dystopia. For instance, a study also showed that DBS could be used to help patients suffering from treatment-resistant depression [9]. A randomized trial of 255 patients even showed that DBS was more effective than the best medical therapy in improving the quality of life for patients with severe Parkinson's disease, although an increased risk of side effects was also observed [10]. DBS in a rat subthalamic nucleus was found to have a neurorestorative effect and might also affect brain functions, thus leading to the frequently observed depression [11]. The effect of DBS on brain functions was also observed using diffusion tensor imaging [12]. However, the mechanisms of actions of DBS are still unclear, especially whether DBS excites or inhibits neural activity. To learn about these mechanisms, researchers investigated different regions of the brain using DBS.

Kringelbach et al produced two literature reviews that can guide us through the exploration of DBS mechanisms [3], [13].

The most common stimulated area in the brain for DBS is the subthalamic nucleus (STN) (figure 2) [14]. Studies showed that DBS at low intensity in rats induced a net decrease of neural activity in the substantia nigra region of the brain, the region damaged by Parkinson's disease. This was confirmed by studies realized on primates that also showed that only high-frequency stimulations were able to improve the symptoms. Studies on humans showed similar results: STN stimulation inhibited local activity and reduced trembling [13].

The global pallidus internal (GPi) was also explored as a possible stimulation location, however the results showed that even if most of the stimulations suppressed thalamic neural activity, only high-amplitude stimulations were able to block the movements, thus draining faster the implanted battery [13].

Pedunculopontine nucleus (PPN) is the most recent region explored, and possesses high potential for being a relevant stimulation area as DBS in PPN can alleviate Parkinson's disease symptoms in humans and animals using lower frequencies and hence reducing the energy consumption [14].

Two possible explanations have been proposed by Kringelbach et al about the working mechanism of DBS: synaptic inhibition or depolarization blockade. However, this inhibition of neural activity is most likely not due to a lack of neurotransmitter as a release of glutamate was observed during DBS [13]. This led to the hypothesis of stimulation-induced modulation of pathological network activity. In Parkinson's disease, the lack of dopamine is believed to create pathological oscillations in the beta frequency band (15-30 Hz) in the STN, and high-frequency DBS in the STN suppress activity in this beta band. Hence DBS most likely modulates the neural activity locally in specific frequency bands rather than simply inhibiting or exciting neural activity altogether. However, much work still need to be done to understand the precise mechanisms and the interactions between the different regions of the brain, dopamine and other neurotransmitters.

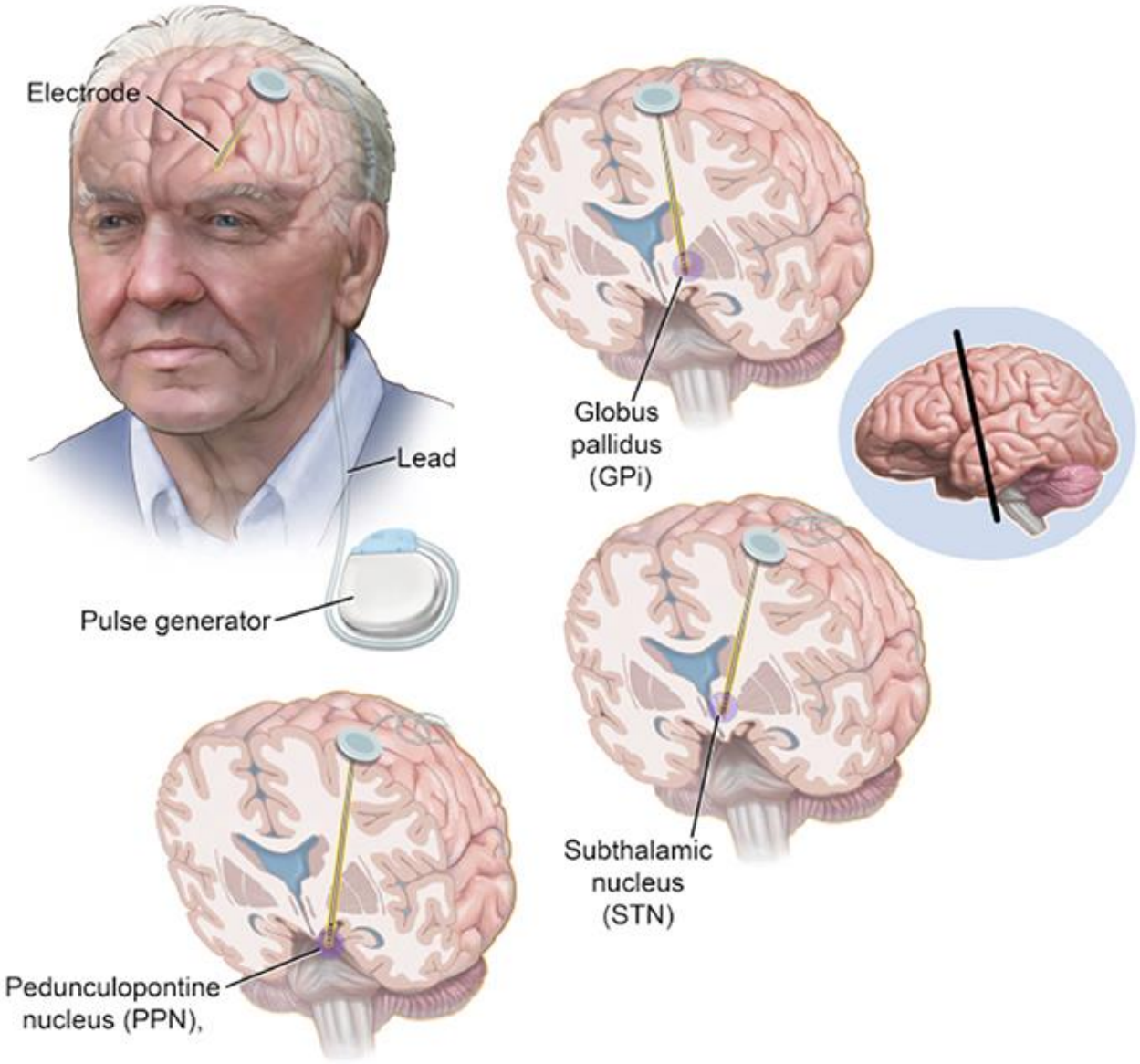

Figure 2: Positions of the recurrently stimulated areas during DBS: GPi, STN and PPN. Taken from Hickey & Stacy [15].

2.1.3 Parameters

The effect of DBS depends not only on the area of implantation but also on intrinsic physiological properties and stimulation parameters. The efficiency of DBS mainly depends on three tunable parameters for the trains of pulses: pulse amplitude, pulse width and frequency. These parameters have mostly been discovered by trial and error, and range from 1 to 9 V at frequencies comprised between 130 and 180 Hz for human patients [3]. The values of these parameters vary drastically

depending on the area of stimulation, with the pedunculopontine nucleus (PPN) requiring lower frequencies [14], and the disorder treated. For instance, Mayberg et al reported an amplitude of 4.0 V, a pulse width of 60 μs and a frequency of 130 Hz for depression [9], whereas Stefani et al reported amplitudes of 1.5 to 2.4 V, a pulse width of 90 μs and a frequency of 185 Hz for Parkinson's disease [14]. However, as multiple studies in humans and rats suggested and confirmed [16], frequencies in the kilohertz range would present a decline in tremor reduction. Brocker et al designed an optimized temporal pattern of stimulation, thanks to computational evolution, and demonstrated that using this temporal pattern the frequency could be lowered to 45 Hz [17].

As this work is concentrated on the rat model for the *in vivo* testing, the rest of this section will focus on DBS parameters for rats. A striking observation is that instead of the voltage-controlled DBS used for most human studies, except some exceptions [18], most studies on rats use current-controlled DBS, with varying amplitudes [11], [19]–[25]. Bronstein et al advocated for this technique to reduce energy consumption and improve patient comfort. Indeed, as time progresses, the impedance of the implanted device increases [21], and for current-controlled DBS the voltage would adapt accordingly to maintain the same amount of stimulation (i.e. current), whereas voltage-controlled DBS would require a regular increase of the voltage amplitude to maintain the same amount of current [26], [27].

Two literature reviews, one by Kuncel and Grill [28] and a more recent one by Cogan et al [29], focused on the specific parameters for an efficient and non-damaging DBS. The first remark is that parameters heavily depend on the dimensions of the electrode. A "large" electrode, with a surface ranging from 0.01 cm^2 to 0.5 cm^2, will follow the Shannon equation (1), linking charge density (D) and charge per phase (Q) (the number of charges exchanged during a stimulation phase, typically during one pulse, or one phase of the pulse for biphasic pulses), to adjust its stimulation parameters to prevent tissues damages [29]:

$$\log(D) = k - \log(Q) \quad (1)$$

It was also shown that the current density influenced the level of tissue damages, and that the dimension, macroelectrodes or microelectrodes, would drastically affect that current density damaging threshold. For instance, the first DBS device from Medtronic, with a surface of 0.06 cm^2, was approved by the FDA for a maximum charge density of 30 $\mu C/cm^2$. However, as expected, the Shannon equation does not directly apply on microelectrodes, with typical surfaces ranging from

200 μm^2 to 2000 μm^2. It has been shown that a charge per phase limit of 4 nC per phase (nC/ph) rather than a charge density limit was more suited for microelectrodes. However, it should be noted that the stimulating microelectrode should provide 1-2 nC/ph (charge by stimulation phase, depends on the amplitude and the duration of the pulse) to elicit a neural response. This leads to a stimulation window of 1 to 4 nC/ph when using microelectrodes for DBS. Still, we should avoid according too much significance to both charge density and charge per phase threshold, as the values heavily depend on the disorder treated and the implantation location. For the pulse duration, Kuncel and Grill suggested that DBS should use the shortest possible pulse duration, as it would reduce charge accumulation and might mitigate some side effects [28]. Another fundamental aspect is charge balance: the use of biphasic charge-balanced pulses is recommended for both corrosion and tissue damages concerns. Biphasic charge-balanced pulses are composed of two consecutives phases, a negative phase followed by a positive phase. The waveform of the two phases can differ (symmetrical or asymmetrical pulses) but the amount of charges exchanged during one phase must equal the one exchanged during the other phase. It is unclear to what extent the waveforms affect the tissues, but a sufficiently unbalanced waveform would cause damages. Last but not least, the voltage should always be limited to avoid electrolysis of water, the limits are quantified by measuring the maximum charge-injection capacity, in Coulomb by surface area, which is the maximum amount of charges a material can inject during a phase without provoking the electrolysis of water.

2.2 Neural electrodes

One of the most efficient ways to interact with the human brain is neural electrodes. They provide direct access to the neurons at a cellular level, which allows great results in recording single unit activity of neurons and for electrical stimulation, such as DBS, of a specifically targeted group of neurons in the brain. Neural electrodes, despite being invasive, are the only way to treat some severe cases of Parkinson’s disease in older patients [15]. In this section, we will review the main designs and materials available for microelectrodes.

2.2.1 Conventional electrodes

2.2.1.1 Microwire-based electrodes

The first use of electrodes dates back to the 1940s, when Renshaw performed recordings with metal wire electrodes, using Ag/AgCl electrodes [30]. The first generations only allowed limited recording duration. The 1970s saw the development of new electrodes based on iridium (Ir), platinum (Pt) and platinum-iridium alloys (PtIr). Those microwire-based electrodes were efficient for chronic recording of single unit electrical activity of neurons, but their performances were decaying over time. Rapidly, it was hypothesized that the inflammatory response of the body due to the device's presence in the brain was responsible for the chronic failure of the microelectrodes [31]. Generally speaking, these MWE consist of a conductive material covered with an insulator, except for the tip, with depending length, shape, geometry, diameter according to the researcher's needs. The most relevant challenge currently is to overcome the general failure during long-term implantation [32], along with possible bending during implantation [33].

2.2.1.2 Silicon-based electrodes

In the 1960s, the development of semiconducting materials and micromachining techniques led to the increasing use of silicon (Si). The first Si electrodes were very similar to the microwire-based ones, with a silicon substrate and an exposed tip for stimulation or recording.

In the 1980s, work at the University of Michigan led to the development of the commonly referred to Michigan-style microelectrodes [34]. Their design consists of a planar structure with multiple conductive sites, allowing recording and/or stimulation at different well-controlled depths. Different groups are using them today, mainly because Michigan-style electrodes are commercially available and useful for recording neuronal activities [32].

Another type of electrode was developed in 1991 at the University of Utah [35]. Their design differs mainly by the number of electrodes: while the previously presented designs were of a single microelectrode, the Utah electrode array consists of an array of several microelectrodes, each of them isolated from its neighbors. A slanted version was developed to facilitate the electrical recording or stimulation at various depths [36]. These arrays, while originally designed for stimulation, are the only high-density recording electrodes approved by the US Food and Drugs Agency (FDA) [32].

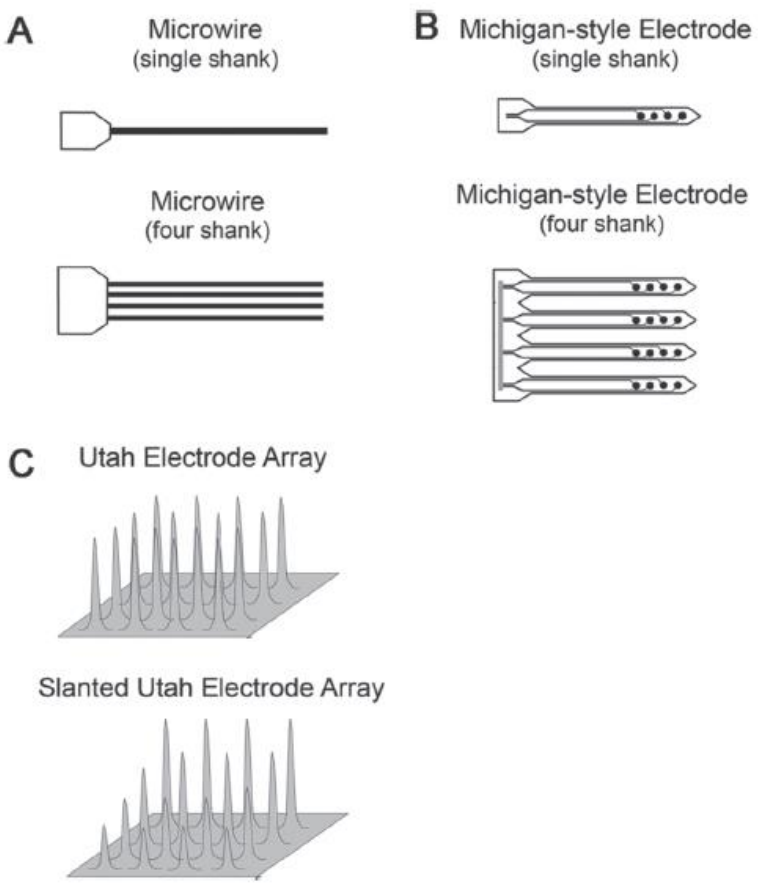

Figure 3: A) microwire-based electrode B) Michigan-style electrode C) Utah-style arrays. Taken from Jorfi et al [32].

For more information about the microelectrodes mentioned here, two reviews on this subject by Jorfi et al [32] and Fattahi et al. [33] are recommended.

2.2.2 Materials

As the variety of designs for electrodes is large, there is also a large choice for materials, not only for the conductive bulk of the electrodes but also for the insulating coating used.

2.2.2.1 Conductive materials

A small number of metals are used for recording and stimulating microelectrodes: platinum, gold, iridium, stainless steel and tungsten [33]. Geddes and Roeder [37] and Wellman et al [38] realized thorough literature reviews about materials for implantable electrodes.

Concerning the biocompatibility, copper and silver were repeatedly reported to be unsatisfactory: they were both found to be cytotoxic. Iron was also found toxic. For the ideal candidates, gold and stainless steel are recommended. Other metals were also found interesting with respect to their biocompatibility such as tungsten, platinum, aluminum. The last one should be avoided because of oxidation. As for alloys, platinum-iridium was found to be a potential candidate.

Along with those biocompatibility considerations, one should consider another relevant parameter for microelectrodes: impedance. The impedance of a system is the ratio of applied voltage to measured current. It is frequency-dependent. The typical model used to describe electrode-solution interaction, known as the Randles model (figure 4), comprises three components: an electrolyte resistance (R_e), a double-layer capacitance (C_{dl}) and a charge-transfer impedance (Z_f). Z_f is divided between the charge-transfer resistance (R_{ct}) and the Warburg impedance (Z_w), which represents the mass transport of electroactive species [39].

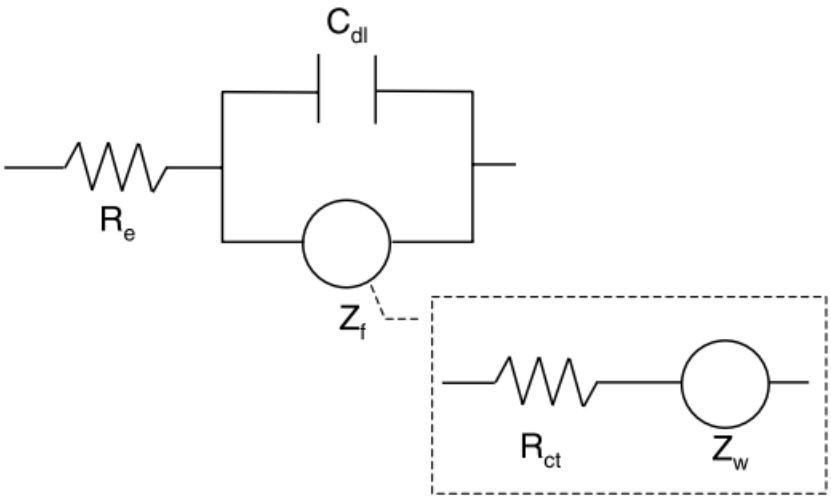

Figure 4: The Randles impedance model for electrode-solution interaction.
Taken from Fernández-Sánchez et al [39].

The Warburg impedances has a real part, its resistances (R), and an imaginary part, its capacitance (C), and it can be described by the following equation (2):

$$(2)\quad Z_w = R - j/(2\pi fC)$$

As the Warburg capacitance increases, the electrode-solution impedance decreases. Knowing this, some studies revealed that the most qualified metals, according to their Warburg capacitance, were: Pt black, PtIr black and PtIr. A Pt electrode is blackened, i.e. covered with finely divided Pt, by

applying a high current density through a sand blasted Pt electrode placed in an HCl solution containing Pt chloride and lead acetate [37]. PtIr is a very interesting alloy because it is characterized by a lower impedance than pure Pt, and is easier to produce than Pt black. A lower impedance is required for most neural applications, as this leads to an easier transfer of charges at the electrode-tissue interface.

Although the use of charge-balanced stimulations reduces the risk of electrode corrosion and damage to the biological tissues, some metals are inherently better suited to withstand corrosion: Pt, Ir, rhodium and palladium [38]. Little corrosion was also found for PtIr electrodes. Tungsten was said previously to be biocompatible but it was reported to suffer from severe corrosion [40], with a corrosion rate as high as 100 μm/year. It was suggested that this was caused by the presence of reactive oxygen species in large quantities near the implanted electrodes [41]. It was also showed that Pt is not only stable against corrosion, but it can also convert the damaging hydrogen peroxide species to water. The reactive oxygen species being heavily involved in the foreign body reaction (see later), this is a very interesting feature [42].

Among all the candidates, the only materials that match both low impedance and high biocompatibility are Pt, PtIr and gold. The PtIr alloy shows good mechanical and electrochemical properties [38]. Clinical neural stimulation devices used today are almost exclusively Pt-based and PtIr-based electrodes [29], [43], [44].

2.2.2.2 Insulating materials

In microwire-based electrodes, except for the tip, the wire is covered by a non-cytotoxic insulator material [33], usually polyimide, Parylene-C or epoxy. Silicon passivation layers have already been reported to degrade *in vivo* due to corrosion [32].

It was reported that polyimide provoked a lesser tissue reaction than epoxy, and Parylene-C reduced greatly the cell attachment on the implanted electrode [45]. Parylene-C and polyimide may also improve the mechanical mismatch between the brain tissue and the conductive material, which is a source of chronic inflammation [33].

It should be noted that polyimide is not the best candidate despite its advantages, because polyimide layers can peel off from the electrode and show signs of cracking as early as 42 days after implantation [40].

2.3 Foreign Body Reaction

The foreign body reaction, also called “reactive gliosis”, glial scar or encapsulation, is a process during which immune cells accumulate near an implanted and non-biodegradable device. The immune cells will form an insulating sheath around it to shield the body from the intruder. This is the main limitation to most long-term implantation in the brain, as the cell sheath leads to an impedance increase over time, blocking the exchange of charges at the interface and diminishing consequently the usefulness of the recording and stimulating devices [21], [46], [47]. The recommended use of current-controlled DBS devices is actually a consequence of the FBR, as the stimulation (i.e. current) is maintained constant for current-controlled devices even when the impedance changes [26]. In this section, we will review the time evolution of the FBR and the cells involved in it. We will then review the main causes believed to generate and maintain the FBR.

2.3.1 Process of encapsulation

Polikov et al [4] and Prodanov et Delbke [42] provided us with complete literature reviews on the response of the brain to chronically implanted devices.

Neurons make up for less than 25% of the brain cells, the majority of the cells are glial (i.e. immune) cells. Astrocytes (figure 5), star-shaped cells, make up for 30 to 65% of these glial cells. After an insertion, or destruction of tissues, these cells become activated or “reactive”, characterized by an enhanced migration and an increased proliferation. A typical way to identify these cells is by immunostaining of glial fibrillary acid protein (GFAP), considered to be a specific marker for astrocytes. The staining can determine the extent of the “reactive gliosis” of the astrocytes and help quantify the degree of inflammation. Microglias (figure 6), another type of glial cells, make up for 5 to 10% of the brain cells. They act as cytotoxic immune cells used to kill intruders. Their shape, ramified in their inactive state, assume a compact form after activation. These immune cells mainly generate chemokines and pro-inflammatory cytokines, recruiting macrophages, immune cells whose role is to phagocytose, i.e. destroy, intruding elements, and other activated microglias. However, microglias also generate cytotoxic and neurotoxic factors, including reactive oxygen species in a process called “respiratory burst”, and reactive nitrogen intermediates, such as nitric oxide.

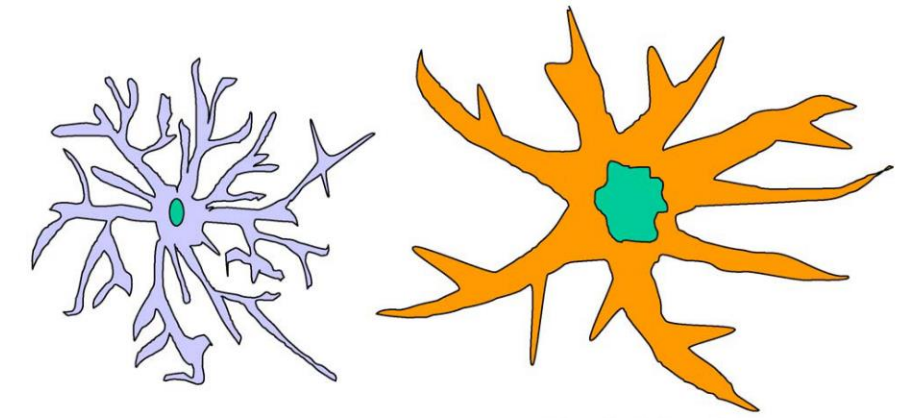

Normal Astrocyte

- 8-10 nm diameter GFAP filaments
- Round nucleus
- 10-40 nm glycogen particles
- Large mitochondria
- Gap junctions with other astrocytes
- Maintain proper neuronal environment
- 30-65% of glial population

Reactive Astrocyte

- Large increase in GFAP filaments, glycogen deposits
- Irregular nucleus
- Increase in mitochondria and multiple Golgi complexes
- Hypertrophy
- Phagocytosis
- Proliferation
- Migration
- Extracellular matrix production
- Production of neurotrophic and inflammatory factors

Figure 5: Astrocytes, brain-native immune cells, in their normal and reactive forms. Taken from Polikov et al [4].

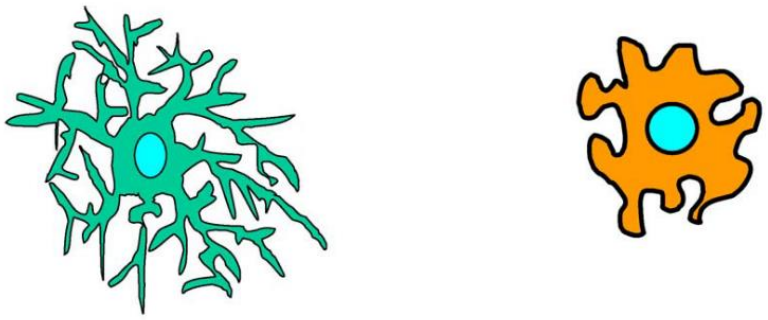

Resting or Ramified Microglia

- No Fc receptors, no macrophage specific receptors
- Large, dense chromatin masses in small flattened nucleus
- 5-10% of glial population
- Many long, thin processes

Activated or Amoeboid Microglia

- Upregulation of lytic enzymes
- Retraction of cytoplasmic processes to stouter, thicker pseudopodia
- Accumulation of phagocytosed material and lipid droplets
- Ameboid and motile abilities
- Release of inflammatory factors MHC I, II expression
- Active Proliferation

Figure 6: Microglias, brain-native immune cells, in their resting and activate forms. Taken from Polikov et al [4].

Upon insertion of the device and destruction of tissues, the acute phase of the FBR starts. After 1 day, a proliferation of activated microglias can already be observed near the implant. Szarowski et al showed that this acute phase heavily depends on the size, geometry and roughness of the device, but they found that there was a following phase, independent from these parameters and from the early reactive response [48]. Indeed, if the presence of the implant persists, a chronic phase, characterized by the presence of reactive astrocytes (i.e. glial scar) and activated microglias, will begin. After their initial accumulation around the implant, the microglias will attempt to phagocytose the intruding device. If the destruction of the device proves impossible, microglias will cluster and form a tissue sheath after 2 weeks and remain present until removal of the device. This resembles the fusion of macrophages into giant multi-nucleated cells during chronic inflammation in the rest of the body. Reactive astrocytes actually form most of this tissue sheath in the brain. Turner et al observed after 2 weeks a massive presence of activated astrocytes, and the formation of the sheath was believed to be complete as early as 6 weeks, as the removal of implanted devices did not result in a collapse of the tissues around the scar (figure 7) [49]. The presence of meningeal fibroblasts that are crucial to the production of the extracellular matrix, has also been reported in the sheath. The reasons behind the formation of this sheath are still under debate, but they all rely on the idea that the encapsulation role is to shield the tissues. Turner et al qualified the sheath as "formidable" after 6 weeks of implantation [49]. The encapsulation does not only obstruct the exchange of charges, but it also pushes the neurons away from the device. Indeed, Biran et al suggested that most of the neuronal loss was associated with the foreign body reaction and the "frustrated phagocytosis" rather than with the initial insertion wound [50]. The "frustrated phagocytosis" (inability for the immune cells to remove the foreign body) leads to a state of persistent release of toxic factors by the microglias, resulting in a "kill zone" or neuronal gap reaching as far as 100 μm away from the device. This phenomena further reduces the efficiency of the implanted devices.

Polikov et al [4] summed up the FBR process as follows:

"The acute phase is a 1–3- week long process in which microglia play a dominant role in response to the insertion trauma. It is unclear how the intensity of the acute response affects subsequent events, which involve both reactive astrocytes and chronically activated microglia. The astrocytic response begins at the time of insertion and is generally completed by 6–8 weeks post-implantation with the development of an encapsulating glial scar. Neuron viability clearly decreases following

device insertion, but the question remains whether the neurons that survive the acute reaction and remain in proximity of the chronic foreign body response remain electrically active or viable in the presence of persistent inflammation. The astrocytic scar remodels nearby tissue, thus further separating neurons from the recording electrodes, and possibly increasing electrode impedance."

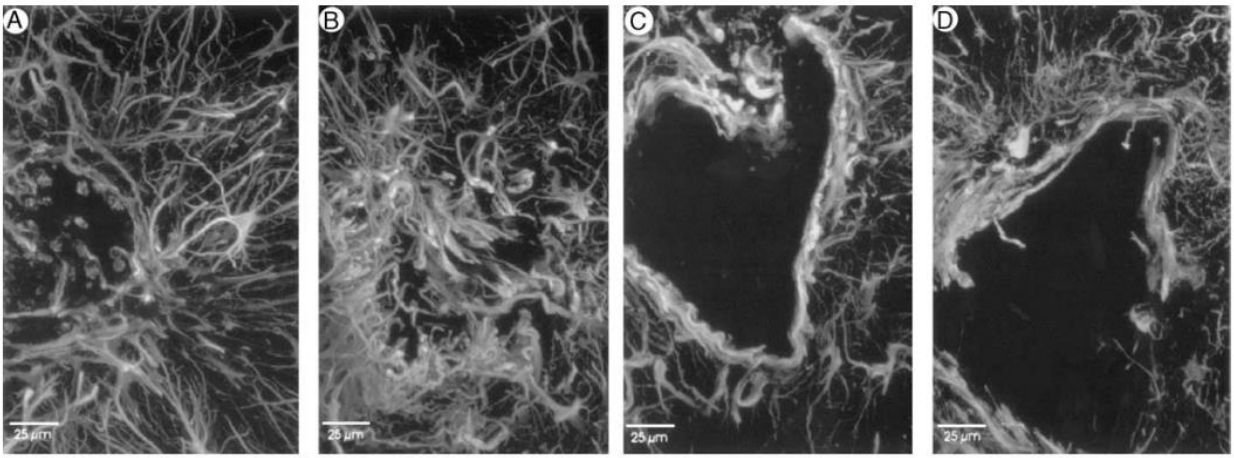

Figure 7: Sheath resulting from chronic implantation of electrodes in brain after extraction of the electrodes at different time periods.
Taken from Turner et al [49].

2.3.2 Causes of the FBR

Besides the evident trauma created by the insertion of a device, several studies proposed hypothesis on how the chronic inflammation begins and is maintained throughout the implantation period.

Woolley et al provided evidence that the infiltration of non-brain cells during insertion contributed substantially to the beginning chronic phase [51]. The disruption of the blood-brain barrier (BBB), allowing non-brain cells to penetrate the brain, is indeed a recurrent theory. It was shown that chronically implanted electrodes demonstrated an inverse correlation between performances and BBB disruption [52]. For the poorly functioning electrodes, the BBB disruption had led to the infiltration of pro-inflammatory myeloid cells, thus initiating the chronic phase. These results were confirmed by another study, as the failures of their arrays were linked to a larger BBB disruption [53]. These results strongly suggest that arrays are far from ideals as they generate much more BBB leakiness than single electrodes, and even create cavities [53]. As suggested by Biran et al [50], the small pro-inflammatory molecules released by the immune cells from the sheath are believed to be

the main cause of destruction following the initial insertion. Further proof was provided when electrodes coated with a thick sodium alginate hydrogel layer managed to significantly reduce the FBR [54]. It was hypothesized that the hydrogel layer acted as a diffusion sink for the pro-inflammatory molecules, reducing their concentration at the biotic-abiotic frontier. These findings indicate that the chronic phase is mostly independent of the initial insertion and depends more on the infiltration of external cells and the following production of toxic substances (figure 8).

The mechanical mismatch between the tissue and the electrode is believed to be the main reason for prolonging the FBR, as vibrations of the electrode lead to more vascular damages and more BBB disruption [42]. Lind et al showed that the density was also a plausible reason for the sustained reactive response [55], as their low-density probes approached no reaction at all. However, increasing the softness of the implanted material is still relevant, as shown by the reduced inflammatory response observed when implanting ultrasoft electrodes consisting of elastomers and conducting polymers [56]. The electrodes consisted of an extruded blend of poly(3,4-ethylenedioxithiophene)-polyethylene glycol (PEDOT-PEG) and polydimethylsiloxane (PDMS), sputtered with gold and insulted by a 5-µm-thick layer of fluorosilicone.

To sum up, the FBR most likely originate from non-brain immune cells leaking through the disrupted BBB. These cells generate pro-inflammatory molecules that destroy tissues and neurons and activate the glial cells, which generate more pro-inflammatory molecules, which leads to further activation of immune cells. This loop is sustained by mechanical and density mismatch between the tissues and the device that regularly provokes more vascular damages and BBB disruption due to vibrations.

However, a long-term study on primates using microelectrode arrays showed that most failures came before reaching one year *in vivo* and that the main reason was the abrupt mechanical failure (48%) rather than observable biological failure (24%) [57]. This result should remind us that even if the FBR remains a relevant problem, other causes of failure should not be ignored.

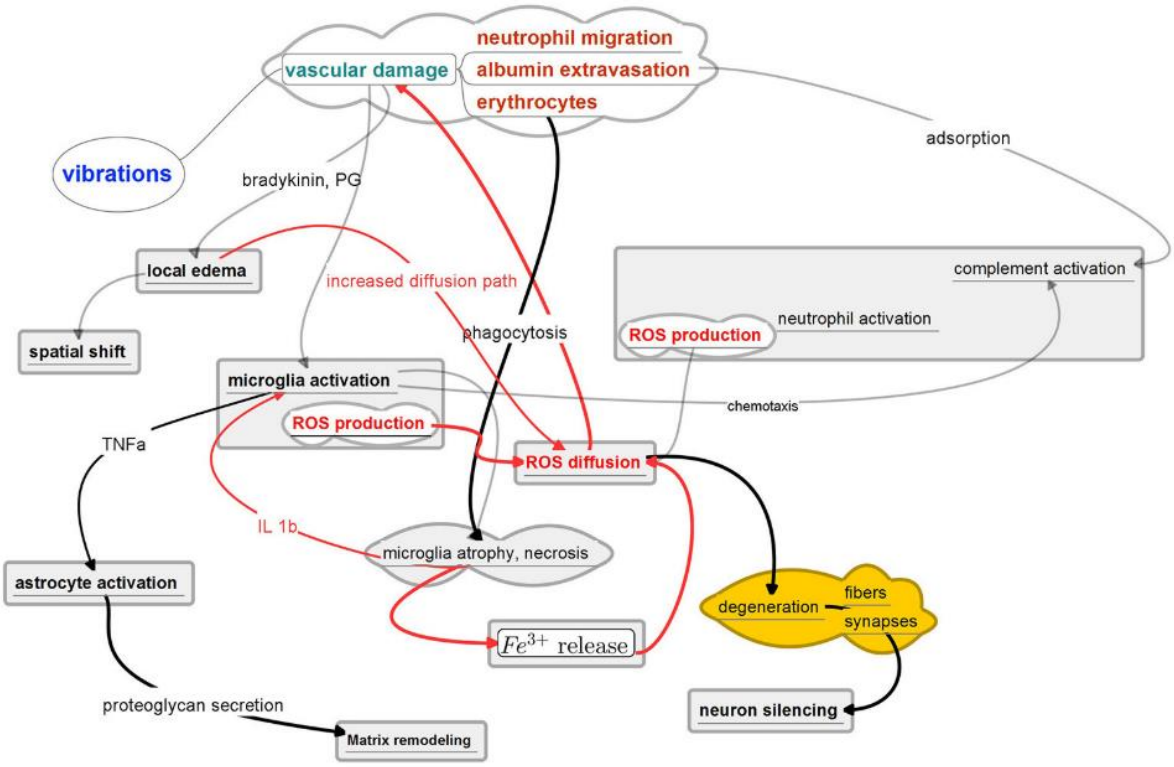

Figure 8: The complex feedback loop mechanisms occurring during the FBR.
Taken from Prodanov & Delbeke [42].

2.4 Conducting polymers

Discovered in the 70s, conducting polymers (CP) revolutionized many fields that includes bioelectronic medicine. Numerous CPs exists, such as polythiophene and its main derivative poly(3,4-ethylenedioxithiophene), polyaniline and polypyrrole (PPy). In this section, we explain how CPs differ from traditional insulating polymers and we will review the main interests of using the most common CP, PEDOT, for neural electrodes.

2.4.1 Electron transport in conducting polymers

CPs are able to conduct electronic charges. This peculiar feature, which distinguishes them from the traditional polymers, is due to their π-conjugated backbone. However, the conductivity of CPs remains very low compared to that of metals and doped semiconductors. High conductivity is achieved via chemical doping. In the following subsections, detailed descriptions of π-conjugation and chemical doping will be presented.

2.4.1.1 π-conjugated structure

A π-conjugated structure is a structure with alternating single and double bonds (figure 9). The first discovered and simplest CP is polyethylene, which consists of alternating single and double bonds. This π-conjugated structure features strongly localized σ-bond and less strongly localized π-bonds, with single bonds containing a σ-bond and double bonds containing both a σ-bond and a π-bond. The overlapping of the p-orbitals of the π-bonds allows the electrons to be delocalized and to move freely between the atoms [58]. Still, as mentioned before, the conductivity remains really low, around 10^{-9} $(\Omega.cm)^{-1}$ for cis-polyacetylene and 10^{-5} $(\Omega.cm)^{-1}$ for trans-polyacetylene.

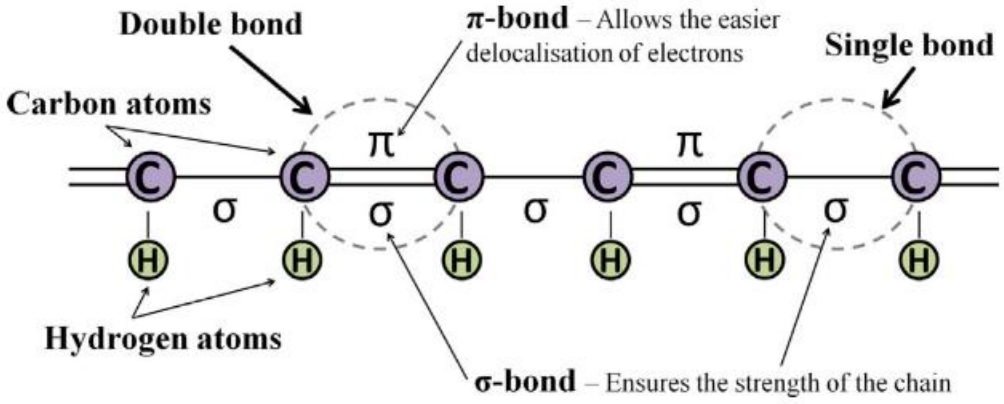

Figure 9: The simple π-conjugated system of polyacetylene.
Taken from Balint et al [58].

2.4.1.2 Doping mechanism

To increase the conductivity, ions, usually anions, are incorporated into the polymer matrix. Despite this process being called "doping", it is actually a redox reaction, unlike doping of inorganic semiconductors. The incorporation of the dopant, or counterion, leads to the oxidation or the reduction of the neutral polymeric chain. The resulting ionic complex will be neutral, with a polymeric cation balanced by anions or a polymeric anion balanced by cations. This ionization of the CP backbone is favored by the weakness of the π bond, from which electrons can be easily removed. The conductivity of polyacetylene increases from 10^{-5} $(\Omega.cm)^{-1}$ to 10^{3} $(\Omega.cm)^{-1}$ after exposure to oxidizing agents. This process introduces new charge carriers into the polymer backbone by removing electrons and generating localized charges (figure 10, A and B) [58]. These

localized charges coupled with lattice distortions are named polarons and act as effective charge carriers (figure 10, C and D) [59].

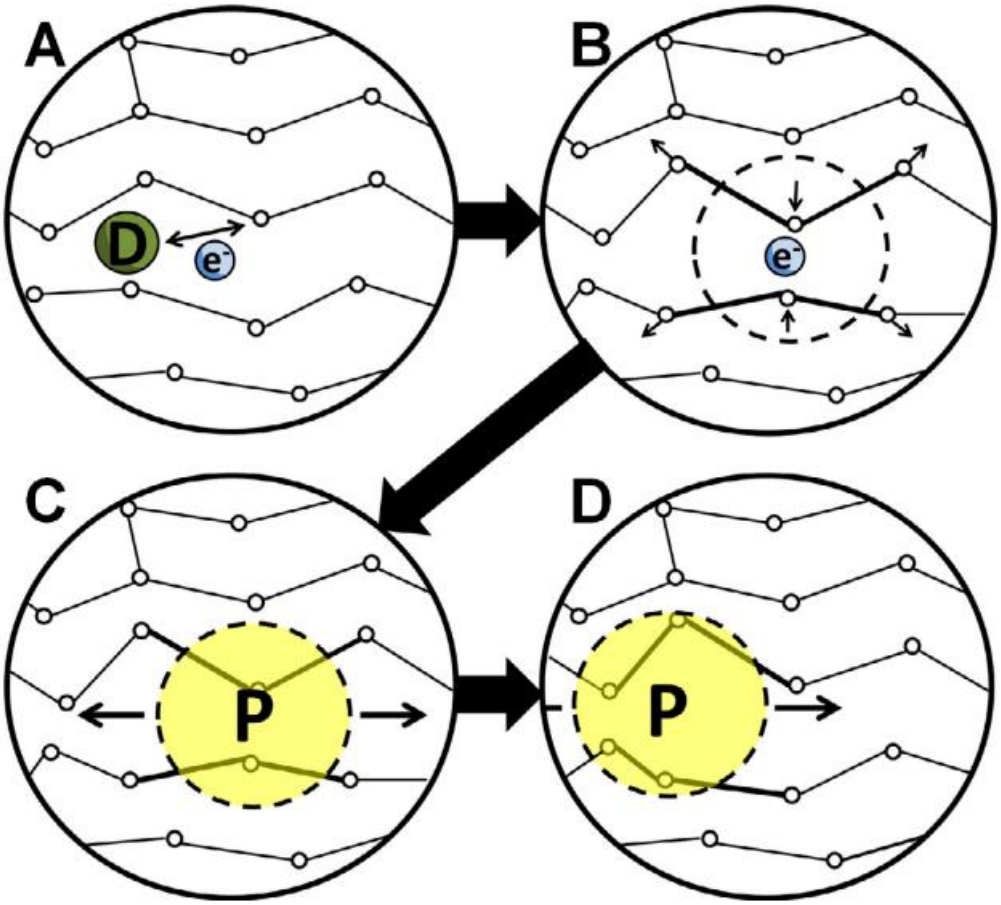

Figure 10: A) Doping mechanism: oxidation or reduction of the polymer backbone, B) Charge carrier coupled with a lattice distortion, C) Polaron acting as an effective charge carrier and D) Travelling polaron.

Taken from Balint et al [58].

A wide variety of dopant exists for PEDOT: large dopants, such as the polymer PSS^-, and small dopants, such as BF_4^-, ClO_4^-, PF_6^-. The ionic complex obtained is usually written PEDOT:dopant. Despite acting similarly as oxidizing agents, these two families of dopant act very differently during dedoping. For instance, PEDOT in PEDOT:PSS is actually incorporated into the matrix of PSS^-. Upon the application of a negative potential that forces the oxidized PEDOT to go back to its original neutral state, the fact that PSS^- cannot move requires cations from the solution to move inside the PEDOT:PSS matrix to balance the remaining negative charge of PSS^-. For smaller

anionic dopants, the application of the negative bias will force the oxidized PEDOT form to go back to initial neutral state, but this time instead of attracting cations, the polymer matrix will likely expulse some of the anionic dopants out of the polymer matrix to maintain its neutrality. In the first case, external cations penetrate the matrix and in the second case, some internal anions, the dopants, leave the matrix.

The doping/dedoping mechanism of CPs is extremely relevant for neural recording and stimulation. Indeed, as explained earlier, biosignals are generated due to ionic movements that polarize or depolarize the cell membrane. The ionic currents in living systems will affect the doping level of PEDOT, thus modulating the amount of current PEDOT can conduct. In a reverse mechanism, the application of a potential bias to doped PEDOT will generate ionic movements similar to the biosignals existing in our body. PEDOT has the ability to transduce electronic into ionic biological signals and to transduce ionic movements into electronic current.

Faradaic behaviors, involving electron transfer through redox processes, are usually avoided for stimulation, as the faradaic reaction for metals electrodes results in corrosion or electrolysis of water [60]. Capacitive behaviors are thus more welcomed despite their limited impact on the ion concentration in the body as they generate weaker ion movements. However, due to its porous morphology and its ability to incorporate ions, PEDOT allows rapid ionic movement in and out of the polymer matrix and access the entire volume instead of just the interface. PEDOT-based coatings for neural electrodes are considered volumetric capacitors, which consists of an accumulation of charges, ions from the solution, in an entire volume using faradaic processes (reduction or oxidation of the PEDOT backbone), compared to the double-layer capacitance of bare metals [8]. PEDOT has a volumetric capacitive behavior that can generate large ion movement, with harmless reversible redox processes, making it an ideal candidate for biotic-abiotic interfaces.

2.4.2 PEDOT coatings for neural electrodes

Besides their conductivity, CPs have other relevant properties as coatings for neural electrodes, such as biocompatibility and enhanced electrochemical properties. An increasing amount of research has been spent into CP-based neural devices, as shown by the number of recent literature reviews mentioning CPs as interesting candidates for implantable devices [1], [5], [8], [32], [58], [61]–[64].

Amongst the CP candidates for neural interfaces, PEDOT and PPy stand out. PPy is the most thoroughly investigated CP [63]. However, despite its proven biocompatibility [58], PPy suffers from poor electrochemical properties and rapid degradation. As early as 1995, Yamato et al observed a loss of 95% of electrochemical activity for their PPy:PSS films after 16 hours of polarization at 400 mV, whereas PEDOT:PSS retained 89% of its initial electrochemical activity [65]. Indeed, PPy is very unstable in aqueous solution and therefore a steady shift towards PEDOT has been observed over the years. PEDOT possesses a dioxyethylene bridging group on the 3- and 4-positions of its hetero-rings which prevents undesired couplings. This leads to the much needed superior electrochemical stability of PEDOT in aqueous environments [66]. PEDOT is nowadays considered to be the most electrochemically stable CP with interesting electrochemical properties.

We will detail in this subsection the useful properties of PEDOT for neural electrodes, as well as their applications in a biomedical context.

2.4.2.1 Improved electrochemical properties

It has been demonstrated that CPs coatings lead to an enhancement of the electrochemical properties of neural electrodes. The two main electrochemical characteristics to observe for neural electrodes are impedance, measured through electrochemical impedance spectroscopy (EIS), and charge storage capacity (CSC), measured through cyclic voltammetry (CV) [67]. The impedance is a frequency-dependent measurement representing the ease, for low impedance, or the difficulty, for high impedance, in charge transfer at the interface with the electrode. During EIS, impedance is usually measured by sweeping the frequency of an input signal, ranging from 1 Hz to 10^5 Hz. Recording electrodes are characterized by their impedance at 1 kHz. For both recording and stimulating electrodes, a low impedance is preferred as it reduces the voltage. This lower voltage will reduce power consumption and prevent damages to the biological tissues and the electrodes. Cyclic voltammetry is a three-electrode measurement during which a potential is cyclically swept across a potential widow, with respect to a reference electrode, at the working electrode of interest, and the current flowing between this working electrode and a counter-electrode is recorded. The CSC, which is the time integral of the cathodic current, can be extracted from the CV. The CSC is an indication of the amount of charges available for stimulation. A high CSC is preferable for stimulating electrodes.

Metals microelectrodes are characterized by small dimensions, as they are required to stimulate and record a small population of neurons. However, the unfortunate consequences of these small dimensions are a high impedance and a low CSC. A lot of work has already been done on increasing the exposed area of microelectrodes, like roughening, but there are limits to these physical modifications. This is where CPs come in handy, as CPs coatings can effectively reduce the impedance and increase the CSC of bare metal microelectrodes. Since the groundbreaking work of Cui and Martin [68], whose electrochemically deposited PEDOT:PSS coatings reduced by two orders of magnitude the impedance of recording electrodes *in vitro*, a lot of research has been conducted to efficiently use PEDOT as coatings for recording and stimulating electrodes. Similar results were obtained using perchlorate (ClO_4) as a dopant instead of PSS^- for ordered surfactant-templated PEDOT [69]. This method was refined to coat Michigan probes with PEDOT:ClO_4 and it was found that PEDOT-coated sites outperformed the uncoated ones for recording purposes [70]. However the typical encapsulation of long-term implantation limited the prospects of these results. Cui & Zhou followed the initial work made on PEDOT:PSS and deposited it on Pt, this time for stimulation purposes [71]. They showed that the PEDOT coatings were stable and effectively decreased the impedance and improved the CSC, leading to lower voltages for PEDOT-coated electrodes during *in vitro* stimulations. Following this work, it was demonstrated that PEDOT:PSS had better electrochemical properties and a better stability when confronted to high current density stimulation than iridium-oxide (IrOx), another candidate for neural electrodes [72]. The better performances of PEDOT:PSS with respect to IrOx and PtIr were later confirmed [73]. It was also found that PEDOT:PSS was stable under stimulation conditions *in vitro* for 24 hours, and it was suggested that the degradation mechanism was more linked to accelerated aging at high temperature than stimulation. Finally, PEDOT-coated PtIr arrays were confronted to *in vivo* testing in rats and signal-to-noise ratio was improved during recording and lower voltages were necessary during stimulation. PEDOT:pTS was electrodeposited on Pt electrodes [74]. As expected, the coatings reduced the impedance by two orders of magnitude and by 85% the maximum voltage recorded for biphasic pulses *in vitro*. However, this reduction decreased to 45% *in vivo.* Accelerated electrical aging *in vitro* for 16 days did not seem to drastically affect PEDOT:pTS. The use of carbon nanotubes (CNTs) coupled with CPs was also explored to further enhance the electrochemical properties of the neural electrodes, as CNTs and CPs are two ways of increasing the active area of the electrode [75]. I reported that PEDOT-CNT was able to sustain millions of

pulses *in vitro* without significant degradation. A study confirmed the usefulness of PEDOT-CNT coatings, as they were able to function *in vivo* for 14 days [44]. Another study using PEDOT-CNT showed that they were better suited for stimulation of retinal interneurons than titanium nitride (TiN), as the voltage required for constant current stimulation was lower. More recently, PEDOT:PSS was again reported to drastically reduce the impedance and increase the charge storage capacity, as PEDOT-coated electrodes were able to record neuronal activity with a quality at least comparable to uncoated ones [76]. An immediate and extremely relevant implication of this reduction of voltage amplitude during stimulation is the reduced power consumption, which could significantly improve the battery's life-span of DBS devices. For instance, Ganji et al calculated a power consumption 88% lower for their PEDOT:PSS/Pt electrodes and 67% lower for their PEDOT:PSS/Au electrodes with respect to Pt and Au electrodes [77].

A striking observation is that despite some early experiments with perchlorate, the vast majority of PEDOT coatings for neural electrodes use PSS^- as dopant. However, Mandal et al demonstrated that other smaller dopants, such as tetrafluoroborate (BF_4^-), provide better electrochemical properties *in vitro* and *in vivo* for both recording [78] and stimulation purposes [79]. Another noticeable point is that despite some occasional short-term experiments *in vivo*, no long-term implantation studies were done. This is an important gap, as the main source of degradation, the FBR, only stabilizes around 6 weeks after implantation.

2.4.2.2 Biocompatibility

The enhancement of electrochemical properties using CP coatings are undeniable. However, these improvements will be mitigated if the FBR remains strong. In the worst case scenario, the use of CPs could even increase the degree of inflammation if they prove to be cytotoxic. Fortunately, it is expected that PEDOT actually reduces the FBR.

The biocompatibility of PEDOT has been recurrently studied *in vitro*. Yang et al showed that their ordered surfactant-templated PEDOT supported SH-SY5Y human neuroblastoma adhesion and neurite extension *in vitro* [69]. It was observed that PEDOT:ClO_4 electrodeposited on stainless steel did not show any sign of cytotoxicity for Hep-2 cells and also presented signs of increased electroactivity when covered by a monolayer of Hep-2 cells [80]. A claim was also made that PEDOT:PBS and PEDOT:PSS coatings were not cytotoxic to mouse myocytes [81]. Given the fact that PBS is biocompatible, it could be deduced that PEDOT is not cytotoxic to this line of cells.

However, despite that PSS^- did not show direct cytotoxicity, it is still possible that it has indirect effects on cellular adhesion and proliferation. Mouse fibroblasts L929 and SH-SY5Y cells were exposed to PEDOT:PSS, and their results pointed strongly toward non-toxicity [82]. Moreover, their PEDOT implants doped with a biomolecule, heparin, did not reveal differences in biological response compared to Pt controls. Green et al observed that electrical stimulation parameters, rather than toxic leachants or PEDOT degradation, were responsible for PC12 cells retarded growth on electrodes [6]. Besides, they suggested that PEDOT:PSS and PEDOT:pTS may lead to an improvement in cell responses because of the lower voltage drop compared to uncoated electrodes for the same applied current. A study, using tetrafluoroborate (TFB) as dopant instead of PSS^-, demonstrated *in vitro* that PEDOT:TFP coatings were not neurotoxic and did not induce any significant inhibition of neuronal activity [78]. A smaller kill zone was observed when using PEDOT-CNT-coated electrodes, with the amount of neuronal death being halved, most likely due to the lower voltage experienced by the tissues around the coated electrodes [44]. Recently, it was observed that SH-SY5Y cells spread homogeneously and proliferated quickly *in vitro* on PEDOT:PSS-coated electrodes, in accordance with previous reports [76]. Good adhesion and viability of fibroblasts cells was also observed on PEDOT:PSS/Pt and PEDOT:PSS/glassy carbon electrodes, in accordance with the preceding findings [83].

The reduction of the voltage drop during current-controlled stimulation seems to be a possible reason for the reduced FBR observed during stimulation tests for PEDOT-coated neural electrodes. Besides, the mechanical mismatch has been proven to be an important factor in the chronic FBR, and PEDOT, like most polymer, is a soft material. Luo et al combined ultrasmooth and thin substrates with PEDOT coatings and observed almost no inflammatory reaction *in vivo* [84]. Despite accumulating evidence about PEDOT biocompatibility *in vitro*, there is a clear lack of long-term implantation studies *in vivo* to confirm these findings, as cell culture differs dramatically from the fluctuating and variously populated tissues of the brain.

2.4.2.3 Adhesion

A recurrent problem of PEDOT coatings is their poor adhesion to inorganic substrates.

Indeed, early experiments from Cui and Zhou showed that cracks would appear during stimulation for thick PEDOT:PSS coatings, eventually leading to delamination [71]. It was later confirmed that PEDOT:PSS was prone to delamination under stimulation conditions, and also that steam

sterilization partially delaminates PEDOT:PSS coatings [6]. In a following study, it was shown that PEDOT:pTS, despite being stable under steam sterilization, displayed cracks following ethylene oxide (ETO) sterilization [74]. The nature of the substrate influenced the adhesion, as PEDOT:PSS on glassy carbon was able to sustain consequent stimulation whereas PEDOT:PSS on Pt began to delaminate fairly quickly [83]. On another side, a strong mechanical stress, such as sonication, led to delamination in a few minutes on gold electrodes [85]. Even more dramatic results were observed as PEDOT:PSS films fell from indium tin oxide (ITO) in 5 seconds [86].

Several methods have been found to promote the adhesion of electrodeposited PEDOT on inorganic substrates. A simple but efficient way to increase the adhesion of PEDOT is to roughen the substrate. Pranti et al used iodine etching on gold electrodes and showed that PEDOT:PSS on iodine-etched gold was able to resist 11 minutes of sonication [85]. More complex methods have also been explored. Povlich et al synthesized an EDOT monomer functionalized with a –COOH group, called EDOTacid [87]. This EDOT-acid was electrochemically co-polymerized with EDOT on gold-palladium and gold with a 1:1 ratio. In a later study, Wei et al used the same EDOT-acid to increase the adhesion of PEDOT. ITO substrates were dipped into an ethanol solution of EDOTacid for 12 hours to ensure the formation of a dense monolayer of EDOTacid. PEDOT:ClO_4 was then electropolymerized on the EDOT moieties of the EDOTacid monolayer. The PEDOT-EDOTacid films were able to withstand 2 minutes of sonication without delamination whereas PEDOT films delaminated before 5 seconds [88]. This indicates that the strong interactions between the EDOTacid monolayer and ITO makes it an ideal candidate as an anchoring layer for PEDOT. The same group developed another method afterwards: Ouyang et al produced an EDOT derivative, EDOT-NH_2, to build an anchoring layer for PEDOT [86]. PEDOT-NH_2 was electrografted on ITO thanks to its amine moieties, forming a covalently-bound layer. In a following step, PEDOT was electrodeposited on the EDOT moieties of PEDOT-NH_2. The resulting polymer layer was able to remain relatively intact after 1 hour of sonication.

Electrografting of amine moieties was also explored in this study. In our previous work, we functionalized a diazonium salt (DS) with a thiophene group [7]. A DS layer was electrodeposited on Pt disks and PtIr microelectrodes, on which PEDOT:BF_4 was later electrodeposited. Electropolymerization of PEDOT was made possible by the thiophene groups exposed on the surface of the DS layer. The covalent bonds created between the DS and the metal surfaces, during the reduction of the amine moieties of the DS, allowed the DS-PEDOT layer to remain strongly

attached on our Pt and PtIr substrates for 10 minutes under sonication conditions whereas PEDOT without the DS anchoring layer delaminated after 10 seconds.

2.5 Processing of PEDOT

One of the many advantages of CPs over other materials for electronics is the variety of methods and ease for processing. In this section, a brief justification of our choice for the deposition method will be provided, followed by a more detailed subsection about this method: electropolymerization.

2.5.1 Choice of deposition method for PEDOT

Chemical deposition is the main method to polymerize PEDOT on most substrates for diverse applications, such as organic transistors or organic light-emitting diodes, and can be used for large scale production [63]. We will not go into details about this method as we did not use it. However, we will justify why electropolymerization was chosen over chemical deposition.

As reported by numerous publications, electropolymerization is the main deposition method for specific applications such as neural electrodes. Neural electrodes are made of conductive materials because of their applications, and this renders them eligible for electropolymerization, which is not the case for most organic substrates used in other applications of organic electronics. Electropolymerization allows precise control over thickness and doping level, and therefore on conductivity [63]. Besides, the targeted area for deposition is usually small for neural electrodes and would require high manipulation skills for a successful chemical deposition on such small targets, whereas in electropolymerization it only requires to have the targeted area inside an electrolytic solution. This last observation combined with the fact that electropolymerization is a one-step procedure, as it does not need post-chemical processing to reach high conductivity [62], gives the advantage of the ease of synthesis to electropolymerization [61].

2.5.2 Electropolymerization of PEDOT

In this subsection, we will describe the principles of electropolymerization, the application in the case of PEDOT and the influence of the several parameters on the obtained PEDOT coatings.

2.5.2.1 Principles of electropolymerization

Electropolymerization is a polymerization method involving electrochemical reactions. It is realized in a cell containing three electrodes immersed in an electrolytic solution: a working electrode, on which the polymerization takes place, a reference electrode, whose fixed potential is used as a reference for the potential measured/applied at the working electrode, and a counter-electrode that collects the current coming from the working electrode. The solution filling the cell contains the monomer and an electrolyte, needed to transport the charges and provide the doping ions. Upon application of a potential bias at the working electrode, the monomers are activated and become activated monomers or radical ions. These radicals will react together to form oligomers. The oligomers will continue to evolve towards insoluble polymer chains that will physically adsorb on the working electrode surface. Continuing the process will increase the amount of polymerized material until the potential bias is stopped or the dissolved monomers are all consumed.

Three main methods are possible for electropolymerization [89]. Potentiostatic (PS) deposition consists of the application of a constant potential for a specified amount of time. Galvanostatic (GS) deposition consists of the application of a constant current for a specified amount of time. Finally, potentiodynamic (PD) deposition consists in cyclically sweeping the potential across a potential window. In this case, the amount of material deposited is controlled by the number of cycles.

2.5.2.2 Electropolymerization of PEDOT

Upon reaching a specific positive potential, dependant on several parameters such as the solvent used, monomer and electrolyte concentrations, EDOT monomers are oxidized at the working electrode (figure 11, (1)). The resulting lone electron on the oxidized EDOT will form a covalent bond with another lone electron from another EDOT radical in the vicinity of the working electrode to create a dimer (figure 11, (2)). Protons will be scavenged from the dimer to allow the replication of the first steps any number of times (figure 11, (3)) [90]. After several repetition, an insoluble PEDOT oligomer is formed. When an area becomes saturated with oligomers, they start to cluster on the working electrode's surface, generating PEDOT nuclei. During the following step, nucleation continues with new nuclei being formed, coupled with the growth of the initial nuclei. At some point, the nuclei fuse together to form the final PEDOT coating [89]. The final roughness of the PEDOT coating depends mainly on the length of the precipitated PEDOT oligomers, with

longer polymeric chains leading to smoother films, but also on the large variety of other parameters that will be described in the following subsection.

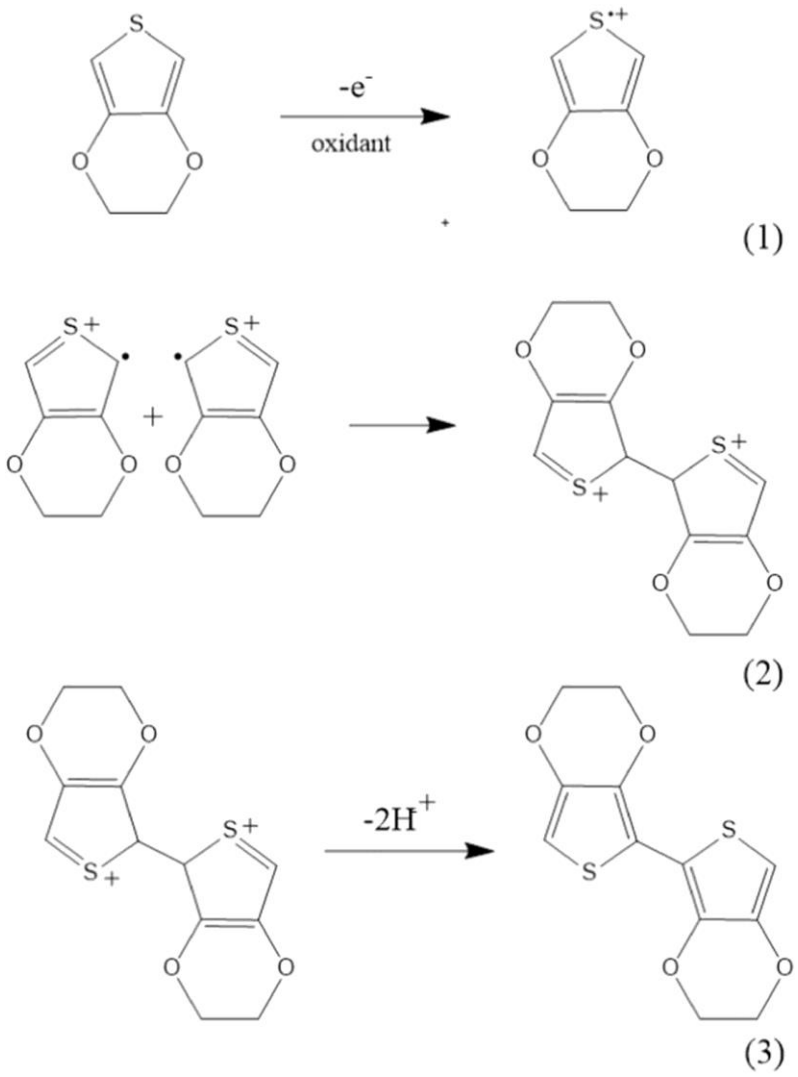

Figure 11: PEDOT polymerization consists of three main steps: (1) oxidation of EDOT, activation of the monomer, (2) EDOT radicals coupling, generation of a PEDOT dimer and (3) deprotonation of the dimer that reforms the π-conjugated structure and allows further polymerization.

Taken from Ismail et al [90].

2.5.2.3 Influence of the parameters

PEDOT's characteristics such as morphology, stiffness, porosity, conductivity, impedance will be heavily influenced by the process of deposition. In the case of electropolymerization, several parameters come into play: electropolymerization technique, solvent, dopant and substrate nature.

The influence of lithium salts dopants for PEDOT electrodeposited galvanostatically on Pt was studied [91]. It was found that the use of very large anion $N(SO_2C_2F_5)_2^-$ gave a compact morphology to the PEDOT film, whereas small anions resulted into a porous structure. These results were confirmed, when a team of researcher electrodeposited PEDOT from aqueous solutions containing different dopant: Cl^-, NO_3^- and PSS^-, on ITO. They also electrodeposited PEDOT:BF_4 from an ACN solution on the same material [92]. The water-processed films had varying morphologies depending on the size of the dopant: PEDOT:Cl possessed an open and loose structure, PEDOT:NO_3 a dense morphology and PEDOT:PSS had an even more compact appearance. On the other hand, ACN-processed PEDOT:BF_4 had a porous and honeycomb-like structure, significantly distinct from the water-processed films. A thorough study of PEDOT:PSS, PEDOT:pTS and PEDOT:ClO_4 galvanostatically deposited from a 50% v/v mixture of acetonitrile and deionized water on Pt and roughened Pt was realized [6]. PEDOT:PSS appeared to be much smoother than the others. However, PEDOT:PSS suffered partial delamination during steam sterilization. PEDOT:PSS also experienced a high loss in electroactivity during accelerated aging in PBS, whereas PEDOT:pTS remained stable and PEDOT:ClO_4 saw an improvement of its electrical properties. During electrical stimulation tests *in vitro*, only PEDOT:PSS delaminated from roughened Pt, with even some materials loss on passive control electrodes. It was observed that the use of PSS^- as a dopant led to an elastic modulus twice higher for PEDOT:PSS films than for the ones doped with the small anion ClO_4 [93]. PEDOT films doped with large anions are smoother but more brittle, and possessed less interesting impedances and CSCs due to their lack of porosity. However, the relative change in stiffness, despite increasing the risks of delamination, did not affect the biocompatibility as both films doped with large and small dopants displayed much higher elastic moduli than the biological tissues. As reported in two studies comparing PSS^- and BF_4^-, PEDOT:PSS provides with less favorable electrochemical properties, such as higher impedance, lower CSC and higher voltage measured during stimulation, than its counter-part PEDOT:BF_4 for neural recording and stimulation purposes [78], [79].

Poverenov et al electrodeposited PEDOT using different dopants ($LiBF_4$, $LiClO_4$, $TBABF_4$, $TBAClO_4$), with PD and PS depositions, in two different solvents: ACN and PC, on ITO [94]. They concluded that their dopant did not influence PEDOT's morphology significantly. While ACN-processed films exhibited a rough and bumpy surface with star-shaped patterns, PC provided a much smoother structure. It was also found that films prepared in PD conditions were rougher than those prepared in PS conditions. They hypothesized that the difference in solubility of PEDOT oligomers, lower in ACN, led to a higher number of terminated short oligomers on the substrate surface, increasing the roughness. Another study compared PEDOT films deposited in water and acetonitrile [95]. Water-processed PEDOT:PSS showed a cauliflower-like compact structure, whereas acetonitrile-processed PEDOT:ClO_4 showed a porous complex morphology. With respect to electrochemical properties, PEDOT:ClO_4 had a lower impedance than PEDOT:PSS. This is most likely due to the higher doping level provided by small anions such as perchlorate, as well as the porous structure provided by organic solvents that increases the electroactive surface. The authors hypothesized that the solubility of PEDOT oligomers at the initial stages might be responsible for the differences in morphology. However, they also invoked that the higher dielectric constant of water may lead to a slower deposition rate and thus a more uniform and compact film. PEDOT:ClO_4 was electrodeposited potentiostatically on Pt and ITO from PC and ACN solutions [96]. A slower deposition was observed for PC, and it was hypothesized that it might be due to the higher viscosity of PC when compared to ACN. The substrate also influenced, as PEDOT on ITO had bigger grains and was therefore rougher, while it appeared smoother on Pt. The effect of several mixtures for PS electropolymerization of PEDOT:ClO_4 was also studied: ACN, ACN:dichloromethane (2:1 v/v), ACN:dichloromethane (4:1 v/v), toluene/ACN (2:1 v/v), toluene/ACN (4:1 v/v) and dichloromethane [97]. Fast kinetics were observed for all the ACN-based solutions, and slower kinetics were noted for the others. However, the study concluded that in order to control a well-ordered growth of PEDOT, toluene/ACN (4:1 v/v) was the ideal mixture as it presented similar deposition performances to the ACN-containing solutions but coupled with slower kinetics. It was reported that PD electropolymerization of PEDOT:ClO_4 in PC led to a thicker PEDOT layer than polymerization in aqueous solution, even when more cycles were used [98]. Indeed, a 4 cycles-deposition in PC provided a thicker film than a 14 cycles-deposition in water.

Castagnola et al compared the three depositions methods for PEDOT:PSS electropolymerization [89]. In their case, PD deposition led to a smoother and more homogeneous layer than the two other methods. Their hypothesis was that the coupling rate between the generated oligomers was slower for PD depositions, which led to more uniform film. The films processed in PD conditions showed the lowest impedance and the highest conductivity due to its compactness and uniformity, and a better resistance to thermal aging. Different electropolymerized PEDOT:ClO_4 coatings on Pt from an ACN solution were compared. Several deposition methods were used: PS depositions at 1.2, 1.3 and 1.4 V and GS deposition [99]. The most conductive film was obtained for PS deposition at 1.4 V due to its high compactness. However, this compactness led to a low exposed area, hence a high impedance, whereas the other films had high double-layer capacitances, hence lower impedances and higher CSCs.

As one could expect, the deposition method seems to have an impact on the electropolymerization process. However other parameters play crucial roles. As for the dopants, PSS^- would appear not to be an interesting candidate. It decreases the conductivity of the material by increasing the spacing between the conductive chains of PEDOT. Besides, it increases the stiffness of the PEDOT film, preventing it to anchor into the imperfection of the substrate and thus leads to an easier delamination. The solvent was clearly proven to have a substantial influence on electropolymerization, as their characteristics such as viscosity, dielectric constant and solubility of PEDOT oligomers can strongly influence the morphology of the PEDOT film.

CHAPTER 3 MATERIALS AND METHODS

3.1 Electropolymerization

All electrochemical depositions and measurements were realized in three electrode-cell using a Pt wire as counter-electrode and a silver/silver-chloride (Ag/AgCl) electrode as the reference and a Bio-Logic VSP-300 Potentiostat equipped the EC-Lab software.

To compare the efficiency of our (4-thien-2-yl) diazonium salt (thien-DS) coatings, we electrodeposited a thien-DS layer subsequently covered by a PEDOT:BF_4 layer on some electrodes and only a PEDOT:BF_4 layer on other electrodes. We controlled the presence of thien-DS using ferrocene and subjected the electrodes to sonication to evaluate the quality of the adhesion. We also investigated the influence of the solvent on the morphology and the adhesion quality of our coatings.

3.1.1 Substrate cleaning

Three different substrates were used as working electrodes: a “large” Pt disk electrode, easier to manipulate for preliminary tests, and two types of PtIr microelectrodes commonly used for recording and stimulating purposes.

Parylene-C-coated PtIr recording microelectrodes (PTM23B05) with a length of 51 mm, a shaft diameter of 231 µm and a sharp exposed tip of 18 µm were purchased from World Precision Instruments. Parylene-C-coated PtIr stimulating microelectrodes (PI201G) with a length of 51 mm, a shaft diameter of 256 µm and a sharp exposed tip of 150 µm were purchased from MicroProbes. The microelectrodes were rinsed with IPA, acetone and DW before any experiment to remove any contaminant.

A Pt flat disk, with a diameter of 3 mm, was polished for 5 minutes on sand paper and for 5 minutes with 1 µm and 0.05 µm alumina polishing powders between every experiments to remove any traces of chemicals from previous experiments. The Pt disk was sonicated for 10 minutes in DW after polishing to remove the alumina particles and rinsed with isopropanol (IPA), acetone and distilled water (DW).

Sonication was realized by an Eumax ultrasonic cleaner (ud100sh-4l) with 100 W ultrasonic power. IPA (C3H8O, 70%) and acetone (C3H6O, 90%) were purchased from Honeywell Research Chemicals.

3.1.2 Solution preparation

Tetraethylammonium tetrafluoroborate ($TEABF_4$) along with the thien-DS were dissolved in acetonitrile (ACN) to reach concentrations of 120 mM for $TEABF_4$ and of 5 mM for the thien-DS. This solution was used for the electrodeposition of thien-DS on the electrodes.

$TEABF_4$ along with ferrocene (Fc) were dissolved in ACN to reach concentrations of 120 mM for $TEABF_4$ and of 5 mM for Fc. This solution was used to control the effective deposition of thien-DS on the electrodes.

$TEABF_4$ along with EDOT were dissolved in ACN, propylene carbonate (PC) and DW to reach concentrations of 120 mM for $TEABF_4$ in all three solvents and of 20 mM for EDOT in ACN and PC and of 10 mM of EDOT in DW. These solutions were used for the electropolymerization of PEDOT:BF_4 on the uncoated electrodes and the thien-DS-coated electrodes.

The chemicals were manually mixed using a spatula until total dissolution.

Weighing of the chemicals was carried out using a Sartorius Quintix Analytical Balance.

ACN non-UV and PC (anhydrous, 99.7%) were purchased from Caledon Laboratories and Millipore Sigma respectively. Ferrocence ($Fe(C_5H_5)_2$, 98%) and EDOT (C_6H_6OS, 97%) were purchased from Millipore Sigma. $TEABF_4$ ($C_8H_{20}NBF_4$, 99%) was purchased from Acros Organics. The thien-DS was prepared by our collaborator from Université du Québec à Montréal (UQAM) following a procedure describe elsewhere [7].

3.1.3 Diazonium salt electrodeposition

A thien-DS layer was electrodeposited on some electrodes to be used as an anchoring layer for the subsequently deposited PEDOT:BF_4 layer. Thien-DS electrodeposition was carried out using a PD deposition of 5 to 15 cycles from -0.5 V to 0.5 V vs Ag/AgCl.

3.1.4 PEDOT electrodeposition

A PEDOT:BF_4 layer was electropolymerized on our electrodes to improve their electrochemical properties. In some cases, PEDOT:BF_4 was deposited on the thien-DS layer.PEDOT:BF_4 electropolymerization was carried out using different methods summed up in the following table:

Table 1: Electropolymerization parameters of PEDOT:BF_4 on different substrates with different methods.

Substrate	Method	Solvent	Limit	Current (GS); Potential (PS); Potential window, sweep rate (PD)
Recording PtIr microelectrode	PD	ACN	5 cycles	-0.5 V to 1.5 V, 100 mV/s
		PC		
	GS	ACN	50 s	17 nA
		PC		
		DW	150 s	6 nA
Stimulating PtIr microelectrode	GS	PC	50 s	315 nA
Pt disk	PD	ACN	15 cycles	-0.5 V to 1.5 V, 100mV/s
		PC		
		DW		-0.5 V to 1.2 V, 100 mV/s
	GS	ACN	400 s	30 μA
		PC		
		DW	1200 s	10 μA

	PS	ACN	12 mC	1.2 V
		PC		
		DW		0.9 V

3.1.5 Electrochemical characterization

To control the deposition of the thien-DS layer, we carried out 3 cycles of CV between 0.2 V and 0.6 V vs Ag/AgCl in the Fc solution before and after thien-DS electrodeposition. Differences in measured currents during CV using ferrocene would indicate the presence of a deposited thien-DS layer, on the surface of the electrode.

To control the presence of the PEDOT:BF_4 layer, we carried out 5 cycles of CV between -0.6 V and 0.6 V vs Ag/AgCl in PBS pH 7.4 before and after PEDOT:BF_4 deposition. EIS measurements between 1 Hz and 10^5 Hz were also conducted before and after deposition, using a 10 mV amplitude for the sine. The phosphate buffer solution (PBS) of pH 7.4 was prepared using PBS tablets purchased from Millipore Sigma.

3.1.6 Imaging

Optical microscope images were obtained using an Olympus SZX7 stereo microscope and an Axio Imager M1 from Zeiss, equipped with an AxioCam Mrm CCD camera. Scanning Electron Microscopy (SEM) was carried out using a Scanning Electron Microscope equipped with a Field Emission Gun (JEOL JSM7600F). The optical images were used to confirm the presence of PEDOT:BF_4 on the microelectrodes, the SEM images were used to characterize the morphology of the deposited coatings.

3.2 Stability tests *in vitro*

Before implanting the microelectrodes, several stability tests were performed *in vitro* including sonication, passive aging, steam sterilization and electrical pulsing.

3.2.1 Sonication test

To assess the adhesion of our PEDOT:BF_4 coatings on the PtIr and Pt substrates, we subjected them to sonication. The electrodes were immersed in DW inside a Becker glass using a clamp holder. The Becker glass was then positioned in the ultrasonic bath of an Eumax ultrasonic cleaner (ud100sh-4l) with 100 W ultrasonic power.

For all samples, an initial sonication time of 30 seconds was used to assess the basic adhesion of the PEDOT:BF_4 coatings. For PtIr microelectrodes, electrochemical measurements and imaging were realized at 30 seconds, 2 minutes and 5 minutes of sonication, to ensure to isolate the delamination period in a narrow enough window. For the Pt disk, electrochemical measurements and imaging were realized at 30 seconds, 5 minutes, 10 minutes, 15 minutes, 20 minutes, 25 minutes and 30 minutes of sonication, we used larger windows as the adhesion was generally better. For thien-DS-PEDOT:BF_4-coated Pt disk, an extra sonication period of 1 hour was used, as the adhesion was very strong.

3.2.2 Passive aging

To determine the PEDOT-coated microelectrodes' passive aging, we immersed them in PBS pH 7.4 for different periods of time. Recording PtIr microelectrodes were immersed for 2 weeks and stimulating PtIr microelectrodes were immersed for 8 weeks, as stimulating electrodes were meant to stay implanted for a longer time. The PBS solution was changed every week to limit contamination and/or crystallisation of salts and electrochemical measurements were carried out every week as well as the first days after immersion.

3.2.3 Steam sterilization

We steam sterilized the PEDOT-coated microelectrodes before implantation and monitored the evolution of the electrochemical properties The microelectrodes were taped to the bottom of a plastic box to prevent unwanted movements that might damage the tip of the electrodes. The electrodes then underwent steam sterilization at 121 °C for 30 minutes. The microelectrodes were characterized in PBS pH 7.4 before and after the process.

3.2.4 Electrical stimulation in PBS pH 7.4

To ensure the stability of our PEDOT:BF_4 layer to repeated stimulations, we sent symmetrical biphasic pulses of 20 μA and 90 μs for the cathodic phase and an interphase period of 10 μs at a frequency of 130 Hz. This corresponds to roughly 30 $\mu C/cm^2$ and 1.8 nC/phase. The electrodes were immersed in a PBS pH 7.4 solution and stimulated for 2 hours and electrochemical properties were monitored before and after the stimulation.

The biphasic pulses were generated by coupling two synchronized monophasic FHC pulsar 6i set up with opposite polarities, the first phase being negative and the second phase being positive with a delay of 100 μs (duration of the first phase plus the delay). The waveform and the maximum intensity amplitude was controlled using a DSO9104A Infiniium Oscilloscope, 1 GHz, Megazoom from Agilent Technologies.

3.3 *In vivo* stimulation

Two female Wistar rats were implanted with two stimulating PtIr microelectrodes, a PEDOT:BF_4-coated one and an uncoated one, in their subthalamic nucleus. Prior to implantation, the microelectrodes were soaked for 24 hours in distilled water.

The rats were anesthetized before the surgery using isoflurane and an isoflurane flow was maintained on the animal's nose during the whole surgery. The head of the animal was shaved using an electrical razor and placed in a stereotaxic apparatus. The shaved skin was cleaned using an iodine solution and bupivacaine was injected under the scalp skin. The scalp skin was then opened with a scalpel in a clean straight line of approximately 2 cm from the between the eyes to the ears. The cut was enlarged using four clamps attached to the skin. Tissues and muscles were removed until the skull was clearly visible. The alignment of the skull was adjusted by measuring the vertical coordinates of the lambda and bregma points of the skull. Two holes were pierced using a drill in the skull at the implantation coordinates necessary to reach the STN (anteroposterior: -3.3 mm, lateral: ±2 mm, from the bregma). Four screws were inserted into the skull around the implantation sites and tied together with a silver wire terminated by a connector to create a counter/reference electrode, as the screws are in contact with brain fluids. Finally, the two electrodes were implanted in the two drill holes (vertical: -6 mm, from the top of the skull) and tethered to the skull with dental cement. An antibiotic cream was spread around the wound at the

end of the surgery to prevent infections and buprenorphine was injected prior to the rat waking up, as well as fluids.

The electrical stimulation were carried out using the same procedure as detailed in section 3.2.4. Both the PEDOT:BF_4-coated and the uncoated PtIr electrodes were stimulated one after the other every day, except the week-ends, for 7 days for the first rat and 16 days for the second rat. The rats were freely moving during the stimulation period. The waveform and maximum applied current was controlled before every stimulation. The voltage excursion observed at the electrodes during stimulation was recorded at the beginning and the end of every stimulation period and regularly monitored in case of disconnection of the cables or strong variation in voltage excursion.

EIS measurements between 1 Hz and 10^5 Hz were conducted before and after every stimulation period using a portable Bio-Logic VSP-150. The potential bias was 0 V and the AC signal amplitude was 10 mV.

CHAPTER 4 RESULTS

We present here the main results of our work. First, we will expose the electropolymerization results, including the thien-DS deposition, the electrochemical properties of PEDOT:BF_4, such as impedance and charge storage capacities (CSCs), and the morphologies of the PEDOT:BF_4 coatings observed by SEM imaging. Following this, we will present the results of the stability tests of the coatings: sonication, passive aging, steam sterilization and electrical stimulations, associated with their respective electrochemical properties and structure robustness. To finish, we will describe the evolution of our PEDOT:BF_4 coatings *in vivo* and the influence of the electrical stimulations.

4.1 Electropolymerization

Different electrodepositions were conducted on different substrates. Thien-DS, Thien-DS-PEDOT:BF_4 and PEDOT:BF_4 were electrodeposited from different solvent: propylene carbonate, acetonitrile and distilled water (PC, ACN and DW) on recording and simulating platinum-iridium (PtIr) microelectrodes as well as on a Pt disk electrode, with different techniques: potentiodynamic, potentiostatic and galvanostatic (PD, PS and GS).

4.1.1 Electrochemical properties

We characterized the electrochemical properties before and after the process of deposition of different organic layers on the metallic surfaces. For the thien-DS layer, an electrolytic ferrocene (Fc) solution was used to control the presence of the layer. For PEDOT:BF_4 layers, either on thien-DS or directly on Pt or PtIr, a PBS pH 7.4 solution was used to control the presence of the PEDOT:BF_4.

4.1.1.1 Diazonium-based anchoring layer

As explained earlier, thien-DS is a molecule that can create a covalent bond with metallic surfaces during the reduction of its amine moieties. During electrodeposition, a strong cathodic peak was detected around 0.15 V vs Ag/AgCl, indicating a reduction (figure 12). A subsequent smaller peak, shifting towards 0.2 V vs Ag/AgCl, was observed for the following cycles. To control the presence of the thien-DS layer on the metallic surfaces, an Fc control solution was used.

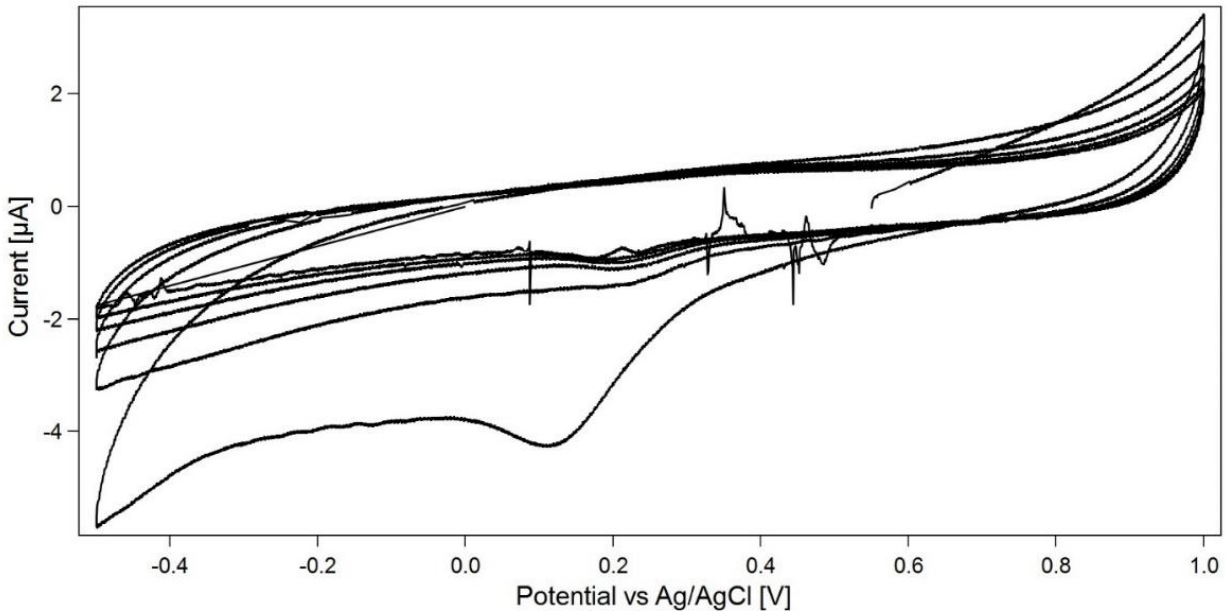

Figure 12: PD deposition of 5 cycles at 100 mV/s of thien-DS on a recording PtIr microelectrode. A clear reduction peak is visible at 0.15 V, indicating the reduction of the amine moieties of the thien-DS.

Ferrocene (Fc) is a molecule that undergoes two reversible redox processes (reduction and oxidation) during CV. However, for electron transfer to happen, the Fc molecule needs to be able to access the surface of working electrode. Hence, the Fc redox process is an interesting method to estimate the electrochemical interactions between a small active surface and an electrolytic solution: a high current indicates that the electron transfer takes place, while a low current indicates a hindered electron transfer.

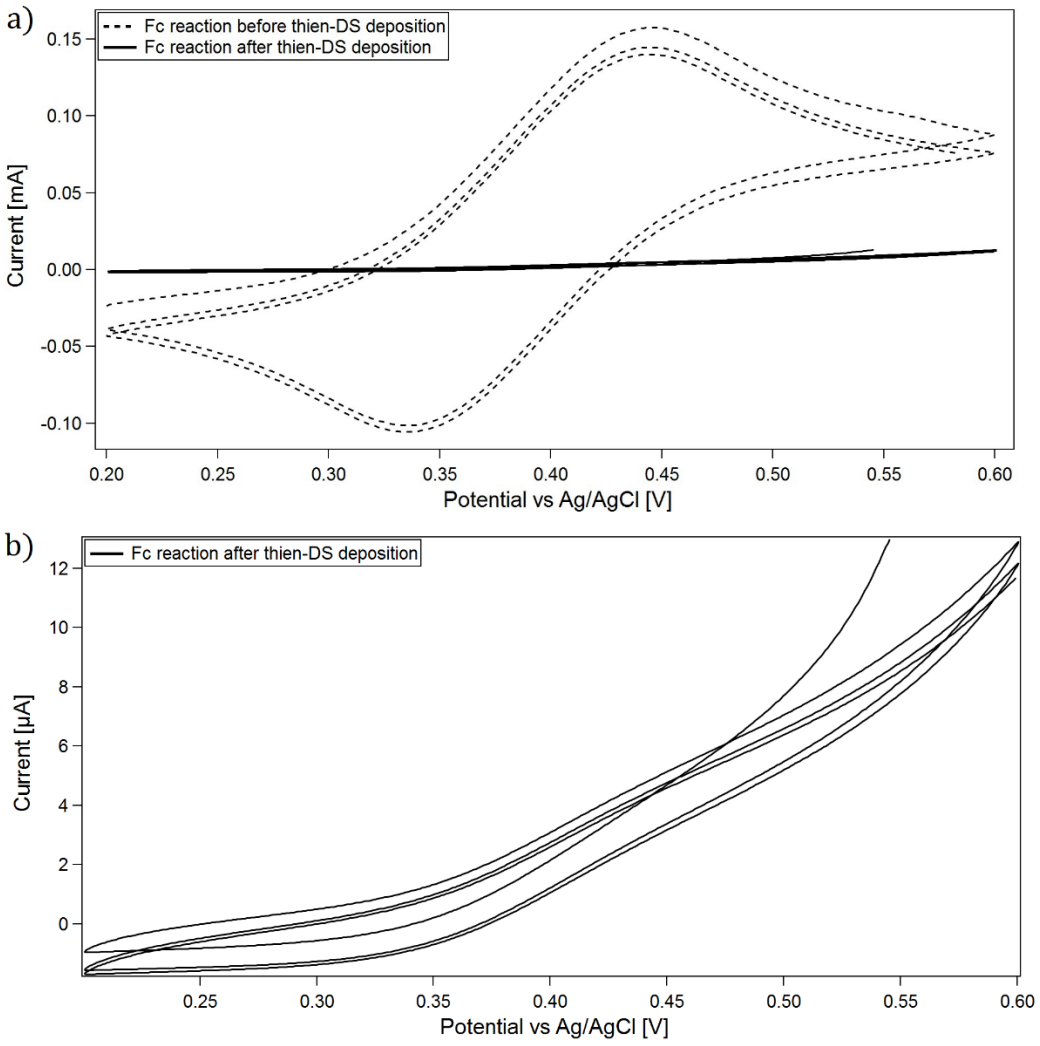

Figure 13: a) CVs (3 cycles, 100 mV/s) in a ferrocene-containing solution before and after electrodeposition of a thien-DS layer on a Pt disk electrode and b) a zoom on the CVs obtained after deposition.

After the thien-DS deposition, a clear drop of current in the ferrocene CV was observed (figure 13), indicating the presence of a thien-DS layer layer preventing the electron transfer between Fc molecules and the electroactive surface.

These results were observed for all substrates: Pt disk and PtIr microelectrodes.

4.1.1.2 PEDOT:BF_4 coating

4.1.1.2.1 Pt disk electrode

Before depositing PEDOT:BF_4 on the PtIr microelectrodes, several electrodeposition tests were conducted on Pt disk electrodes. Electrodeposition of PEDOT:BF_4 was realized with three different methods: PD, PS and GS, in three different solvents: PC, ACN and DW. The aim was to find the parameters leading to the most stable PEDOT:BF_4 coating.

For PD depositions, the current increased after every cycle, indicating an accumulation of conductive material (figure 14, b)). The current for the last cycle of PD deposition in ACN was much higher than the one for the other solvents, especially for DW (figure 14, a)). For PS depositions, a rapid increase of the current over time could be observed, indicating a successful accumulation of PEDOT:BF_4 (figure 14, c)). Here again ACN seemed to provide the fastest deposition kinetics and DW the slowest. For GS depositions, an initial potential spike followed by a decreasing trend, was observed for all the solvents (figure 14, d)). However, whereas PC and ACN could be used with short deposition times, DW needed a lower applied current to prevent unwanted reaction, such as overoxidation of the PEDOT:BF_4 and electrolysis of water, and thus a longer deposition time to reach the same amount of exchanged charges. Overall, ACN provided the fastest deposition kinetics, followed by PC and DW provided the slowest.

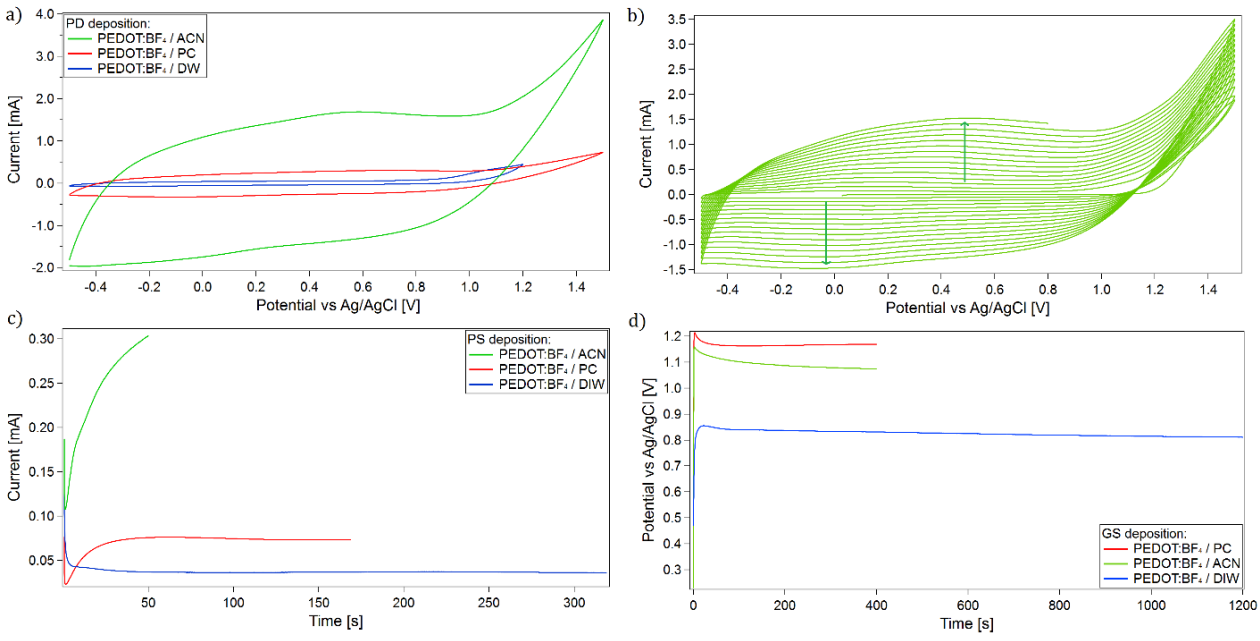

Figure 14: Deposition curves for PEDOT:BF_4 on Pt disk: a) PD depositions in ACN, PC and DW (last cycles out of 15, 100 mV/s), b) PD deposition in ACN (15 cycles, 100 mV/s) c) PS depositions in ACN, PC and DW and d) GS depositions in ACN, PC and DW.

The first main observation post-deposition is that the PEDOT:BF_4 coating decreases the impedance and enhances the CSC for all deposition methods and solvents (figure 15).

Comparing the deposition methods, PD provided a larger amount of materials on the Pt disk, independently of the solvent, than PS and GS, as seen by optical microscopy (not shown) and by electrochemical measurements (figure 15, e) and f)). Indeed, the lowest obtained CSC for PD deposition (DW: 2.6 mC) was more than twice the highest CSC obtained for PS and GS depositions (ACN: 1.245 mC) (figure 15 e)). On the other hand, PS and GS depositions provided similar electrochemical properties when using the same solvent, most likely due to the same amount of charges exchanged and so the same quantity of materials deposited (figure 15, a), b), c) and d)).

When observing the influence of the solvent, one could notice again the difference in deposition kinetics, especially for the PS deposition in DW that lasted more than twice longer than in PC and more than six times longer than in ACN (figure 14 c)). This was reflected on the CSCs measured after PD depositions (figure 15 e)): ACN provided a CSC of 20 mC whereas PC provided 6.45 mC and DW only 2.6 mC. Interestingly, despite large differences in CSCs organic solvents led to similar impedances at 1 kHz, with a reduction of 43 Ω (32% relative change) for PC and of 54 Ω (41% relative change) for CAN (figure 15 f)). However, PEDOT:BF_4 electrodeposition in DW led to no relevant change in impedance at 1 kHz (figure 15, f)). For PS and GS depositions, DW displayed a slightly lower CSC (ACN: 1.245 mC, PC: 1.11 mC and DW: 1 mC, with respect to bare Pt: 0.1 mC) (figure 15 a) and c)), but all three solvent with both methods displayed reductions of impedance at 1 kHz comprised between 11 and 36 Ω (8 and 27% relative change) (figure 15 b) and d)).

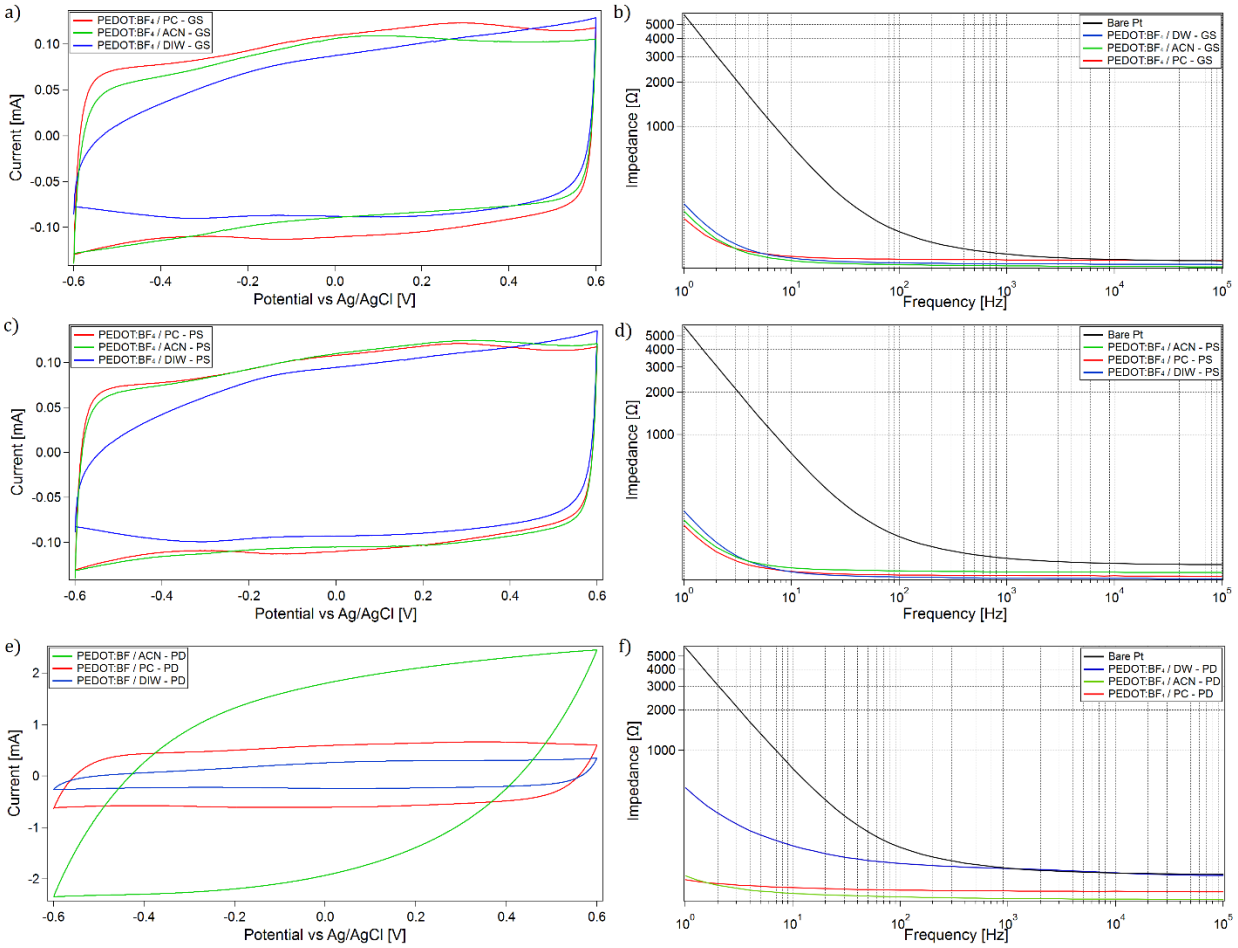

Figure 15: Characterization of electropolymerized PEDOT:BF_4 coatings deposited in ACN, PC and DW using GS depositions: a) CV b) EIS ; PS depositions: c) CV, d) EIS ; PD depositions: e) CV f) EIS. The scan rate for the CVs is 100 mV/s. The measurements were realized in PBS pH 7.4.

To sum up, all solvents allowed for electropolymerized PEDOT:BF_4 to decrease impedances and increase CSCs when compared to the bare Pt disk, except for DW with PD deposition.

4.1.1.2.2 PtIr microelectrodes

Following these tests on Pt disk, PEDOT:BF_4 was electropolymerized on recording (exposed area of 325 μm^2) and stimulating (exposed area of 6000 μm^2) PtIr microelectrodes. An initial PD deposition test was done, but this deposition method was quickly abandoned as it produced too much material (see subsection 4.1.2 PEDOT morphologies). As PS and GS were found to not lead to significant electrochemical differences on the Pt disk (figure 15), recording PtIr microelectrodes

were coated with PEDOT:BF_4 using only GS deposition in the three different solvents: PC, ACN, and DW. The typical curve for GS deposition was observed: an initial spike followed by a slow decrease of potential (figure 16).

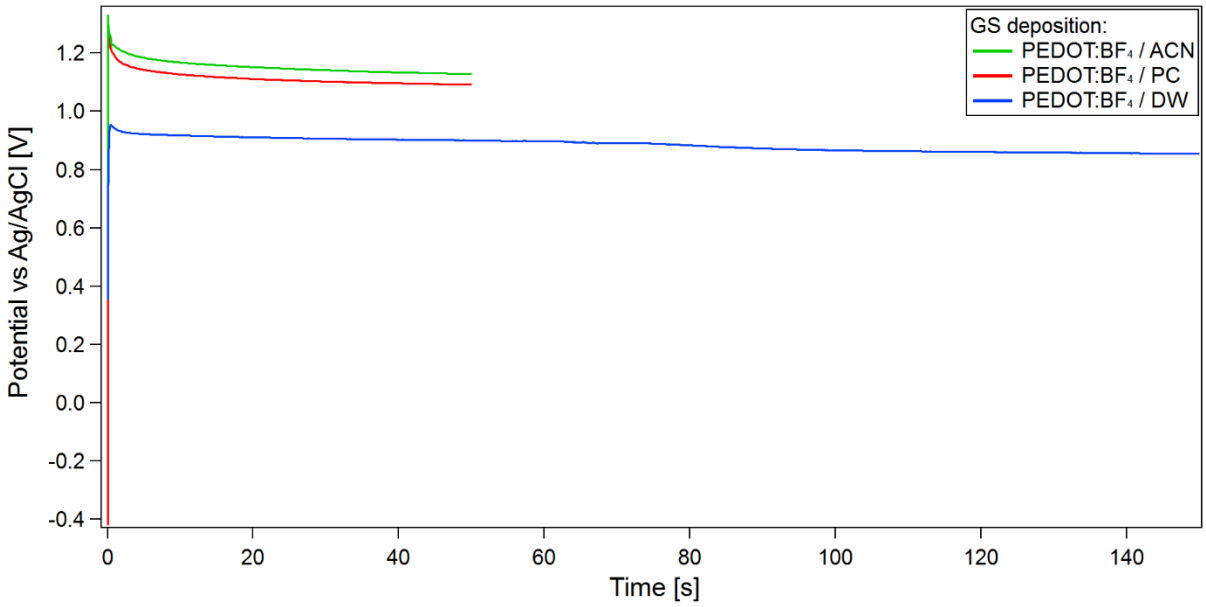

Figure 16: GS deposition curves of PEDOT:BF_4 in ACN, PC and DW on PtIr recording microelectrodes.

The first post-deposition observation confirmed the findings made on the Pt disk: all solvents provided a clear drop of impedance and enhanced CSCs (figure 17). The CSCs and impedances were similar for all three solvents, with DW providing slightly higher impedance and slightly lower CSC. The impedance was reduced by around 810 kΩ (around 2 orders of magnitude), and the CSCs was multiplied several factors (almost 8 times in organic solvents and 5 times in DW) when compared to bare PtIr (CSC: 20 µC). The enormous decrease in impedance for PtIr microelectrodes with respect to the flat Pt disk is mainly due to the fact to the impedance of the Pt disk is already very low, thanks to its large surface area. On the contrary, PtIr microelectrodes have much smaller surfaces thus much higher impedances, so a small amount of PEDOT:BF_4 on the surface can lead to drastic changes to the morphology and therefore to the impedances.

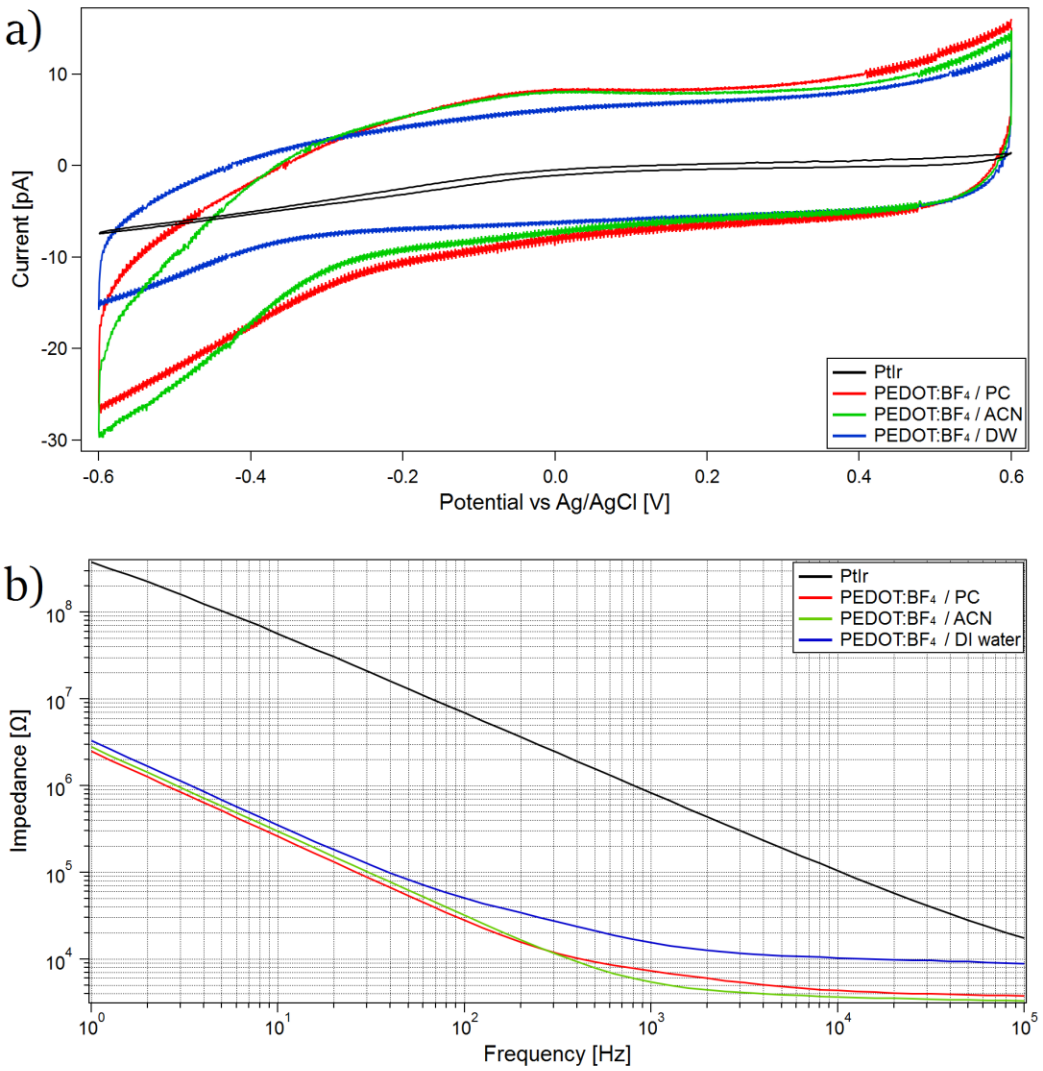

Figure 17: Characterization of electropolymerized PEDOT:BF4 galvanostatically deposited on PtIr recording microelectrodes using a) CV and b) EIS techniques.

Stimulating PtIr microelectrodes were only coated using GS deposition in PC for reasons detailed in the next sections. Here again, the PEDOT:BF_4 layer reduced the impedance and increased the CSC. The impedance decreased from 14.3 kΩ to 1.24 kΩ (1 order of magnitude) and the CSC went from 0.66 mC to 2.5 mC (multiplied 3.8 times).

For the rest of the study, we focused our work on the PtIr microelectrodes, as the Pt disk was not designed for *in vivo* experiments.

4.1.2 PEDOT morphologies

For the PD deposition, PC and ACN led to very different structures. When observing the tip of the microelectrodes, one could notice that ACN led to a coating that followed the tubular shape of the microelectrodes (figure 18, (A)) whereas PC led to a globular shape concentrated on the tip of the microelectrode (figure 18, (B)). ACN also generated random nucleation sites on the insulator, sometimes far away from the electroactive tip. These reasons led us to abandon this deposition method for microelectrodes.

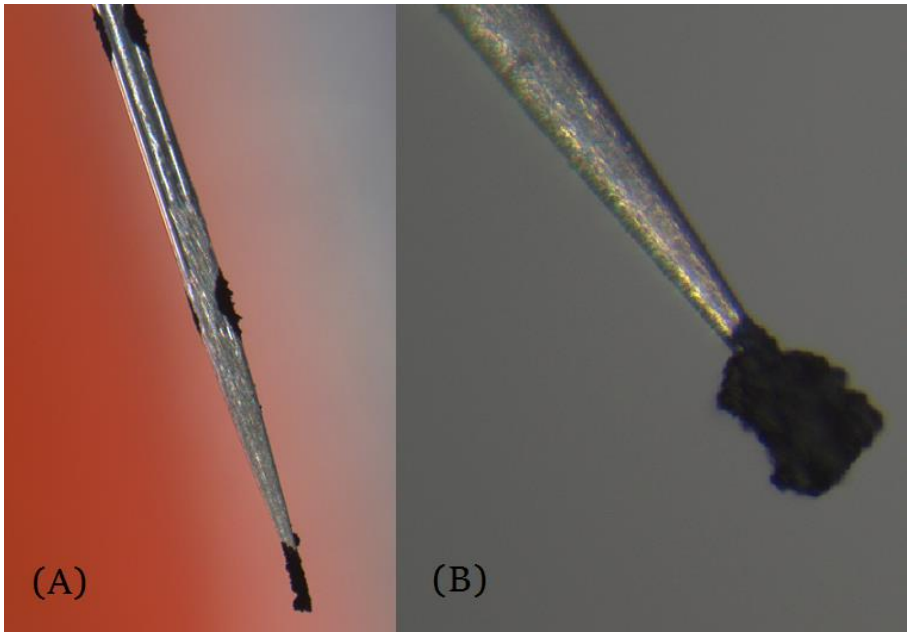

Figure 18: Optical images of electropolymerized PEDOT:BF_4 on recording PtIr microelectrodes using 5 cycles of PD deposition in a) ACN and b) PC.

For the GS method, the coatings were too thin to be observed by optical microscopy. However, very interesting morphologies were observed using SEM imaging for the three solvents on the recording PtIr microelectrodes (figure 19).

At low magnification, all coatings appeared relatively smooth (figure 19, a), c) and e)), with coatings done in PC experiencing some overgrowth (figure 19, a)). At high magnification, PC and ACN led to similar porous morphologies, with coatings processed in ACN showing larger pore diameters (figure 19, d)). However, coatings processed in DW appeared more compact, with a nodular-like morphology really contrasting from the coatings processed in organic solvents (figure 19, f)).

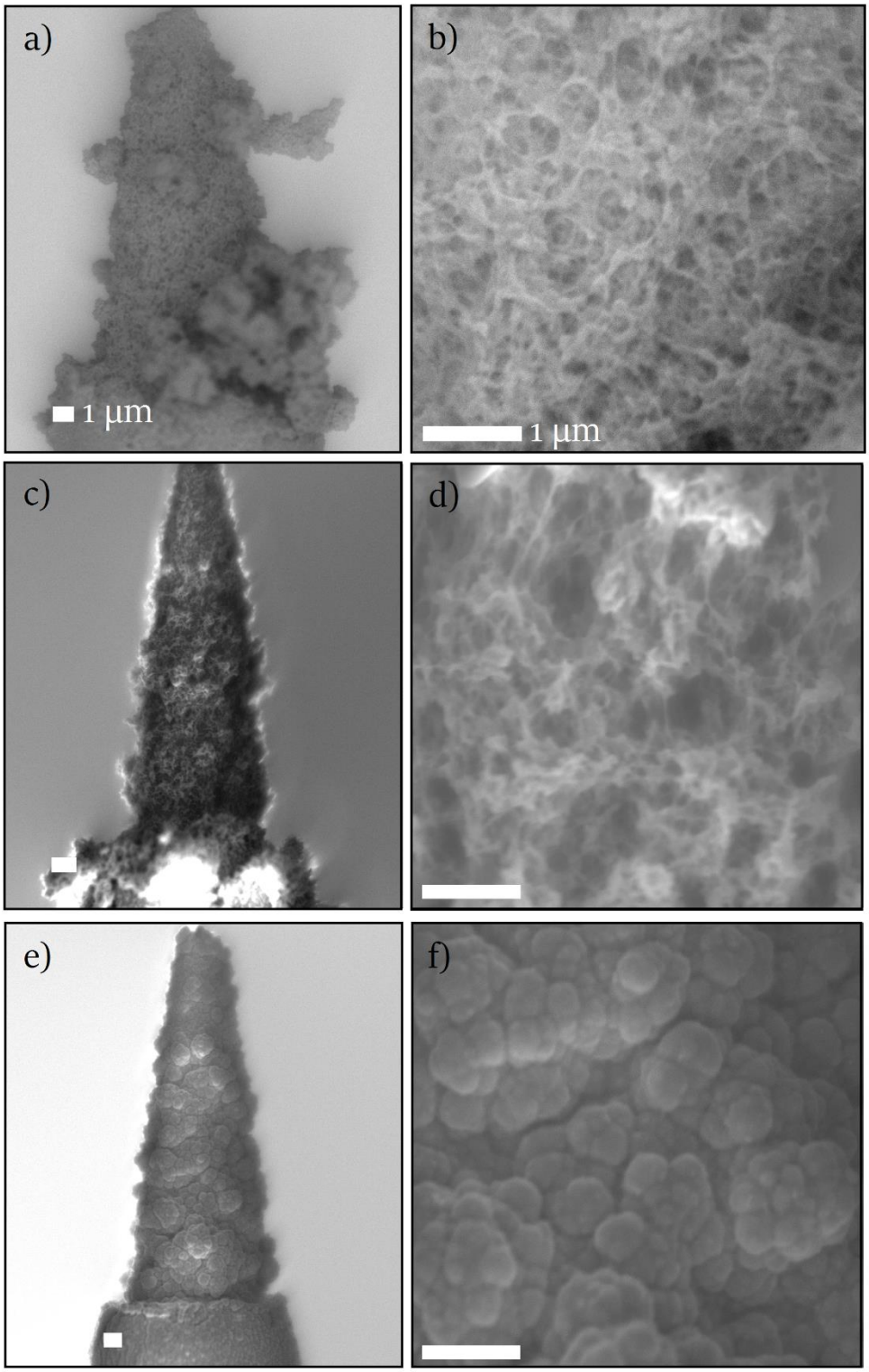

Figure 19: SEM imaging of PEDOT:BF4 on PtIr recording microelectrodes, galvanostatically deposited in PC: a) and b) ; ACN: c) and d) ; DW: e) and f). The acceleration voltage used was of 2.00 kV.

4.2 Stability of the organic coatings *in vitro*

Before any implantation, adhesion and stability tests were realized to assess the efficiency of our electrodepositions. A first harsh sonication test was conducted. If the coatings did survive this initial test, they were then confronted to passive aging, steam sterilization and electrical stimulations *in vitro*. The Pt disk electrode was only confronted to sonication tests.

4.2.1 Sonication test

The electrodes were immersed in DW in a sonic bath in conditions described in the methods section, and sonicated for various amount of time. The results are presented in section 4.2.1.1 and 4.2.1.2.

4.2.1.1 Pt disk electrode

Coatings deposited by PD tended to delaminate quickly, with the majority of the coatings failing before 30 seconds of sonication (figure 20). This was most likely due to a large amount of materials that led to a more brittle coating. PS and GS depositions overall led to similar delamination times for the same solvent, with the coatings usually delaminating before reaching 5 minutes of sonication.

As for the influence of the solvent, ACN led to the highest number of delamination within 30 seconds of sonication, whereas PC led to more resistant coatings (figure 20). DW led to a decent adhesion comprised between the two other solvents.

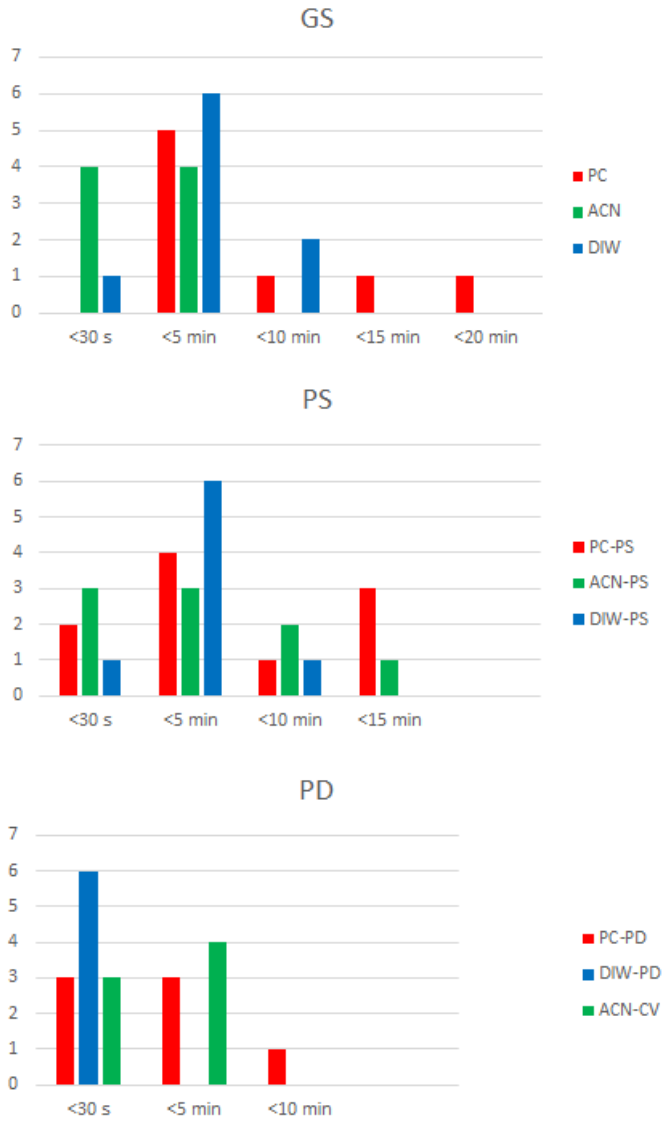

Figure 20: Time before appearance of large cracks and/or sudden changes in electrochemical properties (increase of impedance and decrease of CSC) for the PEDOT:BF_4 coating on the Pt disk during sonication, with different deposition method and different solvent used. The x axis represents the number of samples sonicated.

Another interesting observation was the delamination processes. The different solvents led to different delamination. Coatings processed in PC and ACN delaminated in relatively large portions of PEDOT:BF_4 (figure 21, a), b), c), d), e) and f)), whereas for coatings processed in DW, the delamination process showed the appearance of a multitude of very small holes in the surface of the coatings (figure 21, g), h) and i)).

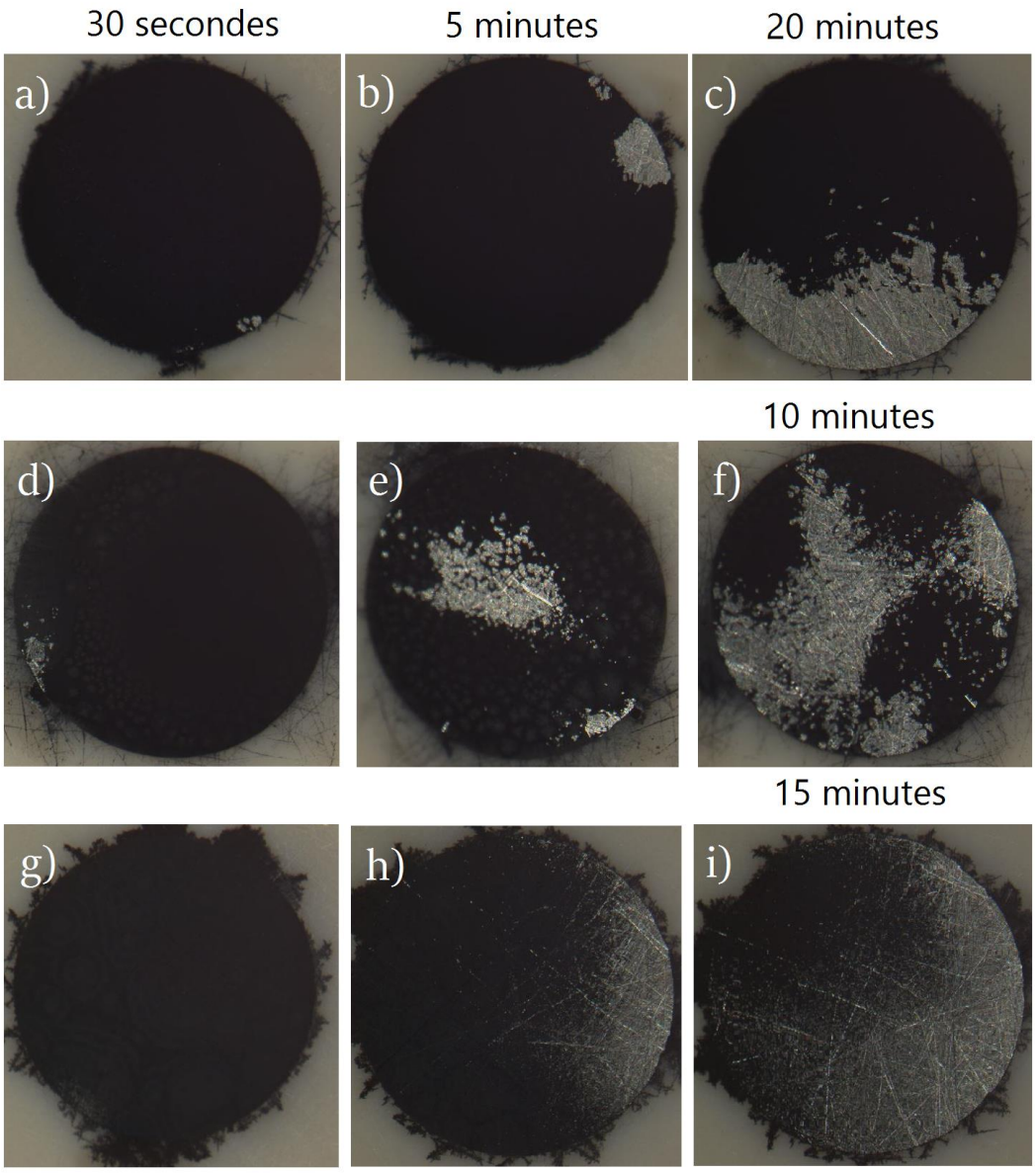

Figure 21: Delamination process of PEDOT:BF_4 galvanostatically deposited on the Pt disk in PC: a), b) and c) ; ACN: d), e) and f) ; DW: g), h) and i), under sonication for different time intervals.

As PD deposition led to low adhesion, we decided to use thien-DS to improve it. When depositing PEDOT:BF_4 using PD deposition on a previously electrodeposited thien-DS layer, a 1-hour long sonication appeared to have little effect on the adhesion, as no damage to the thien-DS/PEDOT:BF_4 layer could be seen. This increase in adhesion was observed for all three solvents.

4.2.1.2 PtIr microelectrodes

The same sonication test was realized on the PtIr microelectrodes. However, the sonication time was limited to 5 minutes in order to prevent the delamination of the Parylene-C insulating layer.

For recording PtIr microelectrodes, the influence of the solvent was studied. The coatings deposited in organic solvents were able to resist the sonication for 5 minutes while retaining more than 80% of their CSCs. On the contrary, coatings prepared in DW delaminated before reaching 5 minutes.

A 15-cycles PD deposition of thien-DS was used in order to improve the adhesion of our coatings. However, when using a thien-DS layer, the adhesion quality would actually be reduced for the PEDOT:BF_4 coating, usually with the delamination occurring before 30 seconds of sonication. Therefore, the use of thien-DS was abandoned for the microelectrodes.

For stimulating PtIr microelectrodes, coatings, processed in PC, were able to resist 5 minutes of sonication while retaining 84% of its initial CSC and experiencing a negligible increase of 65 Ω of impedance.

4.2.2 Passive aging

PtIr microelectrodes were subjected to passive aging at room temperature PBS pH 7.4 solutions. This simple test gave information about the stability of our coatings when allowed to soak in electrolytic solutions.

Recording PEDOT:BF_4-coated PtIr microelectrodes were soaked in PBS pH 7.4 for 2 weeks, and the influence of the solvent was studied (figure 22). Coatings processed in organic solvent were the most affected by the soaking, as their impedance at 1 kHz slightly increased (2.59 kΩ change for the PC-processed electrode and 1.95 kΩ for the ACN-processed electrode). Unexpectedly, their CSCs increased (in PC: roughly 10% and in ACN: roughly 20%). Coatings processed in DW were less affected, as their CSC was the most stable (slight increase of roughly 4.5%), and their impedance even decreased (- 8 kΩ). However, the impedance of coatings processed in DW was initially higher than the ones processed in organic solvents. Overall, all the impedances stayed at much lower levels than the one of bare PtIr.

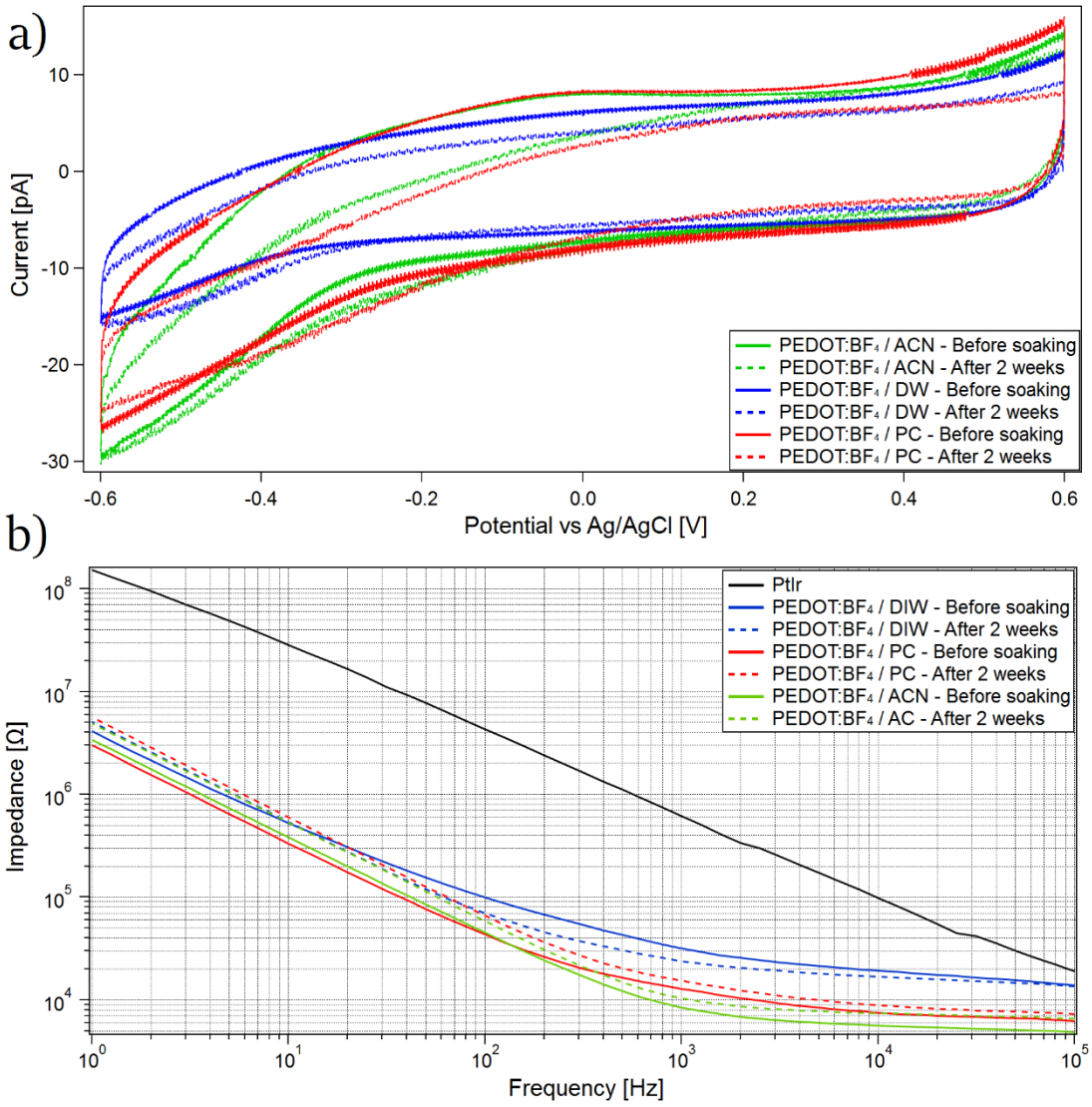

Figure 22: Characterization of PEDOT:BF_4 coatings on PtIr microelectrodes immersed during 2 weeks in PBS pH 7.4: a) CV b) EIS.

A stimulating PEDOT:BF_4-coated PtIr microelectrode (exposed tip 6000 μm^2), processed in PC, was immersed for 8 weeks in PBS pH 7.4. The change in impedance was negligible (increase of 136 Ω) when compared to the initial decrease due to the PEDOT:BF_4 coating (decrease of 19 kΩ, almost 98% relative change) (not shown). The coatings also retained more than 82% of their initial CSC. These changes are similar to the one obtained for 5 minutes of sonication.

4.2.3 Steam sterilization

A commonly used method to sterilize implantable devices is steam sterilization or autoclave. Before implanting our PtIr microelectrodes, we assessed the damages resulting from steam sterilization.

Recording PEDOT:BF_4-coated PtIr microelectrodes were subjected to steam sterilization at 121 °C for 30 minutes, and the influence of the solvent was studied. Coatings processed in organic solvent retained more than 85% of their CSCs, whereas coatings processed in DW only retained around 60%. As for the impedance, coatings processed in organic solvents were mostly unaffected whereas coatings prepared in DW experienced a 15 kΩ increase (figure 23). While this change may seem low compared to the decrease due to the PEDOT:BF_4 coatings, it is still significant as the impedance of coatings prepared in DW were already twice higher than the ones of coatings processed in organic solvents.

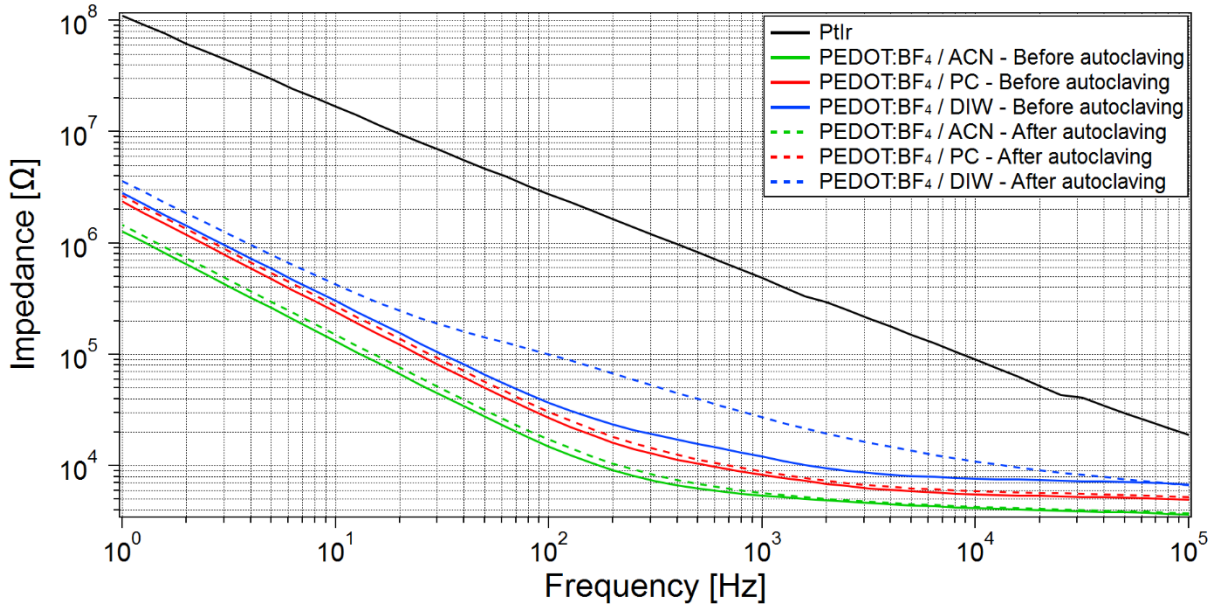

Figure 23: Impedance measurements of PEDOT:BF4 coatings on recording PtIr microelectrodes before and after 30 minutes of steam sterilization at 121 °C.

A stimulating PEDOT:BF_4-coated PtIr microelectrode, processed in PC, underwent steam sterilization. The impedance experienced a negligible increase of 58 Ω, and the CSC maintained 72% of its initial value.

4.2.4 Electrical stimulation in PBS pH 7.4

To ensure the stability of our PEDOT-BF_4 coatings when confronted with repeated stimulations, we stimulated for 2 hours in PBS pH 7.4 using the parameters described in the methods chapter section 3.2.4. Impedance and CSC were measured before and after the stimulations.

The microelectrodes experienced a decrease of around 80 Ω for the impedance, and an increase of their CSCs comprised between 6 and 12% (figure 24). This led us to believe that the stimulation *in vitro* was either beneficial or harmless when tested using PEDOT:BF_4 coating.

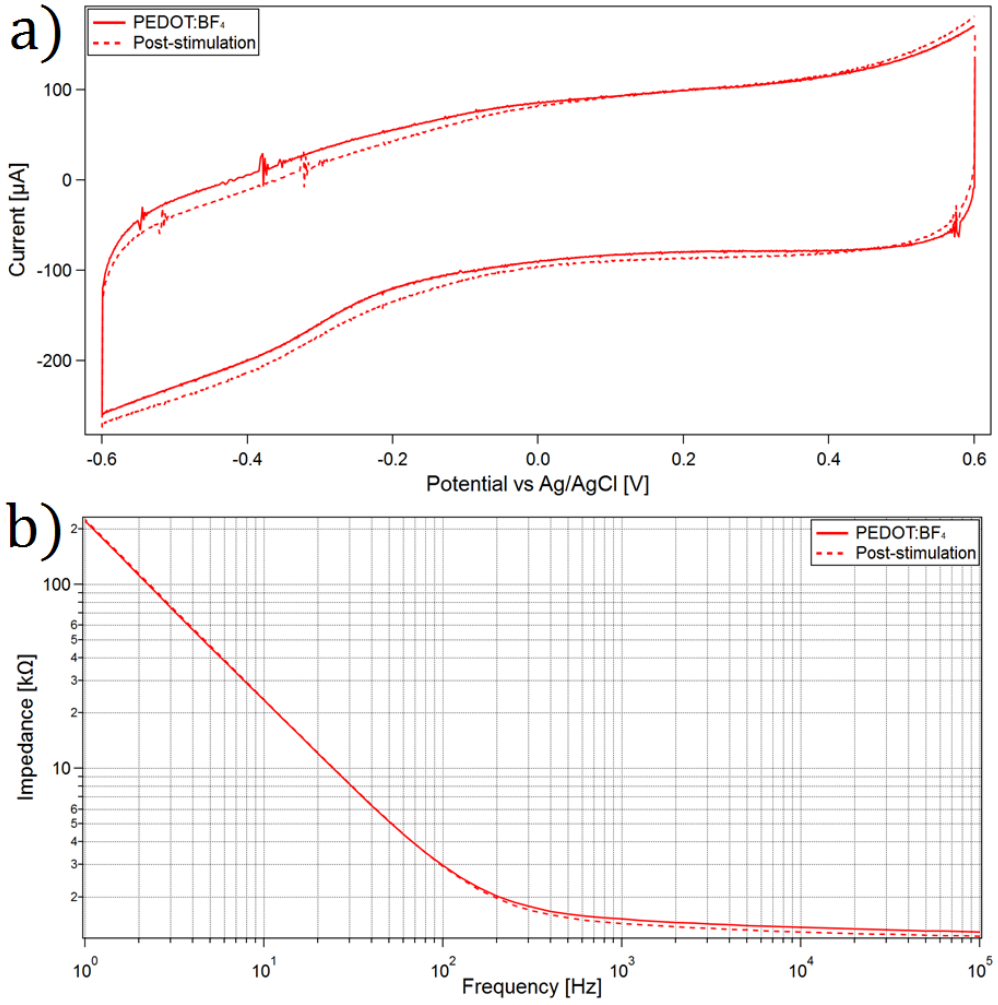

Figure 24: Characterization of stimulating PEDOT:BF_4-coated PtIr microelectrodes before and after 2 hours of stimulations in PBS pH 7.4: a) CV, b) EIS.

4.3 *In vivo* experiments

Chronic implantation of our PEDOT:BF_4-coated PtIr stimulating microelectrodes in a rat brain was realized to observe the evolution of our coatings under DBS conditions. PtIr stimulating microelectrodes were coated with PEDOT:BF_4 galvanostatically processed in PC and implanted in the subthalamic nucleus of two Wistar rats.

4.3.1 Voltage excursion

The voltage at the implanted microelectrodes was monitored when applying biphasic pulses. The parameters were chosen accordingly to the literature [28], [29] and described in section 3.2.4. The biphasic pulses consisting of a first negative pulse followed by a positive pulse, we used the maximum peak of the negative pulse as a way to characterize the efficiency of our microelectrodes. A low negative peak, in absolute value, means a more efficient microelectrode as it reduces the power consumption and the risk of harmful reaction for the coatings and the biological tissues.

For the first animal:

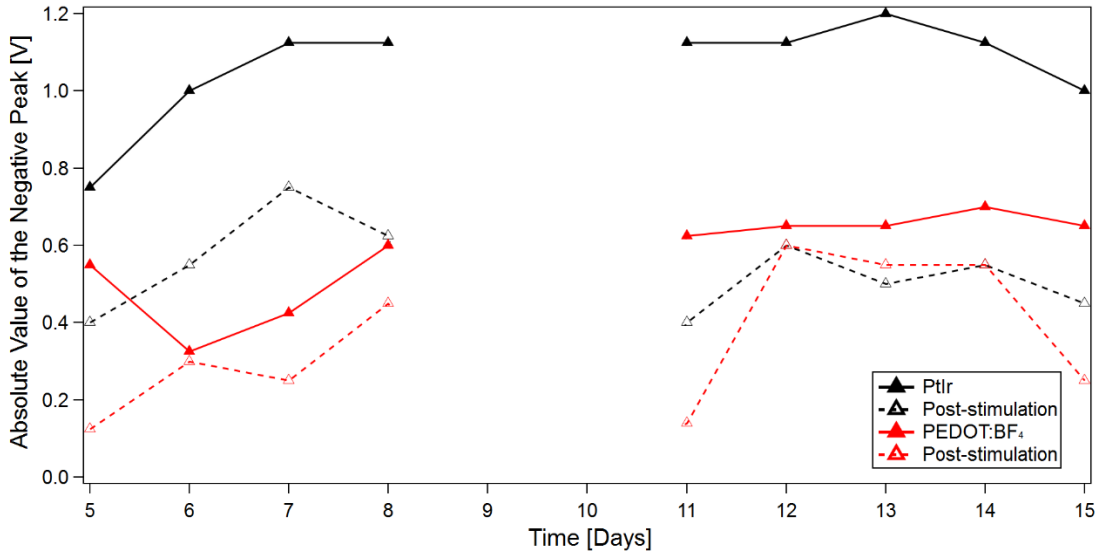

Figure 25: Absolute values of the maximum of the negative peak measured before and after 90 minutes of stimulation at the PEDOT:BF_4-coated microelectrode and the bare PtIr microelectrode implanted in the first animal during the 15 days of stimulation.

The voltage at the uncoated microelectrode was always high at the beginning of the experiment, with the negative peak usually between 0.8 V and 1.2 V (figure 25). However, after 90 minutes of

stimulation, the maximum negative peak (also referenced to as voltage or voltage excursion) decreased. The peak shifted towards values comprised between 0.550 V and 0.750 V. The voltage drop was always between 33% and 64%.

The voltage pre-stimulation at the coated microelectrode was always lower, with the negative peak between 0.400 V and 0.700 V. However, like the uncoated microelectrode, the amplitude was reduced after 90 minutes of stimulation. The peak shifted towards values comprised between 0.125 V and 0.550 V. For the coated microelectrodes the changes were less consistent, with some days the voltage excursion dropping by 77% and another day by only 8%.

The first noticeable point is that at the beginning of the stimulation, the voltage excursion at the PEDOT:BF_4-coated microelectrode was 27 to 67% lower than the voltage excursion at the uncoated microelectrode.

During the first days of stimulation, the voltage difference between coated and uncoated microelectrode post-stimulation remained important, with even cases showing an increased difference post-stimulation of 68%. However, after 12 days of stimulation, the excursion voltage post-stimulation became similar for both microelectrodes, with sometimes the voltage observed at the coated microelectrode being higher. This strongly mitigated the usefulness of PEDOT.

For the second animal:

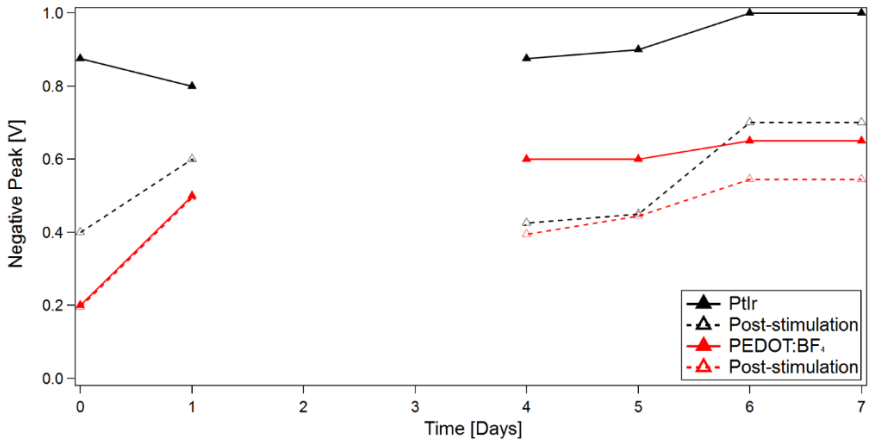

Figure 26: Absolute values of the maximum of the negative peak measured before and after 90 minutes of stimulation at the PEDOT:BF_4-coated microelectrode and the bare PtIr microelectrode implanted in the second animal during the 7 days of stimulation.

The voltage at the uncoated microelectrode was always high at the beginning of the experiment, with the negative peak between 0.800 V and 1 V (figure 26). However, after 90 minutes of stimulation, the amplitude decreased. The voltage shifted towards values comprised between 0.400 V and 0.700 V.

Interestingly enough, unlike the stable voltage of the uncoated microelectrode, the voltage excursion pre-stimulation for the coated microelectrode increased over the 8 days of stimulation, from 0.250 V to 0.700 V. Besides, unlike the behavior of the coated microelectrode for the first animal, only small changes (between 0 and 33%) were observed post-stimulation.

The first observable point is that the pre-stimulation voltage difference between the PEDOT:BF_4-coated microelectrode and the uncoated microelectrode varied from 77% to 35% over the 7 days of stimulation. This strongly mitigated the usefulness of PEDOT, as the difference in voltage became lower over time.

In the first animal, the voltage excursion post-stimulation at the PEDOT:BF_4-coated microelectrode increased until reaching a similar voltage excursion observed at the uncoated microelectrode. In the second animal, the voltage excursion at the PEDOT:BF_4-coated microelectrode remained unaffected by the stimulation, but suffered from a slow and constant increase until reaching a similar voltage excursion observed at the uncoated microelectrode. In both cases, but most likely for different reasons, the voltage after 90 minutes of stimulation was similar for both microelectrodes.

4.3.2 Electrochemical impedance measurements

To complete and control our voltage measurements, we performed impedance measurements before and after every stimulation.

For the first animal:

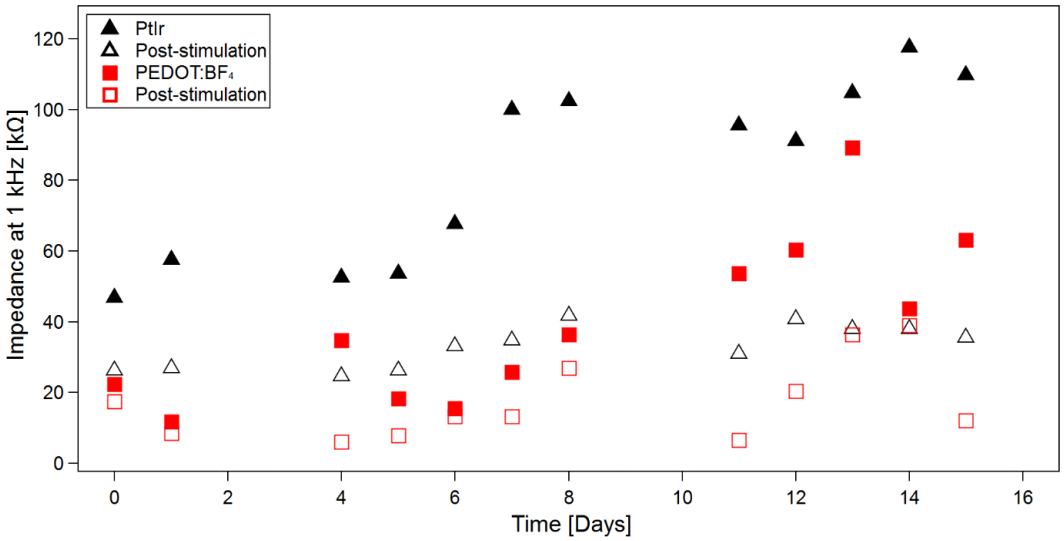

Figure 27: Impedance at 1 kHz before and after stimulation of the PEDOT:BF4-coated microelectrode and the bare PtIr microelectrode implanted in the first animal during the 16 days of stimulation.

The uncoated microelectrode suffered a constant impedance increase over time. However, after 90 minutes of stimulation, the impedance went back every time to a similar value. The relative difference pre and post-stimulation increased, but the post-stimulation impedance did not vary drastically (figure 27). The coated microelectrode also suffered an overall increase in impedance overtime but in a more irregular trend. It can also be observed that the relative change in impedance pre and post-stimulation are always varying, with sometimes an almost insignificant change.

Finally, the impedance values measured seemed to correlate with the measured voltage: the impedance post-stimulation of both microelectrodes are less different than the impedances pre-stimulation.

An interesting result is that the decrease in impedance is limited to high frequencies for the bare PtIr microelectrode whereas the reduction of impedance covered almost the whole frequency range studied for the PEDOT:BF_4-coated microelectrode (figure 28).

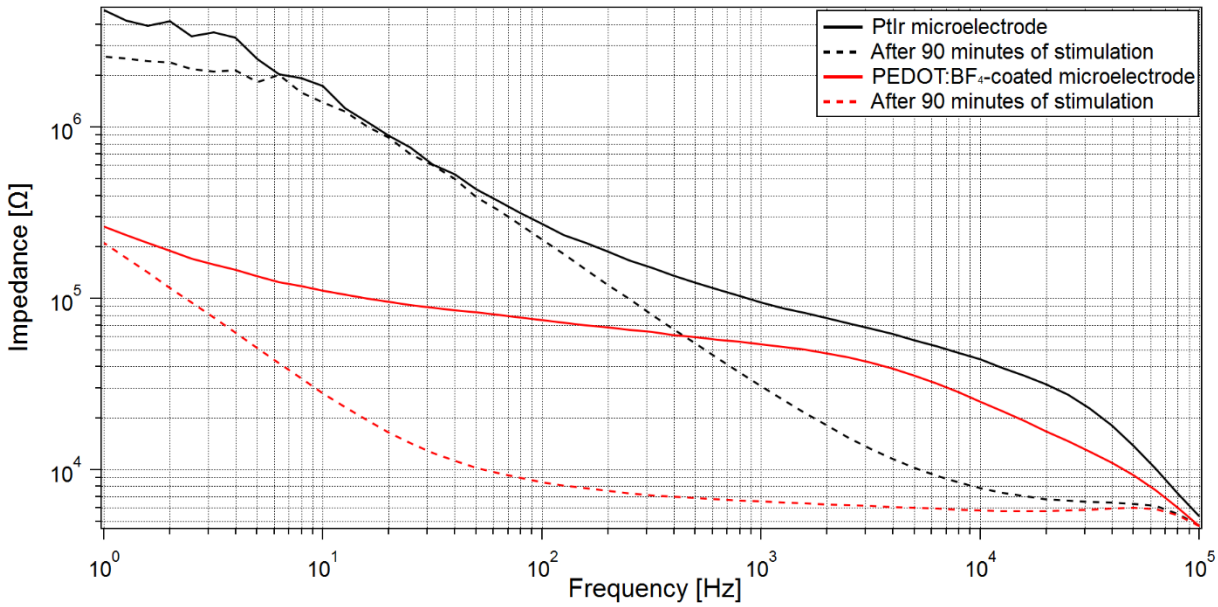

Figure 28: Bode impedance of the microelectrodes implanted in the first animal before and after 90 minutes of stimulation, after 9 days of stimulation.

For the second animal:

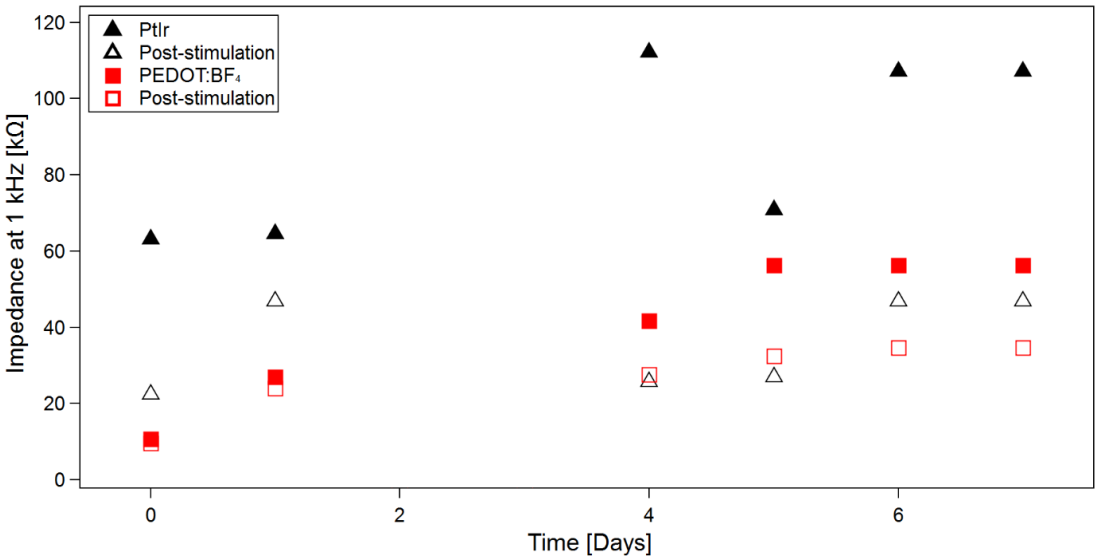

Figure 29: Impedance at 1 kHz measured before and after 90 minutes of stimulation at the PEDOT:BF4-coated microelectrode and the bare PtIr microelectrode implanted in the second animal during the 7 days of stimulation.

There is an overall increasing trend for the pre-stimulation impedances, especially for the uncoated electrode. As observed in the first animal, the difference in impedance pre and post-stimulation increased overtime for the uncoated microelectrode, as the pre-stimulation impedance increased and the post-stimulation stayed relatively constant.

For both animals, the impedance drop was always higher for the uncoated microelectrode than for the coated one. As the impedance increased over the days, the impedances post-stimulation became very similar for both microelectrodes, mitigating the usefulness of the coating. This trend was previously observed for the voltage excursion.

CHAPTER 5 GENERAL DISCUSSION

5.1 Improved electrochemical properties *in vitro*

As expected, the presence of the PEDOT:BF_4 coatings did increase the CSC and reduce the impedance for all substrates: Pt disk, recording PtIr microelectrodes and stimulating PtIr microelectrodes, for deposition carried out in acetonitrile, propylene carbonate and distilled water (ACN, PC and DW). Indeed, the rough morphology of PEDOT morphology increases the electroactive surface area of the electrode, reducing the impedance and enhancing the CSC.

The electrochemical properties of coatings on the Pt disk were characterized after using different deposition methods. PD deposition provided the thickest layer and the largest CSCs. Taking into account the pseudocapacitive behaviour of PEDOT, this characteristic is directly linked to the thickness of the layer: more materials lead to more charges stored in the polymer matrix. PS and GS depositions provided similar results, due to the same amount of charges exchanged and so a similar quantity of PEDOT deposited.

For deposition on PtIr microelectrodes, organic solvents provided similar electrochemical properties, while DW did provide a slightly higher impedance and lower CSC. The most likely explanation for this result is the difference in surface roughness: SEM imaging showed that coatings prepared in ACN and PC had porous morphologies whereas coatings prepared in DW had compact, nodular morphologies. The porosity of the structure for organic solvents further increases the active surface area and facilitates ion transport in and out the polymer matrix. Cysewska et al showed that their compact PEDOT:ClO_4 films had indeed higher impedances and lower CSCs than their more porous films [99].

5.2 Stability *in vitro*

Sonication tests for the Pt disk showed that coatings processed in DW delaminated more easily and appeared more brittle than those processed in organic solvents. This is most likely a consequence of the morphology. The coatings processed in organic solvents seemed less rigid as they were able to resist and conserve a certain cohesion during sonication, whereas the compact-looking water-processed coatings appeared to widely fracture into a multitude of small isolated portions, rapidly losing their film cohesion and their electrochemical properties.

The sonication results on the PtIr microelectrodes confirmed these observations: the organic solvents-processed films were able to survive the sonication whereas the water-processed ones delaminated before 5 minutes of sonication.

The passive aging and steam sterilization did not drastically affect the electrochemical properties of the coatings. However, water-processed coatings did suffer from a slight increase of impedance after steam sterilization.

As mentioned above, a plausible cause can be found in the coating morphology to explain this varying robustness. Green et al observed that smooth and compact PEDOT:PSS films were more fragile than PEDOT:ClO_4 and PEDOT:pTS films when confronted to steam sterilization and accelerated aging [6]. They claimed these films to be stiffer than their counter-parts. This stiffness would make them more brittle and would also prevent them from anchoring into the imperfections of the substrate, all of this contributing to an easier delamination. Baek et al confirmed that the stiffness of PEDOT:PSS films was twice higher than their PEDOT:ClO_4 films [93]. In both cases, the difference in rigidity came from the dopant used and not the solvent. However, in our work, it was the use of water as a solvent that led to compact PEDOT:BF_4 coatings. Therefore, we suppose that the use of water can lead to compact coatings that are more prone to delamination due to their higher stiffness than organic solvent-processed coatings.

5.2.1 Use of thien-DS to improve adhesion

Initially, thien-DS layers proved to be very useful to improve the adhesion of the coatings on the Pt disk. Indeed, the covalent bounds between the Pt surface and the thien-DS layer, generated during the reduction of the thien-DS amine moities, are much stronger than the physical adsorption of PEDOT observed without the thien-DS layer (figure 30). We observed that the electropolymerization of PEDOT:BF_4 on the thien-DS layer could take place in three different solvents (ACN, PC and DW) without diminishing the adhesion improvement provided by the previously deposited thien-DS layer.

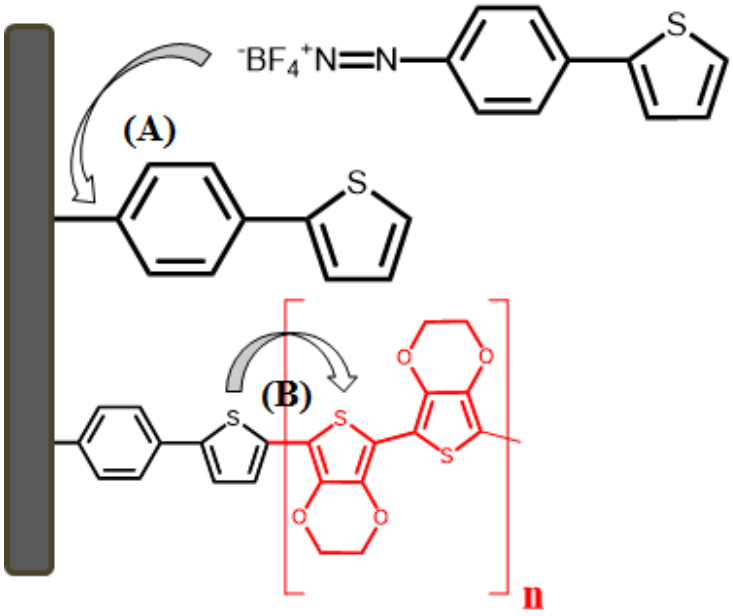

Figure 30:(A) Electrodeposition of the thien-DS layer by reduction of the amine moieties (B) Electropolymerization of PEDOT on the thien-DS anchoring layer.

Unexpectedly, the results indicated a decrease in adhesion quality for PEDOT:BF_4 on PtIr microelectrodes, as some coatings delaminated in less than 30 seconds. An intuitive explanation would be that the 15 cycles of thien-DS provide a too thick layer over a too small surface, and this thickness might hinder the desired development of the subsequent electropolymerized thin layer of PEDOT:BF_4. This would lead to a poorly structured PEDOT layer that would delaminate easily when confronted to sonication. However, this is purely speculative.

In our previous work [7], PEDOT:BF_4 electrodeposition on microelectrodes was realized through 10 cycles of PD deposition. In this case, we can suppose that the quantity of PEDOT:BF_4 was large enough to fully cover the electrode and anchor on the thien-DS layer. However, in this work we could not use the same deposition method as we wanted to limit the quantity of PEDOT on our microelectrodes and 5 cycles of PD deposition already gave us too much PEDOT:BF_4: an important overgrowth could be noticed that would render the use of our microelectrodes inappropriate for recording or stimulation purposes.

The deposition method of the thien-DS should be refined for microelectrode dimensions.

5.3 Differences in deposition kinetics

We discussed previously the critical impact of the morphology on the electrochemical properties and the robustness of the coatings.

As reported in the literature, the solvent used for electropolymerization plays a primary role in smoothness and compactness of the PEDOT films. Several characteristics of the solvent that may influence PEDOT's morphology have been identified in previous studies. Belaidi et al compared water and ACN as solvent [95]. The higher dielectric constant of water (around 80 compared to around 36 for ACN) led to a slower deposition rate. Poverenov et al reported that the difference in solubility of the initial PEDOT oligomers in ACN and PC was responsible for the smoother films produced in PC [94]. Indeed, a low oligomer solubility in ACN would lead to a higher number of small oligomers on the electrode surface, increasing the roughness of the ACN-processed films. Singh & Kumar invoked the higher viscosity of PC as another explanation for the slower deposition rate in PC and the consequently smoother films [96]. Indeed, a higher viscosity results in slower mass transports and lower diffusion coefficients and therefore a slower deposition rate.

In our case, DW led to a slower deposition rate for GS deposition of PEDOT:BF_4 on the PtIr microelectrodes. This was even more evident when looking at the PD and PS depositions curves on the Pt disk (figure 15 a) and c)): the fastest deposition was in ACN, followed by PC, whereas deposition in DW lagged behind. These varying deposition rates may be caused by differences in oligomer solubility, dielectric constant and viscosity. A slower deposition rate facilitates the formation of longer polymeric chains in the solution, the length of these polymeric chains greatly influencing the smoothness of the films. Due to these factors, water-processed coatings inherited a more compact and therefore less flexible and therefore less robust structure.

5.4 Electrochemical properties of PEDOT:BF_4 coatings *in vivo*

As expected, the impedance *in vivo* was substantially higher for both coated and uncoated microelectrodes than the one observed *in vitro*. This is due to the change in medium surrounding the electrodes, protein adsorption and cell accumulation on their surface [47], [100]. However, the differences in impedance *in vivo* between the coated and uncoated microelectrodes was actually higher than *in vitro*. This could mean that PEDOT:BF_4 is even more useful as a coating when

immersed in cerebral fluids inside biological tissues than in laboratory conditions. PEDOT:BF_4 certainly appear to be a better biotic-abiotic interface than bare PtIr.

The slow rise of impedance observed during the implantation period is most likely due to the FBR that gradually encapsulate the intruding microelectrodes, as Williams et al demonstrated when they correlated the increasing impedances of their implanted electrodes with strong inflammatory reactions [46]. Williams et al proposed an impedance model for *in vivo* experiments that could help monitor the degree of inflammation around implanted electrodes and determine if a "confined" or an "extensive" inflammatory response is taking place. Prasad & Sanchez proposed to use daily impedance measurements to find out if the reduction in effectiveness of the implanted electrode originated from biotic factors (tissues) or abiotic factors (the electrode itself) and determine the best course of action to solve the issue [47]. For the PEDOT:BF_4-coated microelectrodes, despite our tests on the stability and the use of non-damaging stimulating currents, we cannot exclude some partial delamination and/or overoxydation. It is difficult to separate the influence of the FBR and the influence of PEDOT on the impedance *in vivo*, as both the FBR [46] and PEDOT delamination [101] decreases the capacitance. An encouraging result is that the impedance increase over the implantation period is faster for the PtIr uncoated microelectrode than for the coated one (figure 27).

The analysis of the impedance at 1 kHz is limited to draw conclusion. It is difficult to correlate impedance with measured voltage, because, as Wei & Grill observed [102], the impedances operate in a non-linear regime for clinically-relevant current densities and is also heavily influenced by the frequency used. Hence our impedance measurements at 1 kHz are only qualitative indicators of the evolution of our coatings and of the brain environment and voltage excursions may be better suited indicators. In addition, in our case the voltage excursions measured overall displayed the same trend as the impedances, with a lower negative voltage peak measured for the PEDOT:BF_4-coated microelectrode, which is in accordance with the lower impedance and the literature [73].

5.4.1 Impact of PEDOT coatings for DBS applications

For our electrodes, the stimulation systematically lowered the impedance and the voltage excursion. This is not new, as Satzer et al identified a reduction of impedance during stimulations in human patients implanted with DBS devices [103]. Early work in animals by Weiland & Anderson had shown that repeated stimulation *in vivo* led to a decrease in impedance at high

frequencies for metallic electrodes [104]. Lempka et al noticed that this change was reversible [100]. They hypothesized that the electrical stimulation polarized the electrode surface, leading to electroporation of adhered cells and desorption of proteins, and "cleaned" it. This phenomenon was not observed *in vitro* for metallic electrodes. *In vitro* stimulations of PEDOT:PSS realized by Wilks et al [72] and Venkatraman et al [73], confirmed that this phenomenon was not observed *in vitro* for PEDOT coatings. This would indicate that this phenomenon is not caused only by the stimulation but by a combination of the presence of biological tissues and electrical stimulation. It is interesting to note that the study from Venkatraman et al did also include *in vivo* stimulations of PEDOT:PSS and did not reveal a following change in electrochemical properties. We can suppose that their stimulation period, not given in the article, was too short to observe any changes in impedances or voltage excursion, in comparison to our 90 minutes-stimulation period. The same remark can be made for the work of Mandal et al about their *in vivo* stimulation using PEDOT:BF_4 coatings: no observations about the influence of long-term stimulations were made because the stimulation period may have been too short [79]. A study by Kolarcik et al measured the evolution of the impedance *in vivo* during stimulation and observed similar results as our own findings [44]. After 1 hour of biphasic charge-balanced stimulation, they observed a decrease in impedance for all their electrodes, both coated and uncoated, and this decrease successfully correlated with a decrease observed for the measured voltages. Their findings combined with ours would suggest that the reduction of impedances *in vivo* after stimulation is also present for PEDOT-coated microelectrodes.

However, in our work, the decrease in impedance *in vivo* was more important for the uncoated PtIr microelectrode than for the coated one. This meant that over time and after stimulation, the usefulness of PEDOT:BF_4 was mitigated, as the impedance and voltage excursion were in some cases very similar for both microelectrodes. These results are definitely worth noting as numerous authors have claimed PEDOT coatings to be a sure improvement for DBS conditions, but most of their results were either acquired *in vitro* or with limited stimulation period *in vivo*. In our study, we observed a mitigation of the usefulness of PEDOT:BF_4 after 90 minutes of stimulation *in vivo*, which could not have been detected *in vitro* nor with short stimulations. Still, we have to mitigate our own findings: only two animals were tested and the stimulation period (90 minutes) was from real medical conditions as human patients are subjected to the stimulation constantly for years.

CHAPTER 6 CONCLUSION AND RECOMMENDATIONS

6.1 Electropolymerization and adhesion

In this work, we made several progress on the electropolymerization procedure and adhesion of PEDOT:BF_4. First, we discovered the difficulty of using thien-DS as an anchoring layer on microelectrodes. However, we found out that organic solvents such as PC and ACN provided coatings with an adhesion strong enough to survive sterilization and implantation in the body.

6.1.1 Thien-DS

Thien-DS, as reported in one of our works [7], may prove to be an ideal solution to solve the adhesion issue of PEDOT. The relevant result reported in this work, is that the electropolymerization of PEDOT can take place in three different solvents (ACN, PC and DW) without reducing the effectiveness of the already deposited thien-DS. However, a lot of work is still required to find the right parameters to deposit the thien-DS layer in a way that does not hinder the following electrodeposition of PEDOT, especially for microelectrodes exhibiting a very low surface available for deposition.

6.1.2 Solvent

Despite the limited usefulness of thien-DS, we managed to obtain stable coatings on PtIr microelectrodes by selecting the most suitable solvent for electropolymerization. We demonstrated that the organic solvents PC and ACN were better suited than DW for the stability under sonication and steam sterilization processes. However, the adhesion was decent enough for the PEDOT:BF_4 coatings processed in DW to be used in a biomedical context.

The differences in adhesion are linked to the important differences observed in morphologies, with DW leading to compact films and organic solvents to porous structures. These varying morphologies depend most likely on the deposition rate affected by diverse factors such as viscosity, dielectric constant and solubility of PEDOT oligomers.

6.2 *In vivo* observations

PEDOT:BF_4-coated microelectrodes, processed in PC, were implanted in rats for stimulations. As observed by impedance measurements, the coatings appeared to be stable and did not indicate any sign of significant delamination during the implantation procedure nor during the following days. This observation reinforces the conclusion concerning the stability of our coatings when used as electrode-tissues interfaces.

Besides the stability of our coatings *in vivo,* we observed an interesting phenomenon. It has already been reported that PEDOT:BF_4 coatings reduces the impedance of neural electrodes both *in vitro* and *in vivo,* and it has also been reported that electrical stimulation *in vivo* reduces the impedance of metallic electrodes by altering the tissue-electrode interface [103], [104]. However, no long-term study has reported the decrease in impedance of PEDOT:BF_4 during electrical stimulations *in vivo*. This is due to the fact that PEDOT has been subjected to electrical pulsing only *in vitro* or during short stimulation period *in vivo*.

In this work, we report a substantial reduction of the impedance of our PEDOT:BF_4 coatings after 90 minutes of biphasic charge-balanced stimulation. This reduction of impedance is most welcomed for stimulation purposes. However, the reduction of impedance was more important for the uncoated microelectrode than for the coated one. Despite the fact that the PEDOT:BF_4-coated microelectrodes always kept a lower impedance than its uncoated counterpart, this difference in reduction mitigated the usefulness of PEDOT coatings, as in some cases the post-stimulation impedances were almost identical. This similar impedance leads to similar voltages at the electrode-tissue interface, which means that the power consumption and the possibly harmful reactions occurring near the microelectrodes are the same for both coated and uncoated microelectrodes. The last observation was that the reduction of impedance for metallic microelectrodes was concentrated on the high frequencies, whereas for the coated microelectrodes the reduction covered almost the entire frequency range studied.

Still, we have to be careful with our own results, as the evolution of the impedance *in vivo* is a complex process and our observations are nothing more than preliminary. All we can advance is that the usefulness of PEDOT:BF_4 as an electrode-tissue interface is reduced by the stimulation but not lost. Longer studies with longer stimulation periods, using more animals, must be conducted to ensure the complete stability and usefulness of our coatings.

6.3 Perspectives

Despite tremendous advances in the bioelectronic medicine field in the last years, our work hinted towards several topics that still require improvement. The electropolymerization process and its influence on the adhesion quality have been extensively studied by the scientific community, but as we reported and characterized important differences when changing the electropolymerization solvent, some parameters, even simple ones such as solvent and dopant, may need further optimization. However, we feel that the study of PEDOT-coated DBS devices should be the main focus in the coming years. The reported use of PEDOT for stimulation purposes were either *in vitro* or incomplete *in vivo* studies that neglected the effect of electrical pulsing on the electrode-tissue interface. Hence, there is an absolute need to further characterize the interactions between neural electrodes, both coated and uncoated, and the biological tissues during stimulation. This could be done both *in vivo* and *in vitro*.

All the experiments were realized by the author.

BIBLIOGRAPHY

[1] S. Löffler, K. Melican, K. P. R. Nilsson, and A. Richter-Dahlfors, "Organic bioelectronics in medicine," *J. Intern. Med.*, vol. 282, no. 1, pp. 24–36, 2017.

[2] J. M. Bronstein *et al.*, "Deep Brain Stimulation for Parkinson Disease," *Arch. Neurol.*, vol. 68, no. 2, pp. 165–171, 2011.

[3] M. L. Kringelbach, A. L. Green, S. L. F. Owen, P. M. Schweder, and T. Z. Aziz, "Sing the mind electric - principles of deep brain stimulation," *Eur. J. Neurosci.*, vol. 32, no. 7, pp. 1070–1079, 2010.

[4] V. S. Polikov, P. A. Tresco, and W. M. Reichert, "Response of brain tissue to chronically implanted neural electrodes," *J. Neurosci. Methods*, vol. 148, no. 1, pp. 1–18, 2005.

[5] D. T. Simon, E. O. Gabrielsson, K. Tybrandt, and M. Berggren, "Organic Bioelectronics: Bridging the Signaling Gap between Biology and Technology," *Chem. Rev.*, vol. 116, no. 21, pp. 13009–13041, 2016.

[6] R. A. Green *et al.*, "Substrate dependent stability of conducting polymer coatings on medical electrodes," *Biomaterials*, vol. 33, no. 25, pp. 5875–5886, 2012.

[7] D. Chhin, D. Polcari, B. Guen, G. Tomasello, F. Cicoira, and S. B. Schougaard, "Diazonium-Based Anchoring of PEDOT on Pt / Ir Electrodes via Diazonium Chemistry," *J. Electrochem. Soc.*, vol. 165, no. 12, pp. 3066–3070, 2018.

[8] M. D. Ferro and N. A. Melosh, "Electronic and Ionic Materials for Neurointerfaces," *Adv. Funct. Mater.*, vol. 1704335, p. 1704335, 2017.

[9] H. S. Mayberg *et al.*, "Deep brain stimulation for treatment-resistant depression," *Neuron*, vol. 45, no. 5, pp. 651–660, 2005.

[10] F. M. Weaver *et al.*, "Bilateral Deep Brain Stimulation vs Best Medical Therapy for Patients With Advanced Parkinson Disease," *JAMA Otolaryngol. - Head Neck Surg.*, vol. 301, no. 1, p. 301(1): 63-73, 2009.

[11] V. Khaindrava, P. Salin, C. Melon, M. Ugrumov, L. Kerkerian-Le-Goff, and A. Daszuta, "High frequency stimulation of the subthalamic nucleus impacts adult neurogenesis in a rat model of Parkinson's disease," *Neurobiol. Dis.*, vol. 42, no. 3, pp. 284–291, 2011.

[12] T. J. Van Hartevelt *et al.*, “Neural plasticity in human brain connectivity: The effects of long term deep brain stimulation of the subthalamic nucleus in Parkinson’s disease,” *PLoS One*, vol. 9, no. 1, 2014.

[13] M. L. Kringelbach, N. Jenkinson, S. L. F. Owen, and T. Z. Aziz, “Translational principles of deep brain stimulation,” *Nat. Rev. Neurosci.*, vol. 8, no. 8, pp. 623–635, 2007.

[14] A. Stefani *et al.*, “Bilateral deep brain stimulation of the pedunculopontine and subthalamic nuclei in severe Parkinson’s disease,” *Brain*, vol. 130, no. 6, pp. 1596–1607, 2007.

[15] P. Hickey and M. Stacy, “Deep brain stimulation: A paradigm shifting approach to treat Parkinson’s disease,” *Front. Neurosci.*, vol. 10, no. APR, pp. 1–11, 2016.

[16] J. Couto and W. M. Grill, “Kilohertz Frequency Deep Brain Stimulation Is Ineffective at Regularizing the Firing of Model Thalamic Neurons,” *Front. Comput. Neurosci.*, vol. 10, no. March, pp. 1–12, 2016.

[17] D. T. Brocker, B. D. Swan, R. Q. So, D. A. Turner, R. E. Gross, and W. M. Grill, “Optimized temporal pattern of brain stimulation designed by computational evolution,” *Sci. Transl. Med.*, vol. 9, no. 371, 2017.

[18] A. I. Tröster, J. Jankovic, M. Tagliati, D. Peichel, and M. S. Okun, “Neuropsychological outcomes from constant current deep brain stimulation for Parkinson’s disease,” *Mov. Disord.*, vol. 32, no. 3, pp. 433–440, 2017.

[19] R. Paulat, W. Meissner, R. Morgenstern, A. Kupsch, and D. Harnack, “Development of an implantable microstimulation system for chronic DBS in rodents,” *Proc. Annu. Int. Conf. IEEE Eng. Med. Biol. Soc. EMBS*, pp. 660–662, 2011.

[20] R. Q. So, G. C. McConnell, A. T. August, and W. M. Grill, “Characterizing Effects of Subthalamic Nucleus Deep Brain Stimulation on Methamphetamine-Induced Circling Behavior in Hemiparkinsonian Rats,” *IEEE Trans. Neural Syst. Rehabil. Eng.*, no. 919, pp. 1–22, 2012.

[21] K. Badstübner, T. Kröger, E. Mix, U. Gimsa, R. Benecke, and J. Gimsa, “Electrical Impedance Properties of Deep Brain Stimulation Electrodes during Long-Term In-Vivo Stimulation in the Parkinson Model of the Rat,” *Commun. Comput. Inf. Sci.*, vol. 357 CCIS, no. January, 2013.

[22] K. J. Lee, I. Shim, J. H. Sung, J. T. Hong, I. S. Kim, and C. B. Cho, “Striatal glutamate and GABA after high frequency subthalamic stimulation in parkinsonian rat,” *J. Korean Neurosurg. Soc.*, vol. 60, no. 2, pp. 138–145, 2017.

[23] K. Badstuebner, U. Gimsa, I. Weber, A. Tuchscherer, and J. Gimsa, “Deep Brain Stimulation of Hemiparkinsonian Rats with Unipolar and Bipolar Electrodes for up to 6 Weeks: Behavioral Testing of Freely Moving Animals,” *Parkinsons. Dis.*, vol. 2017, 2017.

[24] R. Q. So, G. C. McConnell, and W. M. Grill, “Frequency-dependent, transient effects of subthalamic nucleus deep brain stimulation on methamphetamine-induced circling and neuronal activity in the hemiparkinsonian rat,” *Behav. Brain Res.*, vol. 320, pp. 119–127, 2017.

[25] P. Prinz *et al.*, “Deep brain stimulation alters light phase food intake microstructure in rats,” *J. Physiol. Pharmacol.*, vol. 68, no. 3, pp. 345–354, 2017.

[26] J. M. Bronstein *et al.*, “The rationale driving the evolution of deep brain stimulation to constant-current devices,” *Neuromodulation*, vol. 18, no. 2, pp. 85–88, 2015.

[27] T. Pham and J. M. Bronstein, “Neuropsychological outcomes from deep brain stimulation—stimulation versus micro-lesion,” *Ann. Transl. Med.*, vol. 5, no. 10, pp. 217–217, 2017.

[28] A. M. Kuncel and W. M. Grill, “Selection of stimulus parameters for deep brain stimulation,” *Clin. Neurophysiol.*, vol. 115, no. 11, pp. 2431–2441, 2004.

[29] S. F. Cogan, K. A. Ludwig, C. G. Welle, and P. Takmakov, “Tissue damage thresholds during therapeutic electrical stimulation,” *J. Neural Eng.*, vol. 13, no. 2, p. 021001, 2016.

[30] B. Renshaw, A. Forbes, and B. R. Morison, “Activity Of Isocortex And Hippocampus: Electrical Studies With Micro-Electrodes,” *J. Neurophysiol.*, vol. 3, no. 1, 1940.

[31] E. M. Schmidt, M. J. Bak, and J. S. McIntosh, “Long-term chronic recording from cortical neurons.,” *Exp. Neurol.*, vol. 52, no. 3, pp. 496–506, Sep. 1976.

[32] M. Jorfi, J. L. Skousen, C. Weder, and J. R. Capadona, “Progress towards biocompatible intracortical microelectrodes for neural interfacing applications,” *J. Neural Eng.*, vol. 12, no. 1, p. 011001, 2015.

[33] P. Fattahi, G. Yang, G. Kim, and M. R. Abidian, “A Review of Organic and Inorganic

Biomaterials for Neural Interfaces," *Adv. Mater.*, vol. 26, no. 12, pp. 1846–1885, 2015.

[34] S. L. BeMent, K. D. Wise, D. J. Anderson, K. Najafi, and K. L. Drake, "Solid-State Electrodes for Multichannel Multiplexed Intracortical Neuronal Recording," *IEEE Trans. Biomed. Eng.*, vol. BME-33, no. 2, pp. 230–241, Feb. 1986.

[35] P. K. Campbell, K. E. Jones, R. J. Huber, K. W. Horch, and R. A. Normann, "A silicon-based, three-dimensional neural interface: manufacturing processes for an intracortical electrode array," *IEEE Trans. Biomed. Eng.*, vol. 38, no. 8, pp. 758–768, Aug. 1991.

[36] A. Branner, R. B. Stein, and R. A. Normann, "Selective stimulation of cat sciatic nerve using an array of varying-length microelectrodes.," *J. Neurophysiol.*, vol. 85, no. 4, pp. 1585–94, Apr. 2001.

[37] L. A. Geddes and R. Roeder, "Criteria for the selection of materials for implanted electrodes," *Ann. Biomed. Eng.*, vol. 31, no. 7, pp. 879–890, 2003.

[38] S. M. Wellman *et al.*, "A Materials Roadmap to Functional Neural Interface Design," *Adv. Funct. Mater.*, vol. 1701269, pp. 1–38, 2017.

[39] C. Fernández-Sánchez, C. J. McNeil, and K. Rawson, "Electrochemical impedance spectroscopy studies of polymer degradation: Application to biosensor development," *TrAC - Trends Anal. Chem.*, vol. 24, no. 1, pp. 37–48, 2005.

[40] A. Prasad *et al.*, "Comprehensive characterization and failure modes of tungsten microwire arrays in chronic neural implants," *J. Neural Eng.*, vol. 9, no. 5, p. 056015, Oct. 2012.

[41] E. Patrick, M. E. Orazem, J. C. Sanchez, and T. Nishida, "Corrosion of tungsten microelectrodes used in neural recording applications," *J. Neurosci. Methods*, vol. 198, no. 2, pp. 158–171, Jun. 2011.

[42] D. Prodanov and J. Delbeke, "Mechanical and biological interactions of implants with the brain and their impact on implant design," *Front. Neurosci.*, vol. 10, no. FEB, 2016.

[43] S. P. Lacour, G. Courtine, and J. Guck, "Materials and technologies for soft implantantable neuroprostheses," *Nat. Rev. Mater.*, vol. 1, no. 10, p. 16063, 2016.

[44] C. L. Kolarcik *et al.*, "Evaluation of poly(3,4-ethylenedioxythiophene)/carbon nanotube neural electrode coatings for stimulation in the dorsal root ganglion," *J. Neural Eng.*, vol.

12, no. 1, 2015.

[45] B. D. Winslow, M. B. Christensen, W. K. Yang, F. Solzbacher, and P. A. Tresco, “A comparison of the tissue response to chronically implanted Parylene-C-coated and uncoated planar silicon microelectrode arrays in rat cortex,” *Biomaterials*, vol. 31, no. 35, pp. 9163–9172, 2010.

[46] J. C. Williams, J. A. Hippensteel, J. Dilgen, W. Shain, and D. R. Kipke, “Complex impedance spectroscopy for monitoring tissue responses to inserted neural implants,” *J. Neural Eng.*, vol. 4, no. 4, pp. 410–423, 2007.

[47] A. Prasad and J. C. Sanchez, “Quantifying long-term microelectrode array functionality using chronic *in vivo* impedance testing,” *J. Neural Eng.*, vol. 9, no. 2, p. 026028, 2012.

[48] D. H. Szarowski *et al.*, “Brain responses to micro-machined silicon devices,” *Brain Res.*, vol. 983, no. 1–2, pp. 23–35, 2003.

[49] J. N. Turner *et al.*, “Cerebral Astrocyte Response to Micromachined Silicon Implants,” *Exp. Neurol.*, vol. 156, no. 1, pp. 33–49, 1999.

[50] R. Biran, D. C. Martin, and P. A. Tresco, “Neuronal cell loss accompanies the brain tissue response to chronically implanted silicon microelectrode arrays,” *Exp. Neurol.*, vol. 195, no. 1, pp. 115–126, 2005.

[51] A. J. Woolley, H. A. Desai, and K. J. Otto, “Chronic intracortical microelectrode arrays induce non-uniform, depth-related tissue responses,” *J. Neural Eng.*, vol. 10, no. 2, p. 026007, 2013.

[52] T. Saxena *et al.*, “The impact of chronic blood-brain barrier breach on intracortical electrode function,” *Biomaterials*, vol. 34, no. 20, pp. 4703–4713, 2013.

[53] N. F. Nolta, M. B. Christensen, P. D. Crane, J. L. Skousen, and P. A. Tresco, “BBB leakage, astrogliosis, and tissue loss correlate with silicon microelectrode array recording performance,” *Biomaterials*, vol. 53, pp. 753–762, 2015.

[54] J. L. Skousen, M. J. Bridge, and P. A. Tresco, “A strategy to passively reduce neuroinflammation surrounding devices implanted chronically in brain tissue by manipulating device surface permeability,” *Biomaterials*, vol. 36, pp. 33–43, 2015.

[55] G. Lind, C. E. Linsmeier, and J. Schouenborg, “The density difference between tissue and neural probes is a key factor for glial scarring,” *Sci. Rep.*, vol. 3, no. 1, p. 2942, 2013.

[56] Z. J. Du *et al.*, “Ultrasoft microwire neural electrodes improve chronic tissue integration,” *Acta Biomater.*, vol. 53, pp. 46–58, 2017.

[57] F. Liao, H. Xu, N. Torrey, P. Road, and L. Jolla, “Failure mode analysis of silicon-based intracortical microelectrode arrays in non-human primates,” *J. Neural Eng.*, vol. 2, no. 74, 2015.

[58] R. Balint, N. J. Cassidy, and S. H. Cartmell, “Conductive polymers: Towards a smart biomaterial for tissue engineering,” *Acta Biomater.*, vol. 10, no. 6, pp. 2341–2353, 2014.

[59] J. L. and G. B. S. Bredas, G. B. Street, and J. L. and G. B. S. Bredas, “Polarons, bipolarons, and solitons in conducting polymers,” *Acc. Chem. Res.*, vol. 18, no. 4, pp. 309–315, 1985.

[60] Z. Aqrawe, J. Montgomery, J. Travas-Sejdic, and D. Svirskis, “Conducting polymers for neuronal microelectrode array recording and stimulation,” *Sensors Actuators B Chem.*, vol. 257, pp. 753–765, 2018.

[61] N. K. Guimard, N. Gomez, and C. E. Schmidt, “Conducting polymers in biomedical engineering,” *Prog. Polym. Sci.*, vol. 32, pp. 876–921, 2007.

[62] U. A. Aregueta-Robles, A. J. Woolley, L. A. Poole-Warren, N. H. Lovell, and R. A. Green, “Organic electrode coatings for next-generation neural interfaces,” *Front. Neuroeng.*, vol. 7, no. May, pp. 1–18, 2014.

[63] R. Green and M. R. Abidian, “Conducting Polymers for Neural Prosthetic and Neural Interface Applications,” *Adv. Mater.*, pp. 7620–7637, 2015.

[64] J. J. Pancrazio *et al.*, “Thinking Small: Progress on Microscale Neurostimulation Technology,” *Neuromodulation*, vol. 20, no. 8, pp. 745–752, 2017.

[65] H. Yamato, M. Ohwa, and W. Wernet, “Stability of polypyrrole and poly(3,4-ethylenedioxythiophene) for biosensor application,” *J. Electroanal. Chem.*, vol. 397, no. 1–2, pp. 163–170, 1995.

[66] Y. Fang, X. Li, and Y. Fang, “Organic bioelectronics for neural interfaces,” *J. Mater. Chem. C*, vol. 3, no. 25, pp. 6424–6430, 2015.

[67] S. F. Cogan, “Neural stimulation and recording electrodes,” *Annu. Rev. Biomed. Eng.*, vol. 10, pp. 275–309, 2008.

[68] X. Cui and D. C. Martin, “Electrochemical deposition and characterization of poly (3,4-ethylenedioxythiophene) on neural microelectrode arrays,” *Sensors Actuators B Chem.*, vol. 89, pp. 92–102, 2003.

[69] J. Yang, D. H. Kim, J. L. Hendricks, M. Leach, R. Northey, and D. C. Martin, “Ordered surfactant-templated poly(3,4-ethylenedioxythiophene) (PEDOT) conducting polymer on microfabricated neural probes,” *Acta Biomater.*, vol. 1, no. 1, pp. 125–136, 2005.

[70] K. A. Ludwig, J. D. Uram, J. Yang, D. C. Martin, and D. R. Kipke, “Chronic neural recordings using silicon microelectrode arrays electrochemically deposited with a poly(3,4-ethylenedioxythiophene) (PEDOT) film,” *J. Neural Eng.*, vol. 3, no. 1, pp. 59–70, 2006.

[71] X. T. Cui and D. D. Zhou, “Poly (3,4-ethylenedioxythiophene) for chronic neural stimulation,” *IEEE Trans. Neural Syst. Rehabil. Eng.*, vol. 15, no. 1, pp. 502–508, 2007.

[72] S. J. Wilks, S. M. Richardson-burns, J. L. Hendricks, D. C. Martin, and K. J. Otto, “Poly (3,4-ethylenedioxythiophene) as a micro-neural interface material for electrostimulation,” *Front. Neuroeng.*, vol. 2, no. June, pp. 1–8, 2009.

[73] S. Venkatraman *et al.*, “In Vitro and In Vivo Evaluation of PEDOT Microelectrodes for Neural Stimulation and Recording,” *IEEE Trans. Neural Syst. Rehabil. Eng.*, vol. 19, no. 3, pp. 307–316, 2011.

[74] R. A. Green *et al.*, “Performance of conducting polymer electrodes for stimulating neuroprosthetics,” *J. Neural Eng.*, vol. 10, no. 1, p. 016009, 2013.

[75] E. Castagnola *et al.*, “Smaller, softer, lower-impedance electrodes for human neuroprosthesis: a pragmatic approach,” *Front. Neuroeng.*, vol. 7, no. April, pp. 1–17, 2014.

[76] V. Castagnola *et al.*, “Parylene-based flexible neural probes with PEDOT coated surface for brain stimulation and recording,” *Biosens. Bioelectron.*, vol. 67, pp. 450–457, 2015.

[77] M. Ganji, A. Tanaka, V. Gilja, E. Halgren, and S. A. Dayeh, “Scaling Effects on the Electrochemical Stimulation Performance of Au, Pt, and PEDOT:PSS Electrocorticography Arrays,” *Adv. Funct. Mater.*, vol. 1703019, pp. 1–14, 2017.

[78] H. S. Mandal *et al.*, “Improving the performance of poly(3,4-ethylenedioxythiophene) for brain-machine interface applications,” *Acta Biomater.*, vol. 10, no. 6, pp. 2446–2454, 2014.

[79] H. S. Mandal, J. S. Kastee, D. G. McHail, J. F. Rubinson, J. J. Pancrazio, and T. C. Dumas, “Improved Poly(3,4-Ethylenedioxythiophene) (PEDOT) for Neural Stimulation,” *Neuromodulation*, vol. 18, no. 8, pp. 657–663, 2015.

[80] L. J. Valle *et al.*, “Cellular adhesion and proliferation on poly (3,4-ethylenedioxythiophene): Benefits in the electroactivity of the conducting polymer,” *Eur. Polym. J.*, vol. 43, pp. 2342–2349, 2007.

[81] R. M. Miriani, M. R. Abidian, and D. R. Kipke, “Cytotoxic analysis of the conducting polymer PEDOT using myocytes,” *Conf. Proc. ... Annu. Int. Conf. IEEE Eng. Med. Biol. Soc. IEEE Eng. Med. Biol. Soc. Annu. Conf.*, vol. 2008, pp. 1841–4, 2008.

[82] M. Asplund *et al.*, “Toxicity evaluation of PEDOT/biomolecular composites intended for neural communication electrodes.,” *Biomed. Mater.*, vol. 4, no. 4, p. 045009, 2009.

[83] M. Vomero *et al.*, “Highly Stable Glassy Carbon Interfaces for Long-Term Neural Stimulation and Low-Noise Recording of Brain Activity,” *Sci. Rep.*, vol. 7, no. January, pp. 1–14, 2017.

[84] S. Luo *et al.*, “Thin , Ultrasmooth , and Functionalized PEDOT Films with in Vitro and in Vivo Biocompatibility Ultrasmooth , and Functionalized PEDOT Films with in Vitro and in Vivo Biocompatibility,” *Langmuir*, no. c, pp. 8071–8077, 2008.

[85] A. S. Pranti, A. Schander, A. Bödecker, and W. Lang, “PEDOT: PSS coating on gold microelectrodes with excellent stability and high charge injection capacity for chronic neural interfaces,” *Sensors Actuators, B Chem.*, vol. 275, no. July, pp. 382–393, 2018.

[86] L. Ouyang, B. Wei, C. Kuo, S. Pathak, B. Farrell, and D. C. Martin, “Enhanced PEDOT adhesion on solid substrates with electrografted P(EDOT-NH_2),” *Sci. Adv.*, vol. 3, no. 3, p. e1600448, 2017.

[87] L. K. Povlich, J. Cheol, M. K. Leach, J. M. Corey, J. Kim, and D. C. Martin, “Synthesis , copolymerization and peptide-modification of carboxylic acid-functionalized 3,4-ethylenedioxythiphene (EDOTacid) for neural electrode interfaces,” *BBA - Gen. Subj.*, vol. 1830, no. 9, pp. 4288–4293, 2013.

[88] B. Wei, J. Liu, L. Ouyang, C. C. Kuo, and D. C. Martin, “Significant Enhancement of PEDOT Thin Film Adhesion to Inorganic Solid Substrates with EDOT-Acid,” *ACS Appl. Mater. Interfaces*, vol. 7, no. 28, pp. 15388–15394, 2015.

[89] V. Castagnola, C. Bayon, E. Descamps, and C. Bergaud, “Morphology and conductivity of PEDOT layers produced by different electrochemical routes,” *Synth. Met.*, vol. 189, pp. 7–16, 2014.

[90] A. H. Ismail, M. N. Mustafa, A. H. Abdullah, R. M. Zawawi, and Y. Sulaiman, “Effect of Electropolymerization Potential on the Properties of PEDOT/ZnO Thin Film Composites,” *J. Electrochem. Soc.*, vol. 163, no. 2, pp. G7–G14, 2016.

[91] F. Blanchard, B. Carré, F. Bonhomme, P. Biensan, H. Pagès, and D. Lemordant, “Study of poly(3,4-ethylenedioxythiophene) films prepared in propylene carbonate solutions containing different lithium salts,” *J. Electroanal. Chem.*, vol. 569, no. 2, pp. 203–210, 2004.

[92] X. Wang, P. Sjöberg-Eerola, J. E. Eriksson, J. Bobacka, and M. Bergelin, “The effect of counter ions and substrate material on the growth and morphology of poly(3,4-ethylenedioxythiophene) films: Towards the application of enzyme electrode construction in biofuel cells,” *Synth. Met.*, vol. 160, no. 13–14, pp. 1373–1381, 2010.

[93] S. Baek, R. A. Green, and L. A. Poole-Warren, “Effects of dopants on the biomechanical properties of conducting polymer films on platinum electrodes,” *J. Biomed. Mater. Res. - Part A*, vol. 102, no. 8, pp. 2743–2754, 2014.

[94] E. Poverenov, M. Li, A. Bitler, and M. Bendikov, “Major effect of electropolymerization solvent on morphology and electrochromic properties of PEDOT films,” *Chem. Mater.*, vol. 22, no. 13, pp. 4019–4025, 2010.

[95] F. S. Belaidi *et al.*, “PEDOT-modified integrated microelectrodes for the detection of ascorbic acid, dopamine and uric acid,” *Sensors Actuators, B Chem.*, vol. 214, pp. 1–9, 2015.

[96] R. Singh and A. Kumar, “Effect of electrode surface on the electrochromic properties of electropolymerized poly(3,4-ethylenedioxythiophene) thin films,” *Org. Electron. physics, Mater. Appl.*, vol. 30, pp. 67–75, 2016.

[97] J. A. Del-oso *et al.*, “Electrochemical deposition of poly [ethylene-dioxythiophene] (PEDOT) films on ITO electrodes for organic photovoltaic cells : control of morphology ,

thickness , and electronic properties," *J. Solid State Electrochem.*, 2018.

[98] H. Karaosmanoglu, J. Travas-Sejdic, and P. A. Kilmartin, "Comparison of organic and aqueous polymerized PEDOT sensors," *Mol. Cryst. Liq. Cryst.*, vol. 604, no. 1, pp. 233–239, 2014.

[99] K. Cysewska, J. Karczewski, and P. Jasiński, "Influence of electropolymerization conditions on the morphological and electrical properties of PEDOT film," *Electrochim. Acta*, vol. 176, pp. 156–161, 2015.

[100] S. F. Lempka, S. Miocinovic, M. D. Johnson, J. L. Vitek, and C. C. McIntyre, "In vivo impedance spectroscopy of deep brain stimulation electrodes," *J. Neural Eng.*, vol. 6, no. 4, 2009.

[101] J. J. Montero-Rodríguez, D. Schroeder, W. Krautschneider, and R. Starbird, "Equivalent circuit models for electrochemical impedance spectroscopy of PEDOT-coated electrodes," *6th IEEE Ger. Student Conf.*, no. July, 2015.

[102] X. F. Wei and W. M. Grill, "Impedance characteristics of deep brain stimulation electrodes in vitro and in vivo," *J. Neural Eng.*, vol. 6, no. 4, p. 046008, 2009.

[103] D. Satzer, D. Lanctin, L. E. Eberly, and A. Abosch, "Variation in deep brain stimulation electrode impedance over years following electrode implantation," *Stereotact. Funct. Neurosurg.*, vol. 92, no. 2, pp. 94–102, 2014.

[104] J. D. Weiland and D. J. Anderson, "Chronic Neural Stimulation with Thin-Film, Iridium Oxide Electrodes," *IEEE Trans. Biomed. Eng.*, vol. 47, no. 7, pp. 911–918, 2000.